Chemical Engineering Journal

New sustainable flame retardant DOPO-NH-functionalised polyamide 6 and filament yarn

--Manuscript Draft--

Manuscript Number:	CEJ-D-21-03166R2
Article Type:	Research Paper
Keywords:	α-amino-ε-caprolactam; DOPO; Co-monomer; Polyamide 6; Filament yarn; Flame retardance
Corresponding Author:	Ivan Jerman, PhD Kemijski institut Ljubljana, SLOVENIA
First Author:	Marija Čolović
Order of Authors:	Marija Čolović
	Jelena Vasiljević
	Žiga Štirn
	Nataša Čelan Korošin
	Matic Šobak
	Barbara Simončič
	Andrej Demšar
	Giulio Malucelli
	Ivan Jerman, PhD
Abstract:	This work presents a unique approach for the preparation of a flame retardant (FR) polyamide 6 (PA6) polymer with chemically bonded 9,10-dihydro-9,10-oxa-10-phosphaphenanthrene-10-oxide (DOPO) as a pendant group bridged to the polymer via an -NH- group. A novel phosphonamidate co-monomer (DOPO-A-CLM) was synthesized from DOPO and α -amino- ε -caprolactam (A-CLM). This co-monomer was subsequently used in the hydrolytic polymerization with ε -caprolactam (CLM) in different weight ratios to prepare DOPO-NH-functionalized PA6 (PA6-xDC, x = 7, 10, and 15 wt % DOPO-A-CLM). Chemical incorporation of DOPO-A-CLM into the PA6 backbone decreased the molecular weight of the polymer from 15387 for neat PA6 to 12375, 10516 and 9316 for PA6-7DC, PA6-10DC and PA6-15DC, respectively. The DOPO-NH– pendant group accelerated start of the PA6 thermal decomposition and increased the char residues at 500 °C from 1% for PA6 to 4.6, 4.9, and 5.0% for the PA6-7DC, PA6-10DC, and PA6-15DC samples, respectively, indicating crosslinking reactions in the condensed phase. The evolved phosphorus-active species in the gas phase inhibited the PA6 depolymerization, resulting in increased thermo-oxidative stability and about a fourfold higher residue at 500 °C in the case of PA6-15DC compared to PA6. The intrinsically flame retardant PA6 filament yarns with chemically bound FR pendant group were successfully melt spun from PA6-10DC, drawn and wound on bobbin. The DOPO-NH– pendant group decreased filament flammability and inhibited flame propagation, resulting in immediate self-extinguishment after flame removal. Incorporation of DOPO-A-CLM decreased the filament tensile properties compared to the neat PA6, which correlates with the decreased polymer molecular weight.
Response to Reviewers:	Reviewer #4: The authors have revised their paper according to most of my comments. However, each bullet of the highlights is still too long and some numerical values are suggested to be added. Answer: On behalf of my co-authors and me, I would like to thank you for taking your time to review the article once again and give your constructive suggestions. We corrected the highlights and numerical values are added too. We believe that the

	highlights changes greatly improved the quality of the manuscript. The corresponding highlights in the manuscript are given as: •New DOPO-NH-functionalized caprolactam comonomer was synthesized. •New FR PA6 with pendant DOPO-NH– group was produced. •DOPO-NH– group increased thermo-oxidative residue of PA6 at 500 °C by 35%. •FR PA6 was successfully melt spun into multi-filaments of 65 μm in diameter. •Melt spun filaments were self-extinguishing in 1 s by vertical flame spread test.

NATIONAL INSTITUTE OF CHEMISTRY

Professor Todd Hoare

Editor

Chemical Engineering Journal *Ljubljana, June 3 2021*

Dear Proof Hoare,

*Thank you for the positive evaluation of the manuscript entitled "**New flame retardant DOPO-NH-functionalised polyamide 6 and filament yarn**" and for offering us a chance to prepare a revised version. We are pleased to see that reviewers now have a favourable opinion of our work and only minor corrections are suggested before publication acceptance in "Chemical Engineering Journal". We are thankful to all reviewers for their criticism and suggestions, which helped us to improve the quality of the revised manuscript.*

We describe below the revisions and our responses to the comments of the referees.

Reviewer #4:

The authors have revised their paper according to most of my comments. However, each bullet of the highlights is still too long and some numerical values are suggested to be added.

Answer: On behalf of my co-authors and me, I would like to thank you for taking your time to review the article once again and give your constructive suggestions. We corrected the highlights and numerical values are added too. We believe that the highlights changes greatly improved the quality of the manuscript.

The corresponding highlights in the manuscript are given as:

- *New DOPO-NH-functionalized caprolactam comonomer was synthesized.*
- *New FR PA6 with pendant DOPO-NH– group was produced.*

- *DOPO-NH– group increased thermo-oxidative residue of PA6 at 500 °C by 35%.*
- *FR PA6 was successfully melt spun into multi-filaments of 65 μm in diameter.*
- *Melt spun filaments were self-extinguishing in 1 s by vertical flame spread test.*

Having fully addressed the suggestions of all reviewers, we hope that the manuscript is now acceptable for publication in Chemical Engineering Journal.

Yours sincerely,

Ivan Jerman, PhD

Assist. Professor, Department of Material Chemistry

National Institute of Chemistry

NATIONAL INSTITUTE OF CHEMISTRY

Our responses to the comments of the reviewer:.

Reviewer #4:

The authors have revised their paper according to most of my comments. However, each bullet of the highlights is still too long and some numerical values are suggested to be added.

Answer: On behalf of my co-authors and me, I would like to thank you for taking your time to review the article once again and give your constructive suggestions. We corrected the highlights and numerical values are added too. We believe that the highlights changes greatly improved the quality of the manuscript.

The corresponding highlights in the manuscript are given as:

- *New DOPO-NH-functionalized caprolactam comonomer was synthesized.*
- *New FR PA6 with pendant DOPO-NH– group was produced.*
- *DOPO-NH– group increased thermo-oxidative residue of PA6 at 500 °C by 35%.*
- *FR PA6 was successfully melt spun into multi-filaments of 65 µm in diameter.*
- *Melt spun filaments were self-extinguishing in 1 s by vertical flame spread test.*

NATIONAL INSTITUTE OF CHEMISTRY

Highlights

- *New DOPO-NH-functionalized caprolactam comonomer was synthesized.*
- *New FR PA6 with pendant DOPO-NH– group was produced.*
- *DOPO-NH– group increased thermo-oxidative residue of PA6 at 500 °C by 35%.*
- *FR PA6 was successfully melt spun into multi-filaments of 65 µm in diameter.*
- *Melt spun filaments were self-extinguishing in 1 s by vertical flame spread test.*

New sustainable flame retardant DOPO-NH-functionalized polyamide 6 and filament yarn

Marija Čolović[1], Jelena Vasiljević[2], Žiga Štirn[1], Nataša Čelan Korošin[3], Matic Šobak[1], Barbara Simončič[2], Andrej Demšar[2], Giulio Malucelli[4], Ivan Jerman[1]

[1]*National Institute of Chemistry, Hajdrihova 19, 1000 Ljubljana, Slovenia*

[2]*University of Ljubljana, Faculty of Natural Sciences and Engineering, Aškerčeva 12, 1000 Ljubljana, Slovenia*

[3]*University of Ljubljana, Faculty of Chemistry and Chemical Technology, Večna pot 113, 1000 Ljubljana, Slovenia*

[4]*Politecnico di Torino, Department of Applied Science and Technology and local INSTM Unit, Viale Teresa Michel 5, 15121 Alessandria, Italy*

*Author for correspondence (e-mail: ivan.jerman@ki.si)

Graphical abstract

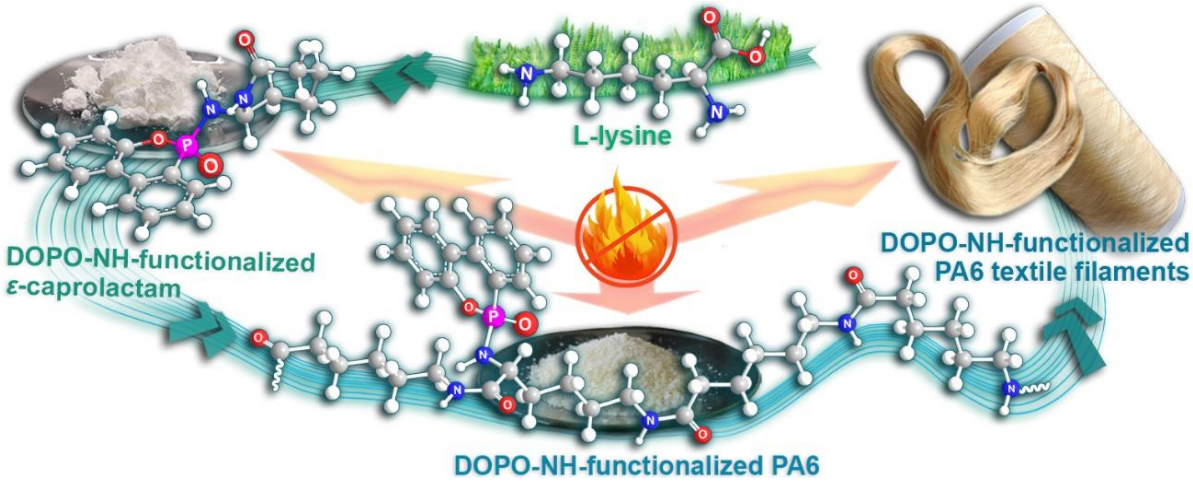

Highlights

- *New DOPO-NH-functionalized caprolactam comonomer was synthesized.*
- *New FR PA6 with pendant DOPO-NH– group was produced.*
- *DOPO-NH– group increased thermo-oxidative residue of PA6 at 500 °C by 35%.*
- *FR PA6 was successfully melt spun into multi-filaments of 65 µm in diameter.*
- *Melt spun filaments were self-extinguishing in 1 s by vertical flame spread test.*

ABSTRACT

This work presents a unique approach for the preparation of a flame retardant (FR) polyamide 6 (PA6) polymer with chemically bonded 9,10-dihydro-9,10-oxa-10-phosphaphenanthrene-10-oxide (DOPO) as a pendant group bridged to the polymer via an -NH- group. A novel phosphonamidate co-monomer (DOPO-A-CLM) was synthesized from DOPO and *α*-amino-*ε*-caprolactam (A-CLM). This co-monomer was subsequently used in the hydrolytic polymerization with *ε*-caprolactam (CLM) in different weight ratios to prepare DOPO-NH-functionalized PA6 (PA6-xDC, x = 7, 10, and 15 wt % DOPO-A-CLM). Chemical incorporation of DOPO-A-CLM into the PA6 backbone decreased the molecular weight of the polymer from 15387 for neat PA6 to 12375, 10516 and 9316 for PA6-7DC, PA6-10DC and PA6-15DC, respectively. The DOPO-NH– pendant group accelerated start of the PA6 thermal decomposition and increased the char residues at 500 °C from 1% for PA6 to 4.6, 4.9, and 5.0% for the PA6-7DC, PA6-10DC, and PA6-15DC samples, respectively, indicating crosslinking reactions in the condensed phase. The evolved phosphorus-active species in the gas phase inhibited the PA6 depolymerization, resulting in increased thermo-oxidative stability and about a fourfold higher residue at 500 °C in the case of PA6-15DC compared to PA6. The intrinsically flame retardant PA6 filament yarns with chemically bound FR pendant group were successfully melt spun from PA6-10DC, drawn and wound on bobbin. The DOPO-NH– pendant group decreased filament flammability and inhibited flame propagation, resulting in immediate self-extinguishment after flame removal. Incorporation of DOPO-A-CLM decreased the filament tensile properties compared to the neat PA6, which correlates with the decreased polymer molecular weight.

Keywords: α-amino-*ε*-caprolactam; DOPO; Co-monomer; Polyamide 6; Filament yarn; Flame retardance

1. Introduction

The widespread use of polymeric materials has increased the demand for new, more sustainable solutions for their production. In fact, the production of plastics has accelerated to the point where 8.3 billion tons of new plastics were created by 2017, 79% of which was confined to landfills or ended up in the natural environment [1]. Considering this issue, environmental legislation, consumer concerns, and stringent waste management approaches are putting increasing pressure on polymer and polymer end-product manufacturers to consider the recyclability and sustainability of their products. The main challenges lie in the development of functional and durable polymer materials with reduced environmental impact and the possibility of implementing a circular economy strategy in their production [2–4].

Polyamide 6 (PA6) has proven to be an excellent candidate for the development of sustainable functional polymer materials. It is known as a high-performance fiber-forming industrial thermoplastic polymer belonging to aliphatic polyamides, the special group of engineering thermoplastics with excellent toughness, elasticity, abrasion resistance, and physical and chemical stability. Consequently, its wide applications include the automotive industry, the technical textile industry, the electrical and electronic industry, construction, and the packaging industry. tThe main advantage of PA6 compared to other engineering polymers is its unique chemical structure, which allows for the chemical recycling of PA6 waste to the monomer ε-caprolactam (CLM) and subsequent re-polymerization into new PA6, while retaining value and usability. This enables the design of a closed loop production process, which is the guiding principle of the sustainability concept. Due to the possibility of obtaining the monomer CLM from the conversion of lysine from biomass fermentation [5,6], PA6 has been classified as a bio-based polymer. According to the literature, the amino acid lysine obtained

by recycling biomass could be advantageously used as a renewable feedstock for the production of CLM [7,8], which is currently derived from fossil resources in petrochemical processing. The use of bio-based CLM in the production of PA6 can make an important contribution to reducing of greenhouse gas emissions and the environmental impact of petrochemical processing [9-11]. However, as the bio-renewable routes are still at an early stage of development, their commercial implementation is still a challenging scientific problem [12].

The development of synthesis reaction for ε-caprolactam from lysine [8] has opened new possibilities for the derivatization of α-amino-ε-caprolactam to produce co-monomers with moieties containing functionalities such as fluorine and benzyl [13,14]. In these studies, functionalized ε-caprolactam molecules were employed as co-monomers with CLM in the polymerization reaction at different weight/molar ratios and conditions to prepare a PA6 backbone with different side chain functionalities. Although there are also some reports on the performance of homo-polymerization of functionalized caprolactam, the resulting polymer shows a much shorter chain length and therefore poorer mechanical properties [15]. However, these studies confirm a multiple role of lysine as a precursor for the synthesis of CLM as well as of CLM-based co-monomers, enabling the development of bio-renewable synthetic routes for the preparation of PA6 co-polymers.

The preparation of functionalized PA6 materials by co-polymerization reactions is considered a practical solution to overcome the drawbacks of PA6 materials, such as their high flammability. The covalent bonding of the functional group to the PA6 structure can prevent the migration and leaching of the flame retardant (FR)from the polymer, while improving the dispersion state of the FR in the polymer matrix, thereby lowering the concentration required for an efficient FR effect. It is well known that the covalent bonding of FRs into the polymer during the polymerization reaction can make an important contribution to solving environmental and fire safety problems [4]. Indeed, the release of FRs into the environment

during the ageing process can cause environmental problems and can simultaneously decrease the FR efficiency of the polymer.

Based on the state of the art in FR polyamides, the use of organic phosphorous compounds as "green" FR alternatives is becoming greatly importance as part of efforts to replace toxic, persistent, and bio-accumulative halogenated FRs [16,17]. Among the phosphorus-based FR compounds, 9,10-dihydro-9,10-oxa-10-phosphaphenanthrene-10-oxide (DOPO) has been extensively explored, as it is known to release highly efficient radical scavenging species such as $PO^{\bullet}$ in the gas phase during its thermal decomposition [18]. Due to its excellent FR properties, DOPO is considered one of the model compounds for studying the effects of FR properties on phosphorous-based chemistry [17].

Various approaches have been conducted for the incorporation of DOPO functionality into the PA6 matrix, mostly involving the physical incorporation of DOPO by melt compounding, reactive extrusion, and the *in situ* polymerization of ε-caprolactam in the presence of DOPO [19-24] or the covalent incorporation of DOPO into the polyamide structure in co-polymerization reactions [25,26]. In this context, DOPO-functionalized dibasic acid and DOPO-functionalized diamine were used as co-monomers in combination with ε-caprolactam or with hexamethylene diamine and adipic acid to prepare polyamides with a different chemical structure. However, by incorporating dibasic acid and diamine into the main polymer chain, the unique backbone structure, characteristic of PA6, was lost. The disadvantage of this approach is that the polymer modification worsens the recyclability of the products. Therefore, to preserve the PA6 backbone and thus the recyclability of the product, the DOPO derivatization of CLM or 6-aminocaproic acid and its incorporation with ε-caprolactam in the co-polymerization reaction remains the only approach, which is still completely unexplored.

The present work aims to synthesize a novel flame retardant DOPO-NH-functionalized PA6 by incorporating the DOPO-NH– functionality as a pendant group into the PA6 backbone

structure. The main idea was to use the cyclic lysine, i.e., *α*-amino-*ε*-caprolactam (A-CLM), as a biomass resource for the one-step Atherton–Todd reaction, in which DOPO-NH-functionalized caprolactam (DOPO-A-CLM) was produced. The proposed co-monomer synthesis can be made more greener by using alternatives to standard chlorinating agents and has a high potential for implementation in an industrial setting. DOPO-A-CLM was further used as a co-monomer with CLM in the hydrolytic ring opening co-polymerization reaction to produce FR DOPO-NH-functionalized PA6 and multifilament yarn.

2. Experimental section

2.1. Materials

L-lysine hydrochloride, (L-Lys × HCl, ABCR, 99%), aluminum oxide, anhydrous (Al_2O_3, Grade I, 60 Mesh, Alfa Aesar), hexanol (Merck, 98%), 9,10-dihydro-9-oxa-10-phosphaphenanthrene-10-oxide (DOPO, ABCR, 97%), sulphuryl chloride (SO_2Cl_2, Sigma Aldrich, 97%), *N*-chlorosuccinimide (NCS, Sigma Aldrich, 98%), potassium hydroxide (KOH, Merck, pellets for analysis EMSURE), tri-ethylamine (TEA, Sigma Aldrich, 99,5%), dichloromethane (DCM, Honeywell, ≥99.8), tetrahydrofuran (THF, Honeywell, ≥99.9), acetone (Honeywell, ≥99.9), hexafluoro-isopropanol (HFIP, ABCR, 99%), and *ε*-caprolactam (CLM) was kindly supplied by L. Brüggemann GmbH & Co. KG (Heilbronn, Germany). All chemicals were used as received.

2.2. Synthesis of DOPO-NH-functionalized PA6 (PA6-xDC)

A new procedure for the synthesis DOPO-NH-functionalized PA6 (PA6-xDC) is presented in Scheme 1. As shown, the synthesis includes three main steps: (a) synthesis of *α*-amino-*ε*-caprolactam (A-CLM) from L-Lys × HCl, (b) synthesis of DOPO-functionalized *α*-amino-*ε*-caprolactam phosphonamidate (DOPO-A-CLM), and (c) synthesis of DOPO-NH-functionalized PA6 (PA6-xDC) with the incorporated co-monomer DOPO-A-CLM at different wt % ratios (x = 7, 10, and 15 wt %).

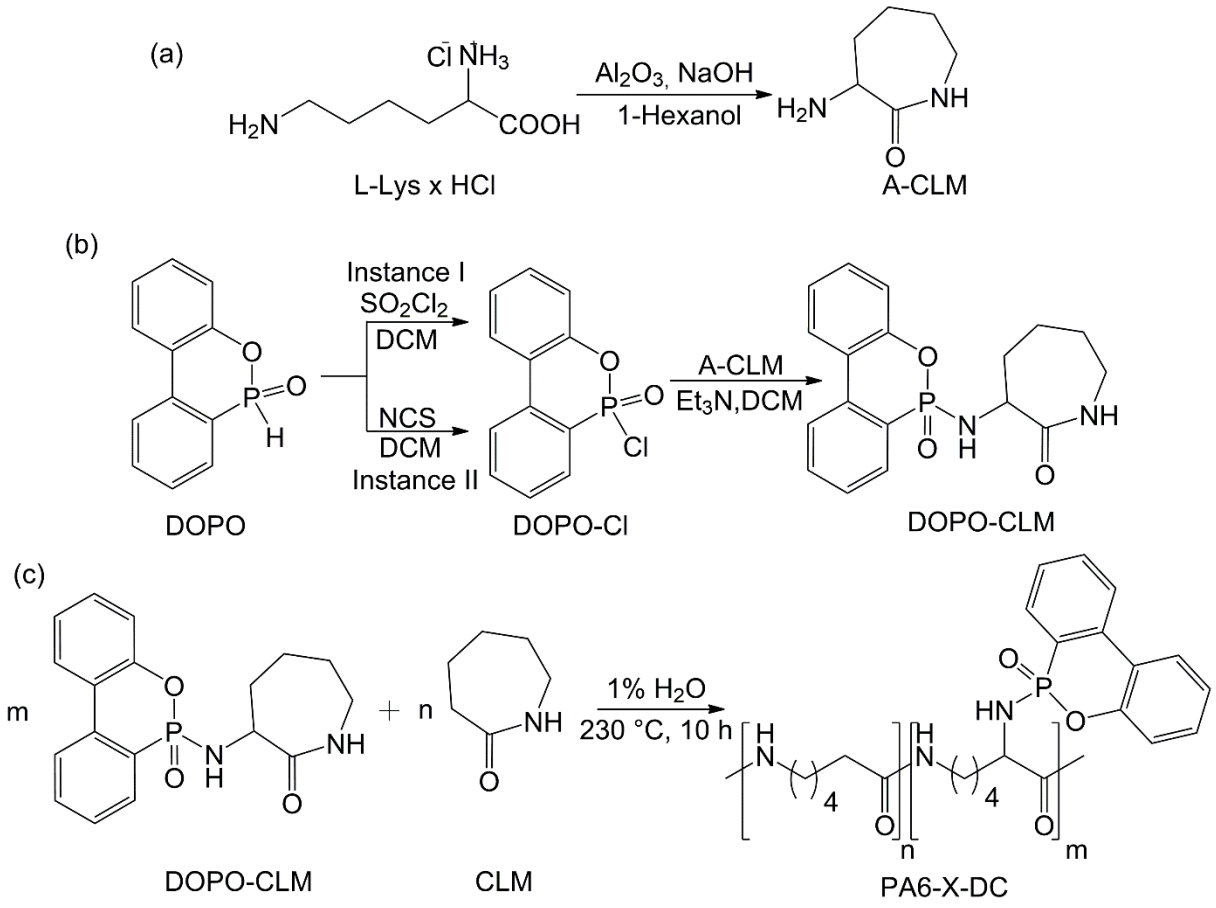

Scheme 1. (a) Synthesis of *α*-amino-*ε*-caprolactam (A-CLM). (b) Synthesis of DOPO-NH-functionalized caprolactam phosphonamidate (DOPO-A-CLM) using two different chlorinating agents, i.e., SO_2Cl_2 (Instance I) and NCS (Instance II). (c) Synthesis of DOPO-NH-functionalized PA6 (PA6-xDC; x = 7, 10, and 15 wt % DOPO-A-CLM).

a) Synthesis of α-amino-ε-caprolactam (A-CLM) according to the modified procedure [6] (Scheme 1a).

In a 10 L reaction vessel equipped with a mechanical stirrer and a nitrogen inlet, a suspension containing 0.8 mol (146.08 g) L-Lys x HCl, 0.8 mol (32 g) NaOH, and 7.2 mol (689.09 g) of Al_2O_3 was prepared in 4 L of hexanol. In a nitrogen atmosphere, the reaction mixture was vigorously stirred for 4 h under reflux (at approximately 155 °C). Afterwards, the cooled reaction mixture was filtered (removal of Al_2O_3), and the solvent evaporated under reduced pressure, which yielded a light orange resin-like substance (70% yield). The obtained A-CLM was used without further purification.

^{1}H NMR (DMSO-d$_6$, δ ppm): 7.57 (s, 1H, CON*H*), 3.41 (d, *J* = 8 Hz, 1H, COC*H*NH_2), 3.12-2.98 (m, 2H, CONHCH_2), 1.85-1.53 (m, 6H, NH_2 and ring) 1.36-1.26 (m, 1H, ring), 1.21-1.11 (m, 1H, ring).

^{1}H NMR spectrum of A-CLM is presented in the supporting information (Fig. S1).

b) Synthesis of DOPO-functionalized caprolactam phosphonamidate (DOPO-A-CLM) (Scheme 1b).

SO_2Cl_2 route (Scheme 1b, Instance I):

In a 2 L round bottom flask equipped with a magnetic stirrer, a nitrogen inlet, and a KOH trap (trapping evolved HCl and SO_2), a solution of 0.4 mol (86.48 g) DOPO in 400 mL of DCM was prepared and subsequently chilled to 0 °C, followed by a slow addition of 0.4 mol (54.24 g) SO_2Cl_2 dissolved in 200 mL of DCM (temperature in the flask did not exceed 10 °C during the addition). Afterwards, the reaction mixture was heated and refluxed for 3 h, removing HCl and SO_2 gases. The reaction mixture was chilled to 0 °C again, and two separate solutions of 0.44

mol (44.52 g) TEA in 200 mL of DCM and 0.4 mol (53.8 g) A-CLM in 200 mL of DCM were slowly added to the reaction mixture (the temperature in the flask did not exceed 10 °C during the addition). Afterwards, the reaction mixture was stirred overnight at room temperature. The solvent was removed under reduced pressure, and crude material was dissolved in THF, removing triethylamine hydrochloride by filtration. Subsequently, THF was removed under reduced pressure and the viscous residue was treated with DCM or acetone, leading to the precipitation of a white powder upon standing at 2–8 °C. The white precipitate was collected and dried, yielding 109.8 g (80%) of DOPO-A-CLM product.

NCS route (Scheme 1b, Instance II):

N-chloro succinimide, NCS (58.7 g, 0.44 mol) was gradually added at 0 °C under nitrogen to a stirred solution of DOPO (86.48 g, 0.4 mol) in 400 mL of DCM. The reaction mixture was left to warm up to ambient temperature and stirred overnight. Afterwards, it was cooled to 0 °C again, followed by dropwise addition of TEA (44.52 g, 0.44 mol) and A-CLM (53.8 g, 0.4 mol) dissolved in 200 mL of DCM. The reaction mixture was stirred overnight and then subjected to extraction with water in order to remove TEA × HCl. The solvent removal gave rise to an oily residue, which was treated with acetone or DCM to precipitate 68.6 g (50%) of a white powder product.

DOPO-A-CLM was found to be in the form of two enantiomeric pairs of diastereomers with a 1:2 ratio between Isomer I and II.

Isomer I (DS-I)

^{1}H NMR (DMSO-d$_6$, δ ppm): 8.19-8.16 (m, 2H, Ar), 8.08-8.04 (m, 1H, Ar), 7.84-7.82 (m, 1H, CON*H*CH$_2$), 7.77-7.74 (m, 1H, Ar), 7.59-7.56 (m, 1H, Ar), 7.46-7.43 (m, 1H, Ar), 7.32-2.29 (m, 2H, Ar), 5.51-5.47 (dd, J_1 = 8.5 Hz J_2 =13.5 Hz, COC*H*NH), 4.17-4.12 (m, 1H, CONHC*H*$_2$), 3.09-3.05 (m, 2H, cyclic), 1.87-1.84 (m, 2H, cyclic and COCHN*H*), 1.71-1.68 (m, 1H, cyclic), 1.57-1.51 (m, 2H, cyclic); **^{31}P NMR (DMSO-d6, δ ppm):** 13.28.

^{1}H NMR (HFIP, insert C_6D_6, δ ppm): 8.13-8.10 (m, 1H, Ar), 8.06-8.04 (m, 1H, Ar), 7.98-7.94 (m, 1H, Ar), 7.84-7.82 (m, 1H, Ar), 7.63-7.60 (m, 1H, Ar), 7.48-7.45 (m, 1H, Ar), 7.38-7.35 (m, 1H, Ar), 7.29-7.27 (m, 1H, Ar), 6.44 (m, 1H, CON*H*CH_2), 4.49 (dd, J_1 = 9 Hz, J_2 = 12, 1H, COC*H*NH), 4.19-4.14 (m, 1H, CONHC*H*), 3.27-3.22 (m, 1H, cyclic), 3.17-3.12 (m, 1H, cyclic), 1.98-1.96 (m, 2H, cyclic and COCHN*H*), 1.79-1.75 (m, 1H, cyclic), 1.68-1.62 (m, 1H, cyclic), 1.59-1.52 (m, 1H, cyclic), 1.42-1.35 (m, 1H, cyclic); **^{31}P NMR (HFIP, insert C_6D_6, δ ppm):** 19.98.

Isomer II (DS-II)

^{1}H NMR (DMSO-d_6, δ ppm): 8.21-8.18 (m, 2H, Ar), 7,89-7,87 (m, 1H, CON*H*CH_2), 7.81-7.74 (m, 2H, Ar), 7.60-7.56 (m, 1H, Ar), 7.47-7.44 (m, 1H, Ar) 7.33-7.28 (m, 2H, Ar), 5.45-5.42 (dd, J_1 = 9 Hz, J_2 = 12, 1H, COC*H*NH), 3.91-3.85 (m, 1H, CONHCH_2), 3.03-2.98 (m, 1H, CONHCH_2), 2.96-2.91 (m, 1H, cyclic), 1.99-1.96 (m, 1H, cyclic), 1.84-1.80 (m, 1H, cyclic) 1.66-1.62 (m, 1H, cyclic), 1.60-1.53 (m, 1H, cyclic), 1.47-1.39 (m, 1H, cyclic), 1.18-1.11 (m, 1H, cyclic). **^{31}P NMR (DMSO-d_6, δ ppm):** 13.29.

^{1}H NMR (HFIP, insert C_6D_6, δ ppm): 8.11-8.09 (m, 1H, Ar), 8.04-8.03 (m, 1H, Ar), 7.85-7.78 (m, 2H, Ar), 7.59-7.55 (m, 1H, Ar), 7.46-7.43 (m, 1H, Ar), 7.36-7.33 (m, 1H, Ar), 7.28-7.26 (m, 1H, Ar), 6.41-6.39 (m, 1H, CON*H*CH_2), 4.62 (dd, J_1 = 9 Hz, J_2 = 12 Hz, 1H, COC*H*NH), 3.91-3.86 (m, 1H, CONHCH_2), 3.20-3.15 (m, 1H, Cyclic), 3.02-2.97 (m, 1H, Cyclic), 2.12-2.09(m, 1H, Cyclic), 1.97-1.93 (m, 1H, Cyclic), 1.74-1.67(m, 2H, COCHN*H* and Cyclic), 1.47-1.40 (m, 1H,Cyclic), 1.38-1.30 (m, 1H,Cyclic). **^{31}P NMR (HFIP, insert C_6D_6, δ ppm):** 20.28.

^{1}H NMR and ^{31}P NMR spectra of DOPO-A-CLM, DC-I and DC-II in DMSO-d_6 and HFIP are presented in the supporting information (Figs. S2 – S11).

c) Synthesis of DOPO-NH-functionalized PA6 (PA6-xDC) with incorporated DOPO-A-CLM (Scheme 1c).

Three different compositions of PA6-xDC with incorporated DOPO-A-CLM synthesized by an NCS route at different wt % ratios (x = 7, 10 and 15 wt %), namely PA6-7DC, PA6-10DC, and PA6-15DC, were produced. Under inert conditions (glove box), 7, 10, or 15 wt % of the co-monomer DOPO-A-CLM was introduced into melted CLM (92, 89, or 84 wt %, respectively). Afterwards, 1% H_2O was introduced outside the glove box, and the reaction mixture was homogenized. In the hermetically sealed autoclave, the reaction mixture was left to react for 10 h at 230 °C. The obtained co-polymers were crunched and refluxed for 24 h, first in water and then in DCM, to remove unreacted reagents and water-soluble oligomers, and then dried in an oven overnight at 90 °C under vacuum before any further analysis. Gravimetrically calculated yield ranged between 85 and 88%.

^{1}H-NMR of 10DC-PA6 (HFIP/benzene-d_6, δ ppm): 8.08-8.04 (m, 2H, Ar), 7.94-7.90 (m, 1H, Ar), 7,77-7.75 (m, 1 H), 7,59-7.56 (m, 1H, Ar), 7.48-7.45 (m, 1H, Ar), 7.37-7.26 (m, 1H, Ar), 6.70-6.67 (m, 1H, CON*H*CH_2-DOPO), 6.38-6.36 (m, 25H (1H),CON*H*CH_2-CL), 3.35-3.31 (m, 50H (2H), chain-CL), 2.34-2.32 (m, 50H (2H), chain-CL), 1.74-1.69 (m, 50H (2H), chain-CL), 1.67-1.62 (m, 50H (2H), chain-CL), 1.47-1.43 (m, 50H (2H), chain-CL).

^{1}H NMR spectrum of PA6-10DC sample is presented in the supporting information (Fig. S12).

d) Synthesis of PA6

PA6 was produced under identical conditions as PA6-xDC. Inside the glove box, the reactor's Teflon insert containing 0.875 mol (99 g) CLM was heated until melting; then, 1 wt % (1 g, 5.56 mmol) water was added into the melt outside the glove box. After homogenization, the

Teflon insert was placed in the autoclave and hermetically sealed. Reaction continued in the oven for 10 h at 230 °C. The obtained product was crunched, refluxed in water for 24 h, filtered, and dried overnight in the oven at 90 °C under vacuum; the final yield was 87%.

^{1}H NMR (HFIP, insert C_6D_6, δ ppm): 6.38 (s, 1H, CON*H*CH_2), 3.38 (m, 2H, CONHC*H*$_2$), 2.35 (m, 2H, chain), 1.7 (m, 4H, chain), 1.46 (m, 2H, chain).

^{1}H NMR spectrum of PA6 is presented in the supporting information (Fig. S13).

2.3. Production of filament yarns by melt-spinning

PA6 and PA6-10DC filament yarns, coded as PA6(f) and PA6-10DC(f), were produced using a laboratory-scale melt-spinning and drawing device (Extrusion System Ltd, Bradford, Great Britain). PA6-15DC(f) filament yarns were not produced due to the poor spinnability with respect to the used melt-spinning process conditions. PA6 and PA6-10DC polymer samples were ground into granules (size: 1-3 mm) and fed into the extruder. The temperature of the extruder (three zones), the metering pump, and the spin pack (two zones) was set at 220 °C for the melt-spinning of PA6(f). In the case of the melt spinning of PA6-10DC(f), the temperature of the extruder was set at 200 °C, and the temperatures of the metering pump and spin pack were set at 190 °C. The extruder screw speed was 3 rpm. The spinneret for multifilament spinning had 10 holes with diameters of 0.35 mm. The extruded filaments were quenched in air at room temperature and were wound using a winder operating at 80 m min^{-1}.

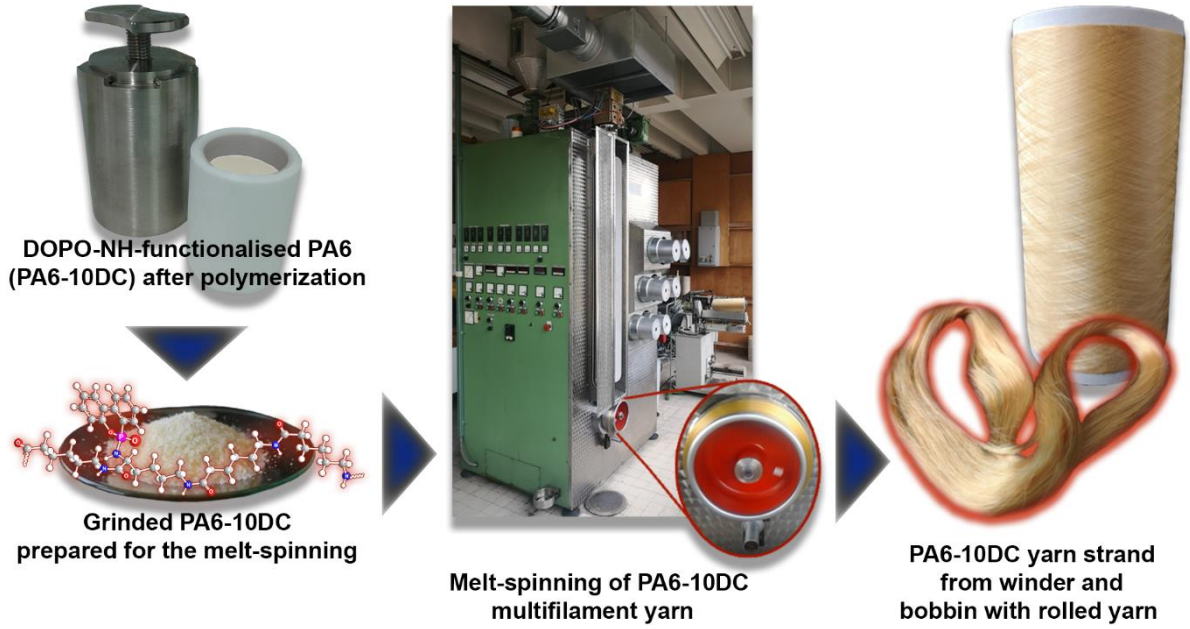

Fig. 1. Illustration of the fabrication process.

2.4. Characterization

^{1}H and ^{31}P NMR spectra were recorded on a Bruker AVANCE NEO 600 MHz NMR or on a Varian 300 MHz NMR Unity INOVA. Samples were prepared in deuterated dimethyl sulfoxide (dmso-d6) with tetramethylsilane (TMS) as an internal standard (δ TMS = 0.0 ppm) and/or in HFIP (hexafluoroisopropanol) with deuterated benzene (C_6D_6) as an internal standard. ^{31}P was calibrated relative to the signal of 85% H_3PO_4.

Ubbelohde viscometer of size 0a was used in order to measure relative viscosity of three polymer solutions with nominal concentrations of 0.01%, 0.05% and 0.09%. Sample solutions were prepared in 85% COOH and measured at 25.0 °C. Huggins (Eq. 1), Kreamer (Eq. 2) and Solomon-Ciuta (Eq. 3) equations were used to evaluate intrinsic viscosities of samples. The obtained intrinsic viscosities were used in Mark–Houwink-Sakurada (Eq. 4) equation to give

molecular weights named as $M_{Huggins}$, $M_{Kreamer}$ and $M_{Solomon\text{-}Ciuta}$ ($M_{Solomon\text{-}Ciuta}$ represents average molecular weight determined from the three used sample concentrations).

$$\frac{\eta_{sp}}{c} = [\eta] + k_2[\eta]^2 c \quad \text{(Eq. 1)}$$

$$\frac{\ln \eta_{rel}}{c} = [\eta] + k_1[\eta]^2 c \quad \text{(Eq. 2)}$$

$$[\eta] = \frac{\left[2\cdot(\eta_{sp} - \ln \eta_{rel})\right]^{1/2}}{c} \quad \text{(Eq. 3)}$$

$$[\eta] = K\mathrm{M}^{\alpha} \quad \text{(Eq. 4)}$$

In the equations, $[\eta]$ represents intrinsic viscosity (dL/g), η_{sp} specific viscosity (/), η_{rel} relative viscosity (/), c is solution concentration (g/dL), K is Mark–Houwink-Sakurada constant (0.000226 dL × mol/g^2) and α is scalar equal to 0.82 and related to stiffness of polymer chains in solvent. Relative viscosities and actual concentrations of sample solutions are presented in the supporting material (Table S1, Figures S16-S18).

Differential scanning calorimetry (DSC) was employed for measuring the melting (T_m) and crystallization (T_c) temperatures using a Mettler Toledo (CH) DSC1 instrument operating from 25 to 230 °C (or just above T_m of each sample) with heating and cooling rates of 10 °C/min in a nitrogen atmosphere (30 mL/min flow rate) and using aluminum-standard 40 µL crucibles with a pierced lid. The second heating runs were analyzed to determine the melting temperatures of each sample.

Thermogravimetric (TG) analyses of 10 mg samples in either air or nitrogen atmosphere at a gas flow rate of 50 mL/min were performed with a Mettler Toledo (CH) TGA/DSC1 Thermogravimetric Analyser from 25 to 800° C with a heating rate of 10 °C/min in open 150 µL platinum pans. Blank curves were subtracted for all measurements. Alternatively, TGA (SDT 2960, TA Instruments) was coupled with infrared spectroscopy (Nicolet iS10 by Thermo-Scientific); these analyses were carried out in a nitrogen atmosphere.

Scanning electron microscopy (SEM) and energy-dispersive X-ray spectroscopy (EDS) were performed on an SEM Cambridge 360 microscope equipped with an energy dispersive X-

ray spectrometer (EDS) INCA 250. The samples were coated with a Cr layer in order to make them electrically conductive.

The tensile properties of the PA6(f) and PA6-10DC(f) multifilament yarns were tested on an Instron 5567 dynamometer in accordance with SIST ISO 2062:1997. For this purpose, the PA6(f) and PA6-10DC(f) multifilament yarns were wound onto bobbins at a 132 and 156 m min^{-1} speed, respectively, wherein they were partially drowned. The method was adjusted so that the gauge length was 100 mm and the deformation rate was 350 m min^{-1}. The linear densities of the partially oriented PA6 and PA6-10DC filament yarns were 386 and 481 dtex, respectively.

The standard vertical flame spread test (ASTM D6413) was performed on fiber strand samples (approximately 12.5 cm long, 1.5 cm wide, and 1.2 cm thick), which were prepared by twisting several filaments together.

Cone calorimetry (Fire Testing Technology, FTT) tests were performed using knitted fabric samples (100 cm × 100 cm) under an irradiative heat flux of 35 kW m^{-2} in horizontal configuration. The fabrics were placed in a sample holder and maintained in the correct configuration by a metallic grid. Time to ignition (TTI), heat release rate (HRR), total heat release (THR), peak of HRR (PHRR), and effective heat of combustion (EHC) were measured. Total smoke release (TSR), the average specific extinction area (SEA), CO, and CO_2 yield ([CO] and [CO_2]) were also evaluated.PA6(f) and PA6-10DC(f) knitted fabric samples with a right–right structure were prepared from the filament yarns wound on bobbin on a hand knitting machine RIMACH operating with 10-gauge needles. For each sample, three multifilament yarns were used for knitting.

3. Results and discussion

3.1. Synthesis strategy of DOPO-A-CLM and PA6-xDC

In this research, a unique approach for the synthesis of flame retardant DOPO-NH-functionalized PA6 (PA6-xDC) is presented. For this purpose, the DOPO-functionalized α-amino-ε-caprolactam molecule (DOPO-A-CLM) was first synthesized and used as a co-monomer with CLM in the polymerization process, since DOPO-A-CLM is compatible with the nature of CLM and its polymerization conditions. As the name of the DOPO-A-CLM molecule suggests, it consists of two structural parts, DOPO and CLM, and the bond between them is established by phosphonamidate bonding.

The DOPO-A-CLM molecule was prepared by reaction of A-CLM with DOPO species. Initially, A-CLM was prepared by converting L-lysine into A-CLM through an intermolecular condensation/cyclization reaction (Scheme 1a) [6]. Since the reaction in butanol at 155 °C in the presence of Al_2O_3 favors an intramolecular over an intermolecular condensation reaction, the reaction preferentially leads to cyclic amide A-CLM over oligomeric or polymeric polyamide linear structures. The use of Al_2O_3 as an efficient water absorber is crucial for achieving a high degree of conversion and a high-yield reaction process (70% isolation yield). The applied synthesis approach for the preparation of A-CLM is classified as green and renewable, since the main component L-lysine is one of the essential amino acids abundant in nature (animal and plant organisms) [27]. Industrial lysine is mainly produced by microbiological fermentation of sugary feeds, and current research is focused on increasing the conversion yield [28]. Butanol, which is used as a solvent in this process, is considered an environmentally friendly and potentially bio-based material [29,30].

The functionalization of A-CLM with DOPO was carried out by the Atherton–Todd reaction under two different synthesis conditions (Scheme 1b). In the first case, SO_2Cl_2 was used as chlorinating agent. However, the release and capture of SO_2 gas as a by-product of the

chlorination reaction poses a financial and possibly an environmental risk in industrial-scale synthesis. To circumvent the aforementioned risk, a second synthesis approach using *N*-chlorosuccinimide (NCS) as a chlorinating agent was used as an alternative, which is more environmentally friendly and greener than SO_2Cl_2 [31]. Moreover, the by-product after the reaction is succinimide, which can be regenerated to NCS. Although in this latter approach the reaction yield was reduced to 50%, adjusting the reaction conditions allowed for an increase in the reaction yield. Nevertheless, this new approach proved the possibility of using NCS as a more environmentally friendly alternative to the chlorinating agent in DOPO-A-CLM synthesis with additional potential for cost savings, as the SO_2 capture and conversion technology is not required.

3.2. Characterization of DOPO-A-CLM

3.2.1. NMR characterization of DOPO-A-CLM

The successful synthesis of DOPO-A-CLM was confirmed by ^{1}H and ^{31}P NMR analyses. The comparison of the ^{1}H spectra of DOPO-A-CLM and the initial compound A-CLM (Fig. 2) reveals significant differences in the molecular structure of these two molecules. The major difference is the presence of aromatic signals in DOPO-A-CLM, corresponding to DOPO functionalization (marked as Ar in Fig. 2). The second obvious and important difference includes the chemical shift and the change in multiplicity for the proton bound to the alpha carbon (marked with number 2 in Fig. 2). The signal shifted from 3.55 in A-CLM to 5.50 ppm in DOPO-A-CLM, while the multiplicity changed from *d* to *dd*, indicating the presence of the second coupling center with ½ spin, such as ^{31}P. All the changes observed in ^{1}H NMR are logical consequences of successful chemical bond formation between P and N atoms of DOPO-

Cl and A-CLM molecules. The presence of ^{31}P was further confirmed by the ^{31}P NMR spectrum shown in Fig. S3.

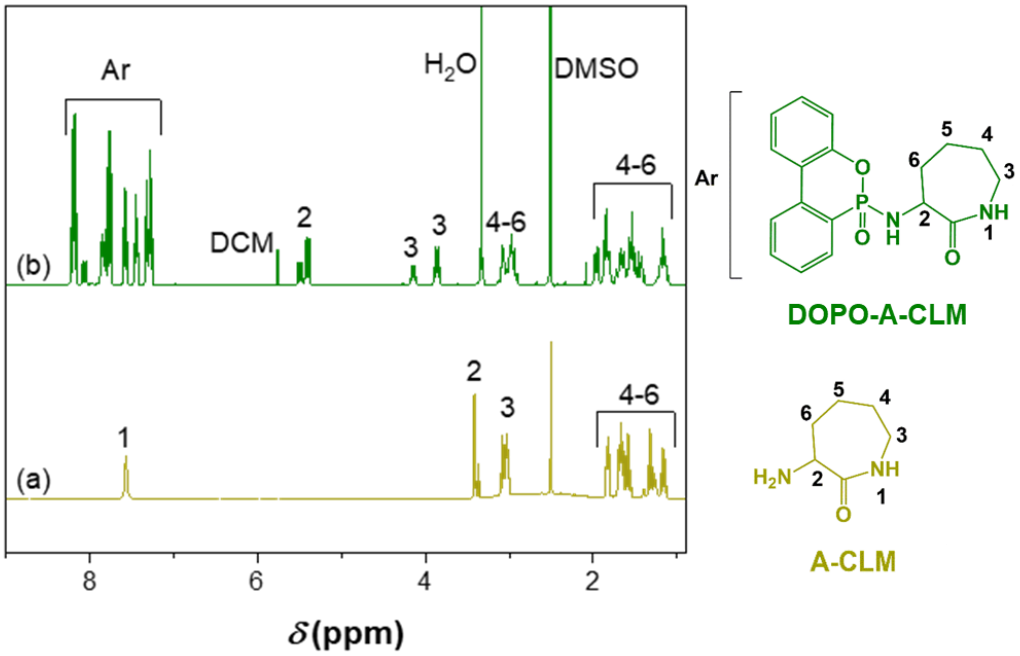

Fig. 2. ^{1}H NMR spectra of A-CLM (a) and DOPO-A-CLM (b).

A closer examination of the ^{1}H NMR (Fig. 3) and ^{31}P NMR (Fig. S3) spectra revealed that DOPO-A-CLM consists of two diastereomeric species, identified as DS-I and DS-II (Fig. 4). The diastereomeric mixture is a consequence of the two chiral centers in the DOPO-A-CLM molecule, the first originating from the A-CLM molecule (alpha positioned C atom next to the carbonyl group) and the second originating from the DOPO molecule (phosphorous atom). Considering that the lysine used as the initial reactant for the preparation of A-CLM was natural L-Lysine, its S_C configuration was retained in the synthesized A-CLM product. On the other hand, the phosphorous atom introduced by the DOPO bond was racemic (50:50 *RP*/*SP* configuration), which accounted for the appearance of diastereomeric compounds classified as R_PSc and S_PSc (Fig. 4). The obtained diastereomeric products were further selectively crystallized and characterized by ^{1}H and ^{31}P and DSC analysis. Although the absolute

configuration of the diastereomers was not determined, their characteristic differences can be identified and described.

Though the differences between the diastereomers found in the ^{1}H NMR spectrum were quite significant (Fig. 3), there are some signals that stand out more than the others and could be classified as characteristic signals for the two diastereomers. In particular in the aromatic region at 8.06 ppm (1 in Fig. 3), the characteristic (isolated) multiple signal integrated for 1 proton and belonging to DS-I can be seen. Furthermore, signals representing the proton bound to α-C related to the CO group in the ε-caprolactam ring were found close to each other at 5.49 and 5.43 ppm (2 and 2' in Fig. 3) for DS-I and DS-II, respectively. The signals in the two diastereomers belonging to the proton bound on δ-C, which is attached to the amide group of the ε-caprolactam ring, exhibited significantly different chemical shifts; the signals at 4.15 and 3.88 ppm (3 and 3' in Fig. 3) correspond to DS-I and DS-II, respectively. The signals at 1.97 and 1.43 ppm, attributable to some of the aliphatic protons of the ε-caprolactam ring, appeared to be isolated and therefore characteristic of DS-II (4' and 5' in Fig. 3). Although many of the signals appear to be characteristic of individual diastereomers, only those at 4.15 and 3.88 ppm (3 and 3' in Fig. 3) provide reliable integration in the case of DS-mix, where one of the diastereomers is present in significant excess relative to the other. The quantitative evaluation of the ^{1}H NMR signals corresponding to DS-I also revealed the traces of DS-II with a DS-I/DS-II ratio equal to 93:7.

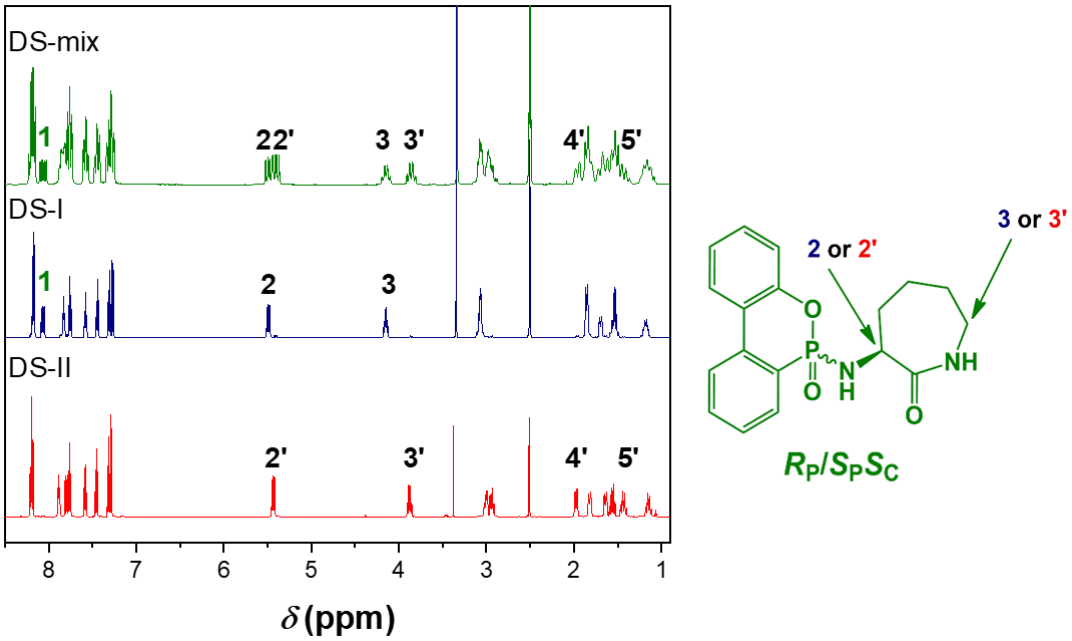

Fig. 3. ^{1}H NMR spectra of DOPO-A-CLM diastereomers DS-I, DS-II, and their 50:50 mixture, DS-mix.

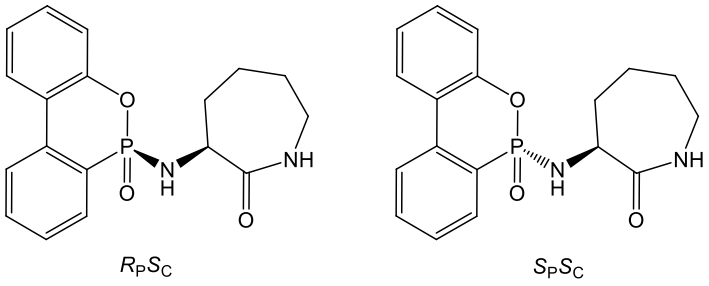

Fig. 4. Two possible diastereomers of DOPO-A-CLM.

3.2.2. DSC characterization of DOPO-A-CLM

Based on DSC analysis (Fig. 5), CLM was found to have the lowest melting point (72 °C), while the highest melting point was observed in the case of DS-II (190 °C), which is significantly higher compared to DS-I (melting point of 123 °C). Interestingly, in the case of a 50:50 mixture of DS-I and DS-II (DS-mix in Fig. 5), there is virtually no detectable endothermic peak that corresponds to the melting of the mixture. The reason for the above phenomena is

probably due to the amorphous nature of DS-mix. Amorphous substances normally become completely liquid over a wider temperature range and are therefore not detected as an endothermic effect by the DSC instrument. Due to this significant difference between the DSs, it is evident that DSC analysis is much more sensitive to the impurity profile than NMR. The observed additional melting peak in the case of DS-I, which occurs at 133 °C, can be attributed to impurities, e.g., traces of DS-II, affecting the melting behavior of the pure DS-I compound. This is consistent with the results of ^{1}H NMR analysis discussed earlier.

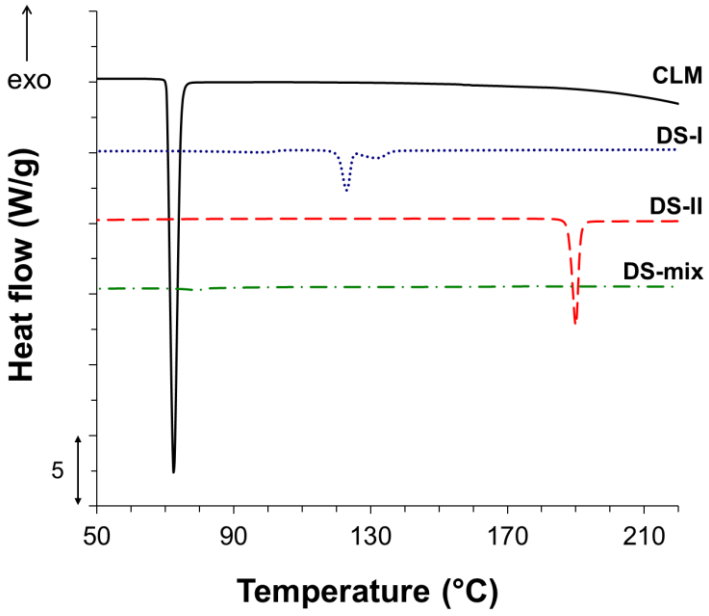

Fig. 5. DSC curves of ε-caprolactam (CLM), DOPO-A-CLM diastereomers DS-I, DS-II, and their 50:50 mixture, DS-mix.

3.3. Characterization of DOPO-NH-functionalized PA6 (PA6-xDC)

3.3.1. NMR characterization of PA6-xDC

The structure of DOPO-NH-functionalized PA6 was confirmed by ^{1}H NMR spectroscopy (Fig. 6), where the presence of signals of aromatic protons indicated the

chemically bound DOPO as a pendant group of the PA6 backbone. The presence of aliphatic proton signals confirmed the opening of the ε-caprolactam ring in the DOPO-A-CLM, while ^{1}H NMR signals of the DOPO-A-CLM molecule were not detected, mainly due to the large molar difference between the monomers used in the co-polymerization reaction (CLM/DOPO-A-CLM was 27:1 in the case of PA6-10DC). Therefore, the aliphatic signals are probably hidden by those belonging to the opened form of CLM.

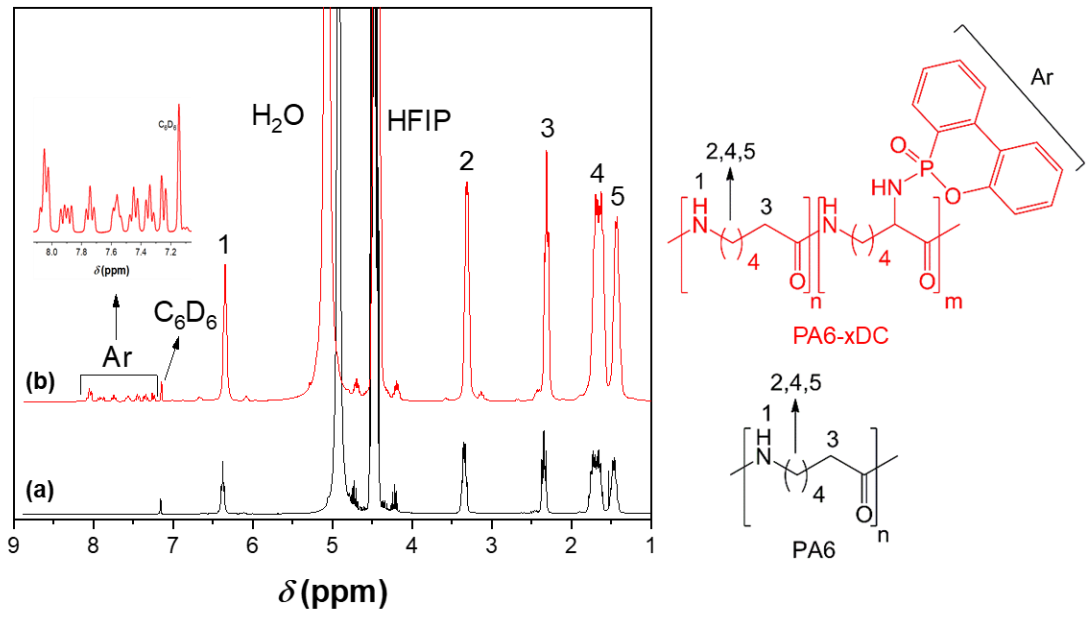

Fig. 6. ^{1}H NMR spectra of PA6 (a) and PA6-10DC (b).

Quantitative analysis of the ^{1}H NMR signals allowed determination of the molar ratio of the DOPO-A-CLM incorporated into the backbone of PA6-xDC (Table 1) based on the aromatic signals (Fig. 6b). The results show that the weight fraction of the incorporated DOPO-A-CLM was slightly higher than the added weight fraction, which was a consequence of the PA6-xDC purification process in water and DCM. Namely, the purification process allowed the removal of unreacted DOPO-A-CLM as well as of the water-soluble CLM-based oligomers.

Obviously, this extraction process slightly increased the concentration of the chemically bound DOPO group, mainly due to the complete extraction of unreacted CLM. The fact that even after the extensive extraction of the samples, the DOPO concentration in the sample remained high proves that the DOPO functionality is chemically bound into the PA6 backbone. Furthermore, this indicates that the DOPO is evenly distributed throughout the PA6 matrix, otherwise a lower level of DOPO functionality would be expected in the final sample due to the leaching of smaller fragments.

The chemical incorporation of the DOPO functionality into the PA6 backbone affected the molecular weight, M_{mean}, of the samples, which gradually decreased from neat PA6 towards PA6-15DC (Table 1, Table S2, Fig. S19). This suggests that the integration of DOPO-A-CLM into the PA6 matrix hindered the chain growth of PA6 backbones.

Table 1. Amounts of added and chemically incorporated DOPO-A-CLM, CLM/DOPO-A-CLM molar rations in different samples of PA6-xDC and the mean value of molecular weight, M_{mean}, calculated form $M_{Huggins}$, $M_{Kreamer}$ and $M_{Solomon-Ciuta}$ (Table S2).

Sample	**DOPO-A-CLM added (wt %)**	**Reaction yield (%)**	**DOPO-A-CLM incorporated (wt %)**	**CLM/ DOPO-A-CLM (molar ratio)**	**M_{mean} (g/mol)**
PA6	0	88	0	100	15387
PA6-7DC	7	88	7.56	40.5	12375
PA6-10DC	10	88	11.40	27.2	10516
PA6-15DC	15	85	16.28	15.9	9316

3.3.2. DSC and TGA characterization of PA6-xDC

A comparison of thermal properties between PA6-xDC and pure PA6 was investigated using DSC and TGA (Figs. 7-10, Tables 2-5). The DSC curves are shown in Fig. 7, and the results for the characteristic melting, T_m, and crystallization, T_c, temperatures, and the degree of crystallinity, *Xc*, are summarized in Table 2. The endothermic melting peaks from the second heating runs corresponding to the melting of the original crystallites of the PA6, PA6-7DC, PA6-10DC, and PA6-15DC samples appeared at 222, 212, 208, and 200 °C, respectively. This trend suggests hindered hydrogen bonding between the PA6 backbones caused by the bulky DOPO-NH– pendant group, which, being chemically bonded to the PA6 backbones, may affect their linear alignment required for the hydrogen bonding and the crystalline phase formation. The second melting peak, which occurred at 215, 206, 201, and 193 °C for the PA6, PA6-7DC, PA6-10DC, and PA6-15DC samples, respectively, was caused by the non-isothermal recrystallization in the DSC analyses and can be attributed to both the γ-crystalline phase and α-crystallites of different sizes and perfection. As the chemically bonded DOPO-NH– pendant group affected the packing of the PA6 backbones, T_m and X_c also decreased as the concentration of the incorporated DOPO-A-CLM increased.

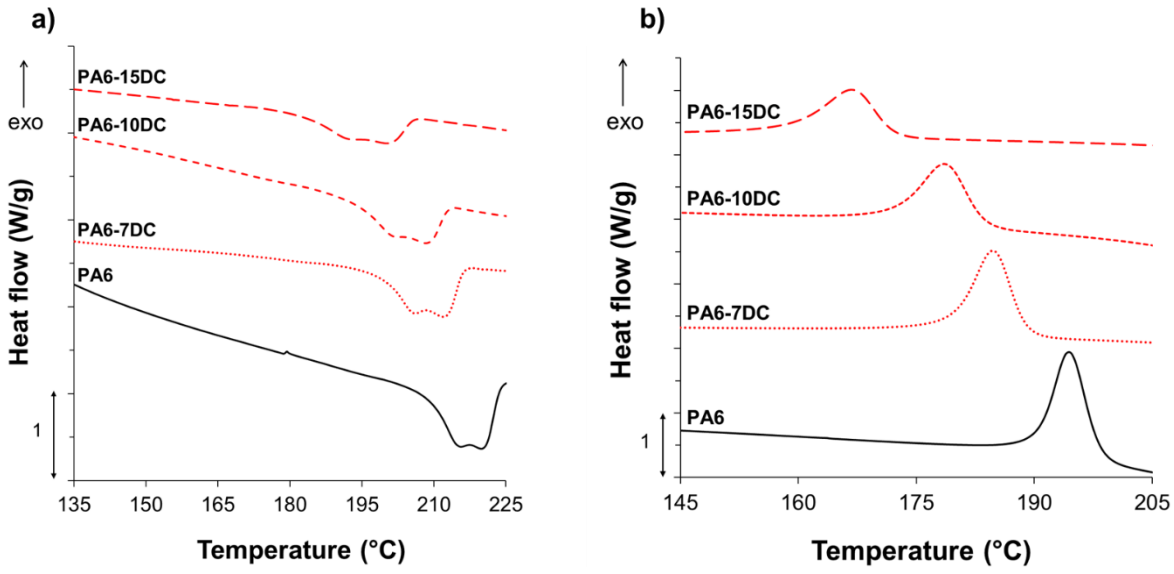

Fig. 7. DSC curves in nitrogen: (a) the second heating run; (b) the first cooling run.

Table 2. Melting temperature, T_m, enthalpy, ΔH_m, crystallization temperature, T_c, and the degree of crystallinity, X_c, of PA6 and PA6-xDC in nitrogen.

Sample	T_m (°C)	ΔH_m (J/g)	T_c (°C)	X_c (%)
PA6	215 / 222	-56.08	196	29.4
PA6-7DC	206 / 212	-46.29	185	28.5
PA6-10DC	201 / 208	-41.99	179	25.9
PA6-15DC	193 / 200	-31.32	167	19.8

To gain insight into the effect of the DOPO-NH– pendant group chemically bonded to the PA6 backbone on the thermal stability of the polymer, the thermal decomposition process of the DOPO-A-CLM, PA6, PA6-7DC, PA6-10DC and PA6-15DC samples were investigated by TGA in a nitrogen atmosphere (Fig. 8 and Table 3). The results showed that the thermal decomposition of DOPO-A-CLM started at about 279 °C (the temperature at 5% weight loss, $T_{5\%}$) and proceeded through two decomposition steps. The second decomposition step on the DOPO-A-CLM thermogravimetric curve, where 69.9% weight loss occurred, was considered as the main decomposition step with the temperature of the maximum of the weight loss rate (T_{max1}) of 417 °C. This step was preceded by an initial decomposition step with the temperature of the maximum of the weight loss rate of 297 °C and the weight loss of 9.1%. Considering that the temperature of the maximum in the weight loss rate for ε-caprolactam is about 120 °C [32] and that ε-caprolactam decomposes without residue, the bridging of DOPO and ε-caprolactam with the –NH– group significantly increased the thermal stability of ε-caprolactam. This finding also confirmed the successful functionalization of the ε-caprolactam ring. It can be assumed that the cleavage of the C–N in the bridge between the ε-caprolactam and DOPO-NH– group

ring occurs concurrently with the cleavage of the peptide C(O)–NH bond or the alkyl-amide NH–CH_2 bond. Since the weight loss during the decomposition step, which preceded T_{max1}, was equal to 9.1%, it can be assumed that some low-molecular-weight gaseous products were formed during this step. However, the chemical interactions occurring between the decomposition products increased the thermal stability of DOPO, as the initial decomposition temperature of DOPO alone is at about 237 °C [18]. Further interactions between the decomposition products formed during the thermal decomposition apparently induce some crosslinking reactions, as the residue fraction of about 10% remains stable in the temperature range from 500 to 800 °C. Since the initial decomposition temperature of DOPO-A-CLM is 279 °C, it can be suggested that this co-monomer could be safely processed at temperatures up to, for example, 260 °C.

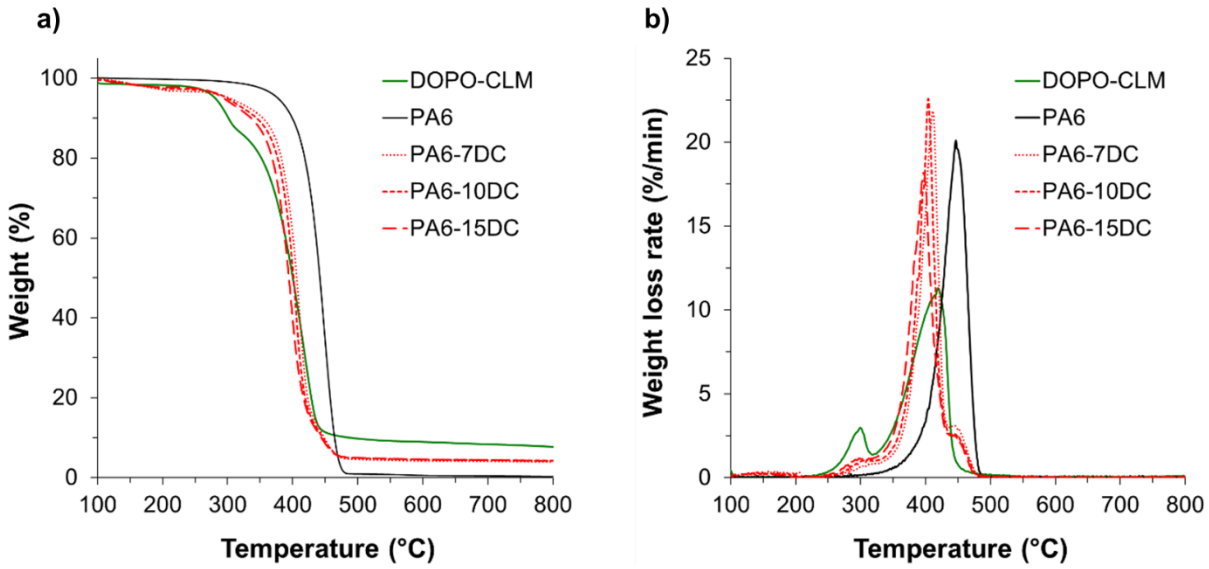

Fig. 8. (a) TG and (b) dTG graphs of DOPO-A-CLM, PA6, PA6-7DC, PA6-10DC, and PA6-15DC analyzed in a nitrogen atmosphere.

Table 3. TG data obtained in a nitrogen atmosphere.

Sample	$T_{5\%}$ (°C)	T_{max1} (°C)	Residue at T_{max1} (%)	T_{max2} (°C)	Residue at T_{max2} (%)	Residue at 500 °C (%)
DOPO-A-CLM	279	417*	30.1	-	-	9.8
PA6	379	449	40.5	-	-	1.0
PA6-7DC	303	412	39.8	448	10.7	4.6
PA6-10DC	301	405	43.8	447	10.3	4.9
PA6-15DC	295	399	44.8	448	9.7	5.0

* In the case of DOPO-A-CLM, this step was preceded by the initial decomposition step at 297 °C.

While the decomposition of PA6 under a nitrogen atmosphere is a one-step process, the thermal decomposition of PA6-7DC, PA6-10DC, and PA6-15DC samples was characterized by two decomposition steps, T_{max1} and T_{max2}. Chemical bonding of the DOPO-NH– pendant group to the PA6 backbone shifted $T_{5\%}$ and T_{max1} of the PA6-7DC, PA6-10DC, and PA6-15DC samples toward lower temperatures compared to those of the PA6 sample by 76, 78, and 84 °C, respectively, for $T_{5\%}$ and by 37, 44, and 50 °C, respectively, for T_{max1} (Fig. 8 and Table 3). This phenomenon intensified when the concentration of the incorporated DOPO-A-CLM was increased. The decrease in $T_{5\%}$ and T_{max1} could be attributed to the accelerated start of the thermal decomposition of PA6 due to the decomposition of organophosphorus group, as already reported in the literature [19,33] with respect to the MW of the studied polymers. Since the dTG curves of the PA6-7DC, PA6-10DC, and PA6-15DC samples also show shoulder at about 300 °C, as in the case of DOPO-A-CLM (Fig. 9b), it can be assumed that thermal decomposition of the PA6-7DC, PA6-10DC, and PA6-15DC samples is initiated with the cleavage between the DOPO-NH– group and the PA6 backbone. From the heat flow rates, which were measured

simultaneously with the weight change during thermal decomposition (Fig. S14), it can be concluded that DOPO-A-CLM decomposes exothermically, indicating the exothermic cleavage of the C–N in the bridge between the PA6 backbone and the DOPO-NH– group. This could also promote the start of the thermal decomposition of PA6-7DC, PA6-10DC, and PA6-15DC at a lower temperature compared with that of PA6.

Furthermore, the occurrence of the second decomposition step, T_{max2}, in the temperature range 447-448 °C for samples PA6-7DC, PA6-10DC, and PA6-15DC may coincide with T_{max1} of PA6. This phenomenon could be explained by a partial block structure in the PA6-7DC, PA6-10DC, and PA6-15DC polymers [34]. Moreover, the increase in char residues at 500 °C from 1% for PA6 to 4.6, 4.9, and 5.0% for the PA6-7DC, PA6-10DC, and PA6-15DC samples, respectively, suggests that the DOPO-NH– pendant functionality promotes the crosslinking reactions in the condensed phase of the polymer during the main decomposition step.

To further understand the decomposition pathway, an investigation of the gaseous products of the thermal decomposition of PA6 and PA6-10DC was carried out using TG-FTIR. The evaluated results for the gaseous products formed are shown in Fig. 9, while the assignments of the detected FTIR bands are collected in Table 4. The decomposition of PA6 in a nitrogen atmosphere was followed by the generation of ε-caprolactam, NH_3, CO, CO_2, and H_2O, as well as primary aliphatic amines and hydrocarbons, and carboxylic acid monomer (Fig. 9a and Table 4). These products were confirmed in the spectra collected at $T_{5\%}$, T_{max1}, and 500 °C. Spectra corresponding to the PA6-10DC sample showed significantly reduced band intensities (2400–2266 cm^{-1}, 668 cm^{-1}) in the case of CO_2 emission compared to PA6. The source of the CO_2 emission bands is probably the decarboxylation reaction of the acidic ends that occurs during the hydrolytic cleavage of the peptide C(O)–NH bonds [34]. Therefore, it can be assumed the cleavage of the peptide C(O)–NH bonds and, thus, the depolymerization of the PA6 backbone was inhibited during the thermal decomposition of the PA6-10DC sample in

comparison to that of PA6. This was confirmed by the disappearance of the band at 1761 cm^{-1} in the spectra of the PA6-10DC sample recorded at $T_{5\%}$, T_{max1}, and 500 °C, where the band at 1761 cm^{-1} represents the C=O stretching vibration belonging to the carboxylic acid monomer. Additional bands at 1234, 1219, 1095, and 753 cm^{-1}, which appeared in the spectra of PA6-10DC at 500 °C, are assigned to the phosphorus compounds (Table 4), confirming the existence of the phosphorus-active species in the gas phase. Moreover, the time-evolution profiles for the total absorption intensity and the intensity of the peaks characteristic of ε-caprolactam and ammonium (Fig. 9b,c,d) confirmed that the DOPO-NH– pendant functionality initiated the release of the gaseous products of the decomposed PA6 at lower temperatures with respect to PA6.

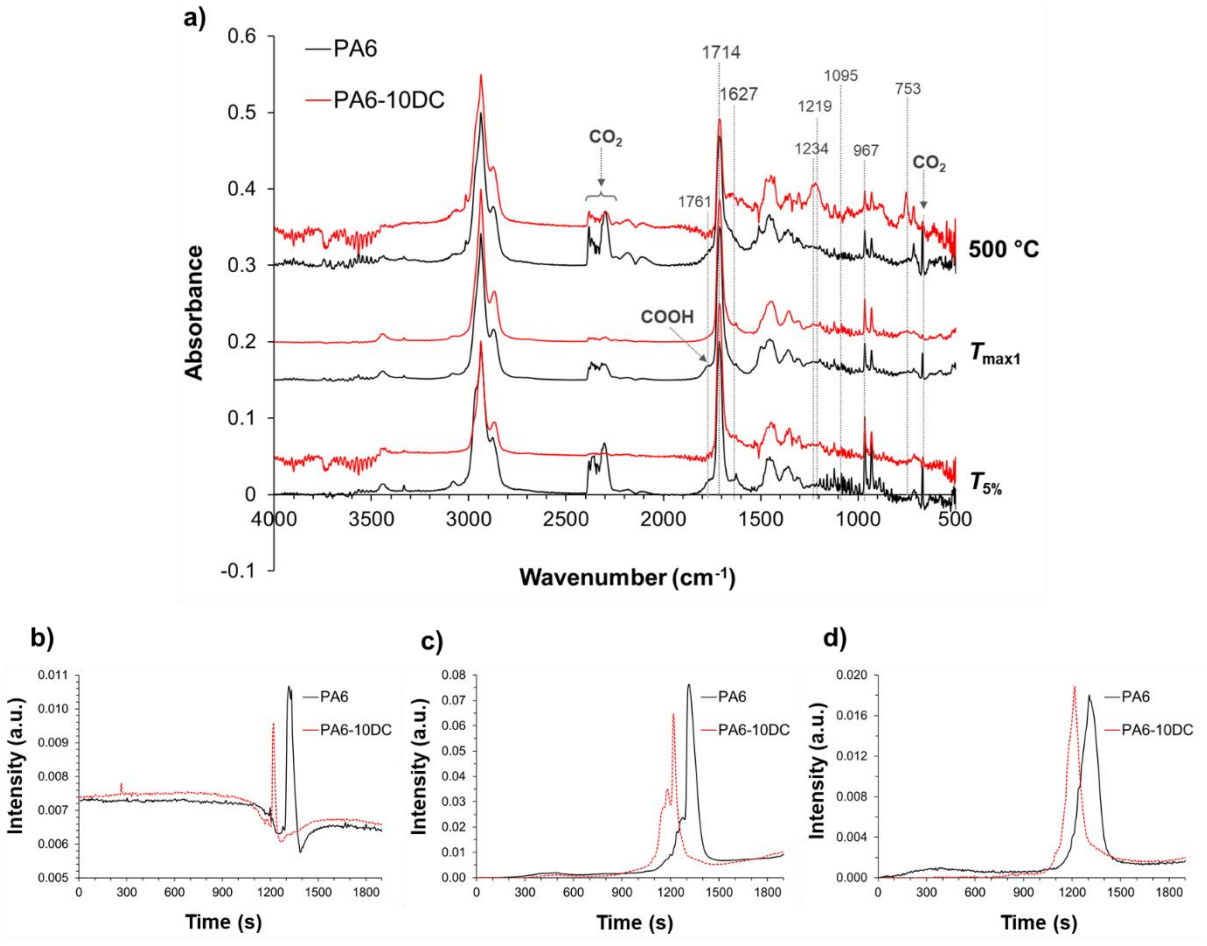

Fig. 9. (a) FTIR spectra of the evolved gases during the thermal decomposition of the PA6 and PA6-10DC at $T_{5\%}$, T_{max1}, and 500 °C; (b) the total absorbance intensity calculated as the root mean square (RMS) plotted as as a function of decomposition time; (c) intensity of the band at 1714 cm^{-1} representing the ε-caprolactam peak plotted as a function of decomposition time; (d) intensity of the band at 967 cm^{-1} representing ammonium peak plotted as a function of decomposition time.

Table 4. FTIR peak assignment [35,36].

Wavenumber (cm^{-1})	Vibration assignment	Functional group or compound
3441, 3332	amine N-H stretching vibrations	Primary aliphatic amines
2938, 2873	CH_2 stretching vibrations	ε-caprolactam
1713	C=O stretching vibration in the CONH group (Amide I)	
2400 – 2266, 668	CO_2 asymmetric stretching and bending vibrations	CO_2
2185, 2107	CO stretching vibration, doublet	CO
1761	C=O stretching vibration band in the COOH	Carboxylic acid monomer
1470-1360	C-H deformation vibrations	Hydrocarbons
964, 930	NH_3 bending vibrations	NH_3
753	P-C stretching vibration	Organic phosphorus
1095	P-O stretching vibration	Organic phosphorus
1219, 1234	P=O stretching vibration, doublet	Organic phosphorus

The results of thermo-oxidative decomposition may give an indication of the ability of the polymer to resist combustion since the flaming combustion is preceded by interaction of the polymer with heat and oxygen. When heat-induced decomposition is assisted by oxygen, the decomposition products react chemically with oxygen, shifting the onset of polymer decomposition to lower temperatures compared to the decomposition under a nitrogen atmosphere. The thermo-oxidative decomposition of PA6, PA6-7DC, PA6-10DC, and PA6-15DC samples in an air atmosphere confirmed that the chemically bonded DOPO-NH– pendant group caused a shift of $T_{5\%}$ (Fig. 10a, Table 5) to lower values compared to PA6. The T_{max1} of PA6-7DC, PA6-10DC, and PA6-15DC samples also decreased as compared to PA6, but the DOPO-NH– group significantly decreased the rate of weight loss during the first main decomposition step, resulting in increased residues at T_{max1} and 500 °C (Table 5). Comparing the initial decomposition step for DOPO-A-CLM occurring at 288 °C with the initial decomposition steps for PA6-7DC, PA6-10DC, and PA6-15DC samples occurring at 333, 325 and 320 °C, respectively, it can be observed that the thermo-oxidative stability of the DOPO-NH– functionality bound to the PA6 backbone is more stable compared to that in DOPO-A-CLM. The increased thermo-oxidative stability resulted in about a fourfold higher residue at 500 °C in the case of PA6-15DC compared to PA6. In addition, the increased thermo-oxidative stability of PA6-7DC, PA6-10DC, and PA6-15DC residues shifted T_{max2} to higher temperatures as compared to PA6, leading to the increased char residues in this decomposition step. The increased thermo-oxidative stability of the PA6-7DC, PA6-10DC, and PA6-15DC samples also resulted in decreased heat flow rates (Fig. S15) compared to PA6, which confirmed the successful inhibition of oxidative radicals by the phosphorus radical scavenging species. Additionally, since the $T_{5\%}$ corresponding to DOPO-A-CLM is significantly lower in comparison to the $T_{5\%}$ corresponding to PA6, it could be assumed that the physical

incorporation of DOPO-A-CLM into the PA6 matrix, would cause DOPO-A-CLM to decompose prematurely at temperatures lower than the onset of PA6 decomposition. This would result in the premature evolution of the flame retardant radical species into the gas phase, which would not be able to provide the increased residue at 500°, as was the case with the chemically bonded DOPO-NH–group to the PA6 backbone.The dTG curves of the PA6-7DC, PA6-10DC, and PA6-15DC samples (Fig. 10b) clearly showed an additional third decomposition step occurring above 650 °C, which was not observed for the PA6 sample. This finding can be ascribed to the blocky structure of the PA6-7DC, PA6-10DC, and PA6-15DC samples. Based on the collected evidence, the chemically bonded DOPO-NH– pendant group may provide the flame retardant effect for the PA6 in both gas and condensed phases.

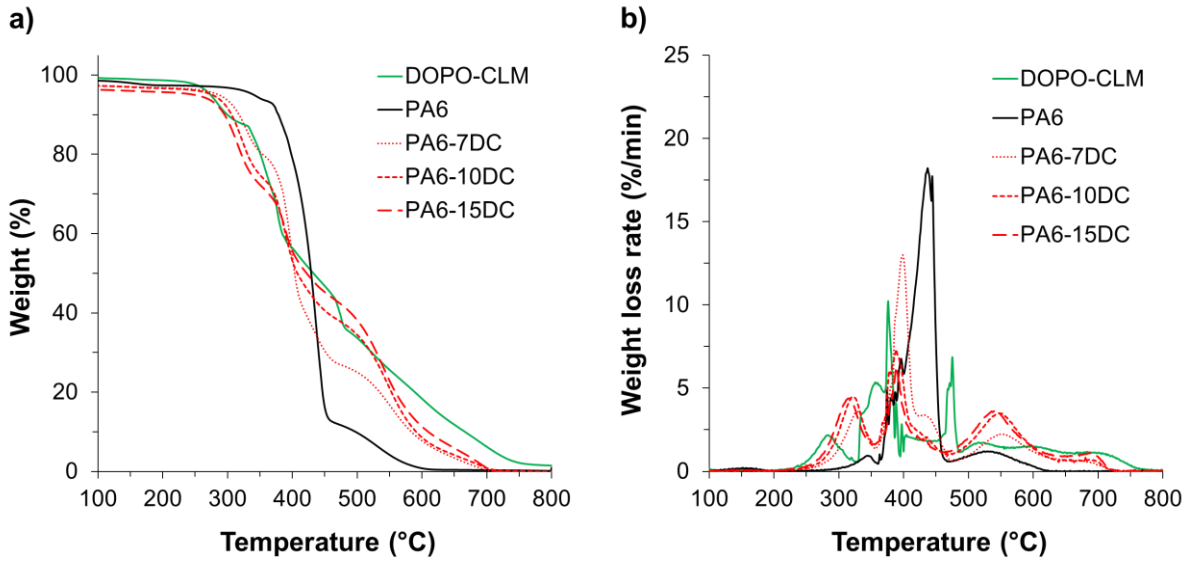

Fig. 10. (a) TG and (b) dTG graphs of DOPO-A-CLM, PA6, PA6-7DC, PA6-10DC, and PA6-15DC samples analyzed in an air atmosphere.

Table 5: TG data obtained in an air atmosphere.

Sample	$T_{5\%}$ (°C)	T_{max1} (°C)	Residue at T_{max1} (%)	T_{max2} (°C)	Residue at T_{max2} (%)	T_{max3} (°C)	Residue at T_{max3} (%)	Residue at 500 °C (%)
DOPO-A-CLM	277	379	66.5	478	39.0	-	-	34.1
PA6	343	449	36.5	527	7.2	-	-	10.0
PA6-7DC	290	403	57.0	552	17.0	656	2.9	25.2
PA6-10DC	280	392	61.1	551	22.0	679	2.2	34.9
PA6-15DC	253	392	61.0	543	26.8	684	2.5	38.8

3.4. Characterization of PA6-10DC(f) filament yarn

3.4.1. Morphology

Some typical SEM images of the PA6(f) and PA6-10DC(f) filament yarns are shown in Fig. 11. A comparison of the PA6(f) and PA6-10DC(f) filament surfaces revealed no significant differences in the surface morphology of the filament yarns. In both cases, the surface was relatively smooth, while oligomeric microfibrils were visible on both the PA6(f) and PA6-10DC(f) filament surfaces. SEM images also showed that the diameter of the PA6-10DC(f) sample was 65.4 ± 2.2 μm, which is slightly larger than that of PA6 (62.7 ± 1.4 μm).

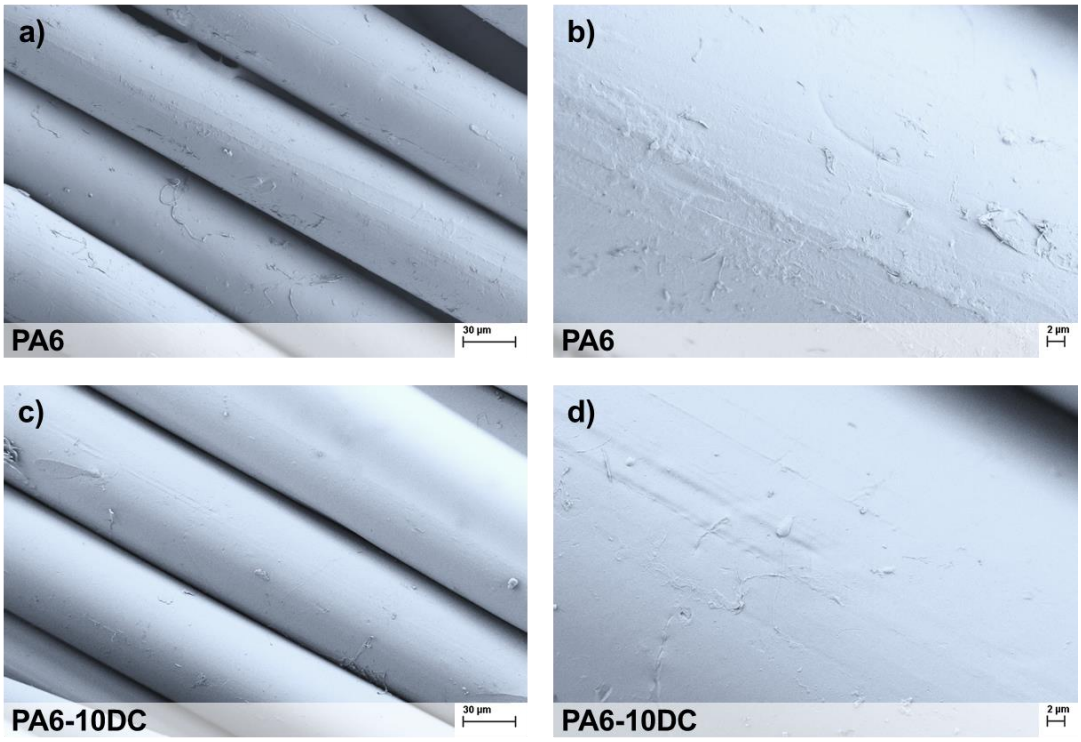

Fig. 11. Typical SEM images of longitudinal views of multifilament yarns: (a,b) PA6(f); (c,d) PA6-10DC(f) (lower (a,c) and higher (b,d) magnification).

3.4.2. Tensile properties

Tensile analysis was performed to evaluate the effects of incorporating the DOPO-NH– functionality on the mechanical properties of the multifilament yarns. The force versus tensile strain curves obtained for the PA6(f) and PA6-10DC(f) samples are shown in Fig. 12a. The results show that the tenacity and tensile strain at break decreased for PA6-10DC(f) compared to PA6(f). This finding can be attributed to the influence of chemically bonded DOPO-NH– functionality as the pendant group in the PA6 backbone, which reduces the H-bonding occurring between the PA6 chains, as well as slowing down the polymer crystallization and orientation. Therefore, further efforts should be made to investigate the chemical systems with a minimal effect on the mechanical properties of PA6 bulk materials. There is also much scope for optimizing the melt spinning process conditions, as they are known to have a direct effect

on the mechanical properties of the filament yarns. However, in this work, it was shown that the PA6-10DC(f) filament yarn could be successfully melt-spun as well as drawn and wound on bobbins (Fig. 12b).

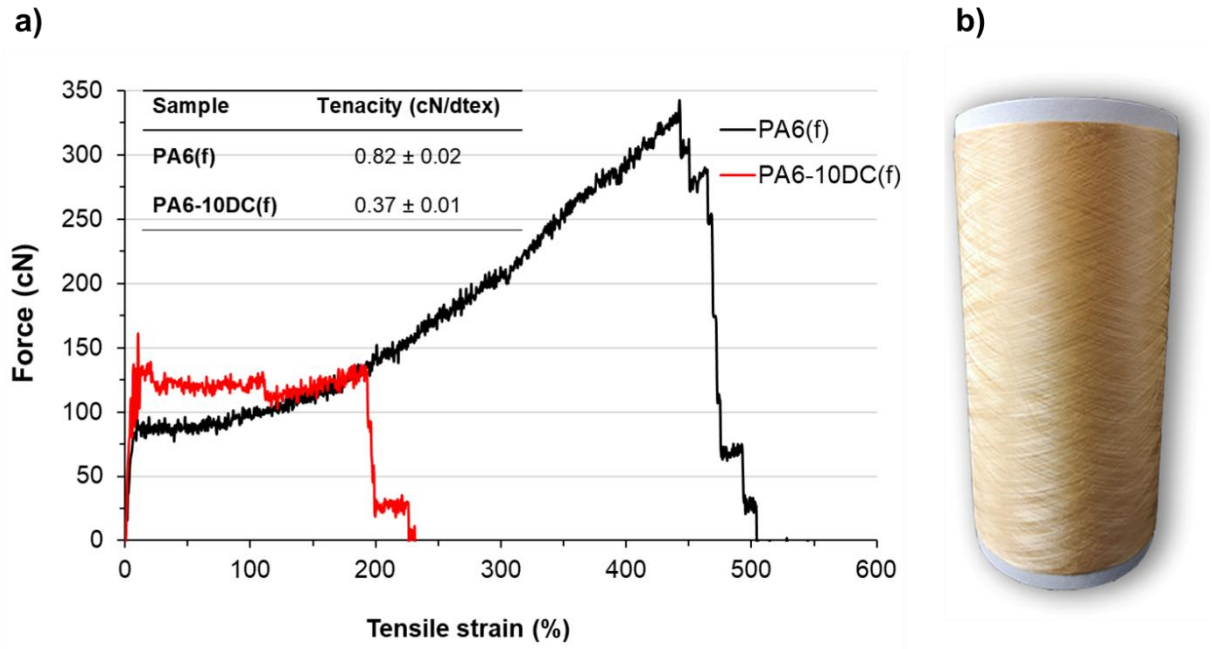

Fig. 12. (a) Force-tensile strain curves; (b) PA6-10DC(f) multifilament yarn wound on bobbin.

3.4.3. Vertical flame spread and forced-combustion tests

The vertical burning behavior of PA6(f) and PA6-10DC(f) filament samples was investigated according to the standardized vertical flame spread test (ASTM D6413); the results are shown in Fig. 13 and Table 6. The high surface-to-volume ratio of the fiber strand samples prolonged the burning and dripping of PA6(f). The flame retardant action of the DOPO-NH– pendant functionality successfully retarded both burning and melt-dripping, and provided self-extinction within 1 s for the PA6-10DC(f) sample (Fig. 13a). Self-extinction occurred immediately after the first drop, which significantly reduced the weight loss.

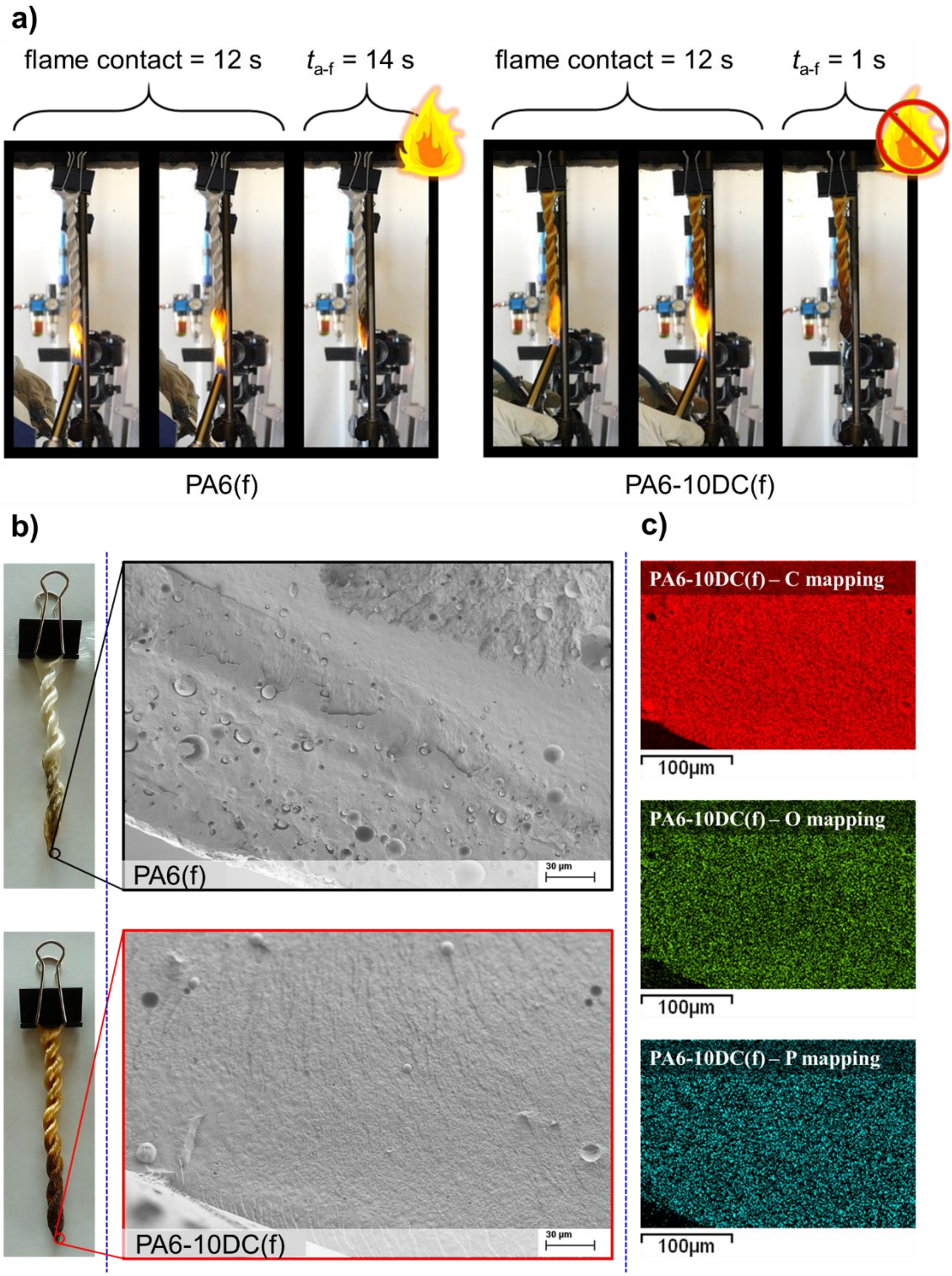

Fig. 13. (a) Snapshot photos from the videos of the ASTM D6143 vertical flame spread testing of the PA6(f) and PA6-DC(f) fiber strand samples and the corresponding residues after testing, (b) SEM images of the polymer bulk near the surface of bottom edge samples being exposed to

the flame, and (c) EDS carbon, oxygen, and phosphorus mapping of the surface of bottom edge of the PA6-DC(f) fiber strand being exposed to the flame.

Some typical SEM images of the polymer bulk spots in close proximity to the charred surfaces of the PA6(f) and PA6-10DC(f) fibre strand residues that were in direct contact with the flame are presented in Fig. 13b. The PA6(f) polymer bulk appeared to be much more porous as compared to that of PA6-10DC(f). The observed voids resulted from the released gases formed during the decomposition of the polymer, which was much more intense in the case of PA6(f) than PA6-10DC(f), which appeared to be much more compact. These results undoubtedly confirm that the thermo-oxidative stability of the PA6 backbone provided by the chemically bonded DOPO-NH– pendant group in the PA6-10DC(f) sample was efficient enough to confer acceptable flame retardant properties to PA6. In addition to the action of the flame retardant radicals in the gas phase during the decomposition of the DOPO-NH– pendant groups, their partial effect in the condensed phase can also be suspected, as the EDS mapping of the PA6-10DC polymer bulk near the surface of the lower edge sample exposed to the flame (Fig. 13c) confirms the presence of phosphorus.

Table 6. The results of the ASTM D6143 vertical flame spread tests performed on PA6(f) and PA6-10DC(f) fibre strand samples.

Sample	$t_{a\text{-}f}$ [a)] (s)	Weight loss (%)	Number of drips
PA6(f)	14	22.5 ± 3.2	12
PA6-10DC(f)	1	3.5 ± 1.1	1

[a)] $t_{a\text{-}f}$ – after flame time.

The resistance of the PA6(f) and PA6-10DC(f) knitted fabric samples to a heat flux of 35 kW/m^2 was investigated by cone calorimetry (Fig. 14, Tables 7 and 8). These results confirmed that the chemically bonded DOPO-NH– pendant functionality decreased the time to ignition (TTI, Table 7) and increased the mean heat release rate (HRR, Fig. 14a) and total heat released (THR, Table 7) of the PA6 polymer. These findings seem to contradict the results from the vertical flame spread tests, as the presence of the chemically bonded DOPO-NH– pendant group in the PA6-10DC(f) sample degrades the forced-combustion behavior of PA6. However, since the forced flaming combustion of polymers in cone calorimetry proceeds as a pyrolysis process with limited oxygen diffusion, the increased HRR, PHRR, and THR could be primarily attributed to the limited condensed phase effect, as the flame retardant DOPO's radicals act primarily in the gas phase [37]. Additionally, the exothermic effect of the cleavage between the DOPO-NH– group and the PA6 backbone, as determined by DSC analyses (Fig. S14) could also additionally degrade the forced-combustion behavior of PA6. The decrease in the mean effective heat of combustion (EHC, Table 7) of the volatiles generated during the decomposition of the PA6-10DC(f) sample compared to that of the PA6(f) indicates inhibited combustion in the gas phase. At the same time, the chemical interactions occurring in the gas phase caused a significant increase of the total smoke release (TSR, Fig. 14b) and the mean specific extinction area (SEA, Table 8) of the PA6-10DC(f) sample compared to those of the PA6(f). This was followed by a 4-hold higher mean [CO] yield and a 30% lower mean [CO_2] yield for the PA6-10DC(f) sample compared to that of the PA6(f) (Table 8).

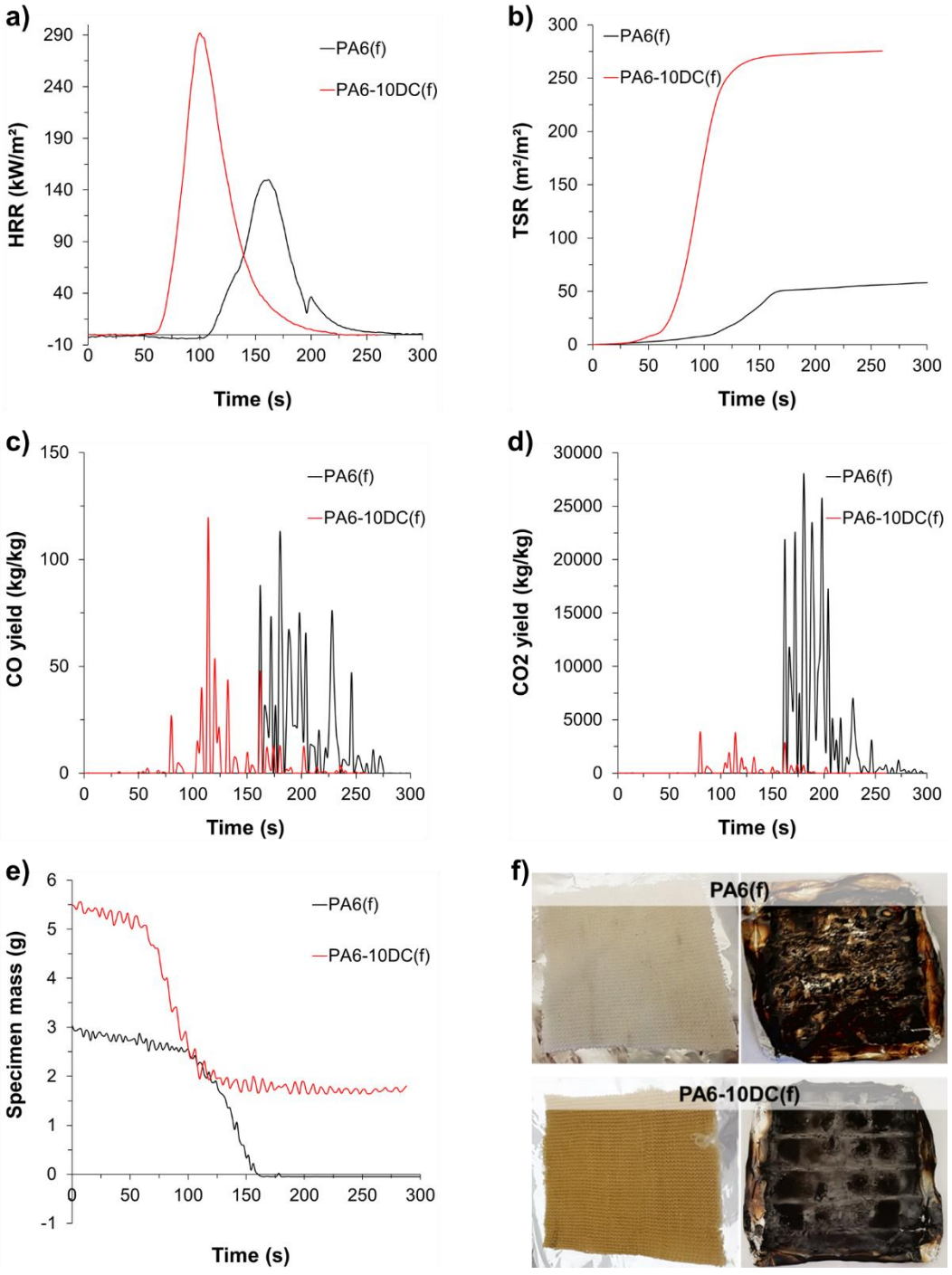

Fig. 14. (a) Heat release rate (HRR) vs. total combustion time, (b) total smoke release (TSR) vs. total combustion time, (c) and (d) carbon monoxide and carbon dioxide yields, respectively, vs. total combustion time, (e) specimen mass loss vs. total combustion time for the PA6(f) and PA6-10DC(f) knitted fabric samples, and (f) photographs of the PA6(f) and PA6-10DC(f) knitted fabric samples and their charred residues after cone calorimetry tests.

Table 7. Combustion data collected by cone calorimetry (heat flux: 35 kW/m^2).

Sample	TTI (s)	PHRR (kW/m^2)	THR (MJ/m^2)	EHC (MJ/kg)
PA6(f)	110 ± 30	190 ± 5	8.0 ± 0.2	32.8 ± 2.9
PA6-10DC(f)	51 ± 5	295 ± 12	13.3 ± 0.4	27.7 ± 0.4

Table 8. Smoke data collected by cone calorimetry (heat flux: 35 kW/m^2).

Sample	SEA (m^2/kg)	[CO] yield (kg/kg)	[CO_2] yield (kg/kg)	[CO]/[CO_2]
PA6(f)	191 ± 27	0.010 ± 0.001	2.911 ± 0.169	0.004
PA6-10DC(f)	546 ± 9	0.046 ± 0	1.985 ± 0.089	0.023

Furthermore, it can be observed that the production of both CO and CO_2 for the PA6-10DC(f) sample occurred at lower combustion times compared to those of the PA6(f) (Fig. 14c,d). However, the mass of CO_2 yield per mass of the PA6-10DC(f) sample burned was significantly lower compared to the PA6(f) (Fig 14d), confirming the results of the TG-FTIR analysis. Consequently, the ratio between the [CO] and [CO_2] yields (Table 8) was fivefold higher for the PA6-10DC(f) sample with respect to that of the PA6(f) sample, which could be due to the retardation of the OH• radicals in the oxidation of CO to CO_2 as well as the inhibited cleavage of the peptide C(O)–NH bonds. This eventually leads to the inhibited decomposition of the PA6-10DC(f) sample in the solid phase, as evidenced by the sample mass loss values shown in Fig. 14e. The charred residue of the PA6-10DC(f) sample, also displayed in Fig. 14f, was significantly higher as compared to that of the PA6(f). The initial weights of the 1 dm^2 samples of PA6(f) and PA6-10DC(f) knitted fabrics were 3.0 and 5.5 g, respectively, which could be partly responsible for the increased HRR and THR, since almost twice the mass of the

PA6-10DC(f) sample was burned under the continuous heat flux compared to PA6(f). However, the increased TSR is characteristic of the phosphorus-based FRs active in the gas phase, and this phenomenon should be further researched by simultaneously introducing smoke suppressants and investigating their influence on the flame retardant effects of DOPO-NH– functionality [33,38,39].

4. Conclusion

In this work, the idea of producing FR PA6 by chemical modifications of the polymer chain, while completely preserving the structure of the PA6 backbone, was fulfilled for the first time. For this purpose, a novel phosphonamidate derivative of A-CLM, containing the DOPO-NH– pendant functional group, was synthesized for the first time by a one-step Atherton–Todd reaction. Due to the presence of two chiral centers, DOPO-A-CLM consists of two diastereomeric species DS-I and DS-II. The co-polymerization of DOPO-A-CLM with CLM was conducted as a hydrolytic polymerization process, and DOPO-A-CLM was successfully integrated into the polymer matrix at different weight ratios.

The results showed that the bridging of DOPO and ε-caprolactam with the –NH– group significantly enhances the thermal stability of ε-caprolactam. Consequently, the chemical bonding of the DOPO-NH– pendant group to the PA6 backbone increases the thermal stability of polymer in nitrogen and air, as compared to PA6. The promoted thermal decomposition at lower temperatures, and the inhibition of the cleavage of peptide C(O)–NH bonds and thus depolymerization of PA6, increased char residues at 500 °C with respect to PA6. The increased thermal stability of PA6-xDC was enhanced by increasing the concentration of the incorporated DOPO-A-CLM co-monomer.

The chemically bonded DOPO-NH– pendant group affected the packing of PA6 backbones, leading to decreased crystallinity. This phenomenon caused a decrease in the tensile properties of PA6-10DC as compared to PA6. However, the filament yarns were successfully melt-spun from PA6-10DC, then partially drawn during winding onto bobbins, and knitted into the fabric samples. The surface morphology of the PA6-10DC(f) filament yarns was not significantly different from that of PA6.

The flame retardant effect of the DOPO-NH– functionality successfully slowed down both the burning and melt dripping of the PA6-10DC(f) sample that achieved self-extinction within 1 s, immediately after the first drop. The presence of phosphorus near the surface of the lower edge sample exposed to the flame confirms, in addition to the gas phase action of DOPO, a possible effect taking place in the condensed phase.

We believe that the discussed high-performance flame retardant polyamide yarn material fabricated from bio-mass holds great potential for a wide variety of future products in, e.g., the automotive, aerospace, and technical textile industries, where safety plays an important role.

Acknowledgements

This work was supported by the Slovenian Research Agency (Basic Postdoc Project Z2-9250, Programmes P2-0213, P2-0393, and P1-0134b, the Infrastructural Centre RIC UL-NTF), and the European COST Action CONTEXT, "European Network to connect research and innovation efforts on advanced Smart Textiles". The authors thank Helena Spreizer and Gregor Žitko for technical support in the synthesis of co-polymer, Tomaž Stergar for technical support during the melt-spinning process, and Andrej Vilar for the preparation of the knitted fabric samples.

Appendix A. Supplementary information

References

[1] R. Geyer, J.R. Jambeck, K.L. Law, Production, use, and fate of all plastics ever made, Sci. Adv. 3 (2017) e1700782. https://doi.org/10.1126/sciadv.1700782.

[2] J.C. Worch, A.P. Dove, 100th Anniversary of Macromolecular Science Viewpoint: Toward Catalytic Chemical Recycling of Waste (and Future) Plastics, ACS Macro Lett. (2020) 1494–1506. https://doi.org/10.1021/acsmacrolett.0c00582.

[3] J.B. Williamson, S.E. Lewis, R.R. Johnson, I.M. Manning, F.A. Leibfarth, C−H Functionalization of Commodity Polymers, Angew. Chemie Int. Ed. 58 (2019) 8654–8668. https://doi.org/10.1002/anie.201810970.

[4] A.B. Morgan, The Future of Flame Retardant Polymers–Unmet Needs and Likely New Approaches, Polym. Rev. 59 (2019) 25–54. https://doi.org/10.1080/15583724.2018.1454948.

[5] B. Claus, K. Rudolf, S. Joachim, W. Reinhard, Process for the production of caprolactam from waste containing polyamide, 2002.

[6] Frost W. John, Synthesis of caprolactam from lysine, WO2005123669A1, 2005.

[7] Frost W. John, Catalytic Deamination for Caprolactam Production, US20100145003A1, 2008.

[8] J. Sebastian, M. Zheng, Y. Jiang, Y. Zhao, H. Wang, Z. Song, X. Li, J. Pang, T. Zhang, One-pot conversion of lysine to caprolactam over Ir/H-Beta catalysts, Green Chem. 21 (2019) 2462–2468. https://doi.org/10.1039/c9gc00415g.

[9] J. Zhang, X. Mi, S. Chen, Z. Xu, D. Zhang, M. Miao, J. Wang, A bio-based hyperbranched flame retardant for epoxy resins, Chem. Eng. J. 381 (2020) 122719. https://doi.org/10.1016/j.cej.2019.122719.

[10] W. Huang, X. Hu, J. Zhai, N. Zhu, K. Guo, Biorenewable furan-containing polyamides,

Mater. Today Sustain. 10 (2020) 100049. https://doi.org/10.1016/j.mtsust.2020.100049.

[11] H. Vahabi, H. Rastin, E. Movahedifar, K. Antoun, N. Brosse, M.R. Saeb, Flame Retardancy of Bio-Based Polyurethanes: Opportunities and Challenges, Polymers (Basel). 12 (2020) 1234. https://doi.org/10.3390/polym12061234.

[12] R. Beerthuis, G. Rothenberg, N.R. Shiju, Catalytic routes towards acrylic acid, adipic acid and ε-caprolactam starting from biorenewables, Green Chem. 17 (2015) 1341–1361. https://doi.org/10.1039/c4gc02076f.

[13] D. Tunc, H. Bouchekif, B. Améduri, C. Jérôme, P. Desbois, P. Lecomte, S. Carlotti, Synthesis of aliphatic polyamide bearing fluorinated groups from ε-caprolactam and modified cyclic lysine, Eur. Polym. J. 71 (2015) 575–584. https://doi.org/10.1016/j.eurpolymj.2015.08.030.

[14] D. Tunc, C. Le Coz, M. Alexandre, P. Desbois, P. Lecomte, S. Carlotti, Reversible cross-linking of aliphatic polyamides bearing thermo- and photoresponsive cinnamoyl moieties, Macromolecules. 47 (2014) 8247–8254. https://doi.org/10.1021/ma502083p.

[15] J. Chen, M. Li, W. He, Y. Tao, X. Wang, Facile Organocatalyzed Synthesis of Poly(ε-lysine) under Mild Conditions, Macromolecules. 50 (2017) 9128–9134. https://doi.org/10.1021/acs.macromol.7b02331.

[16] C. Hirsch, B. Striegl, S. Mathes, C. Adlhart, M. Edelmann, E. Bono, S. Gaan, K.A. Salmeia, L. Hoelting, A. Krebs, J. Nyffeler, R. Pape, A. Bürkle, M. Leist, P. Wick, S. Schildknecht, Multiparameter toxicity assessment of novel DOPO-derived organophosphorus flame retardants, Arch. Toxicol. 91 (2017) 407–425. https://doi.org/10.1007/s00204-016-1680-4.

[17] M.M. Velencoso, A. Battig, J.C. Markwart, B. Schartel, F.R. Wurm, Molecular firefighting—How modern phosphorus chemistry can help solve the challenge of flame

retardancy. Angew. Chem. 2018, 57, 10450–10467. https://doi.org/10.1002/anie.201711735..

[18] N.M. Neisius, M. Lutz, D. Rentsch, P. Hemberger, S. Gaan, Synthesis of DOPO-Based Phosphonamidates and their Thermal Properties, Ind. Eng. Chem. Res. 53 (2014) 2889–2896. https://doi.org/10.1021/ie403677k.

[19] A. Buczko, T. Stelzig, L. Bommer, D. Rentsch, M. Heneczkowski, S. Gaan, Bridged DOPO derivatives as flame retardants for PA6, Polym. Degrad. Stab. 107 (2014) 158–165. https://doi.org/10.1016/j.polymdegradstab.2014.05.017.

[20] L. Long, W. Zhou, Y. Xiang, J. Li, S. Huang, S. Qin, G. Xu, J. Yu, Function of the aryl group in bis DOPO phosphonate on reducing fire hazards of polyamide 6 composites, J. Appl. Polym. Sci. 137 (2020) 49188. https://doi.org/10.1002/app.49188.

[21] M. Li, Y. Zhong, Z. Wang, A. Fischer, F. Ranft, D. Drummer, W. Wu, Flame retarding mechanism of Polyamide 6 with phosphorus-nitrogen flame retardant and DOPO derivatives, J. Appl. Polym. Sci. 133 (2016) n/a-n/a. https://doi.org/10.1002/app.42932.

[22] P. Simonetti, R. Nazir, A. Gooneie, S. Lehner, M. Jovic, K.A. Salmeia, R. Hufenus, A. Rippl, J.P. Kaiser, C. Hirsch, B. Rubi, S. Gaan, Michael addition in reactive extrusion: A facile sustainable route to developing phosphorus based flame retardant materials, Compos. Part B Eng. 178 (2019) 107470. https://doi.org/10.1016/j.compositesb.2019.107470.

[23] J. Vasiljević, M. Čolović, N. Čelan Korošin, M. Šobak, Ž. Štirn, I. Jerman, Effect of Different Flame-Retardant Bridged DOPO Derivatives on Properties of in Situ Produced Fiber-Forming Polyamide 6, Polymers (Basel). 12 (2020) 657. https://doi.org/10.3390/polym12030657.

[24] J. Vasiljević, M. Čolović, I. Jerman, B. Simončič, A. Demšar, Y. Samaki, M. Šobak, E. Šest, B. Golja, M. Leskovšek, V. Bukošek, J. Medved, M. Barbalini, G. Malucelli, S.

Bolka, In situ prepared polyamide 6/DOPO-derivative nanocomposite for melt-spinning of flame retardant textile filaments, Polym. Degrad. Stab. 166 (2019) 50–59. https://doi.org/10.1016/j.polymdegradstab.2019.05.011.

[25] G. Mourgas, E. Giebel, T. Schneck, J. Unold, M.R. Buchmeiser, Syntheses of intrinsically flame- retardant polyamide 6 fibers and fabrics, J. Appl. Polym. Sci.136 (2019) 47829. https://doi.org/10.1002/app.47829.

[26] D. XUAN, F. XINXING, J. LIPENG, W. XING, WENHUA XIAO, Preparation method of halogen-free flame retardant nylon 66 polymer, CN104211954A, 2014.

[27] I. Leinonen, P.P.M. Iannetta, R.M. Rees, W. Russell, C. Watson, A.P. Barnes, Lysine Supply Is a Critical Factor in Achieving Sustainable Global Protein Economy, Front. Sustain. Food Syst. 3 (2019) 27. https://doi.org/10.3389/fsufs.2019.00027.

[28] F.K. do C. Félix, L.A.J. Letti, G. Vinícius de Melo Pereira, P.G.B. Bonfim, V.T. Soccol, C.R. Soccol, L-lysine production improvement: a review of the state of the art and patent landscape focusing on strain development and fermentation technologies, Crit. Rev. Biotechnol. 39 (2019) 1031–1055. https://doi.org/10.1080/07388551.2019.1663149.

[29] B.O. Abo, M. Gao, Y. Wang, C. Wu, Q. Wang, H. Ma, Production of butanol from biomass: recent advances and future prospects, Environ. Sci. Pollut. Res. 26 (2019) 20164–20182. https://doi.org/10.1007/s11356-019-05437-y.

[30] E. Ketabchi, L. Pastor-Pérez, T.R. Reina, H. Arellano-García, Catalytic upgrading of acetone, butanol and ethanol (ABE): A step ahead for the production of added value chemicals in bio-refineries, Renew. Energy. 156 (2020) 1065–1075. https://doi.org/10.1016/j.renene.2020.04.152.

[31] P. Losch, J.F. Kolb, A. Astafan, T.J. Daou, L. Pinard, P. Pale, B. Louis, Eco-compatible zeolite-catalysed continuous halogenation of aromatics, Cite This Green

Chem. 18 (2016) 4714. https://doi.org/10.1039/c6gc00731g.

[32] K. Shakeela, V.L. Sinduri, G.R. Rao, Hydrophobic supramolecular assemblies of Keggin anions with lactam-lactim cationic tautomers, Polyhedron. 137 (2017) 43–51. https://doi.org/10.1016/j.poly.2017.07.023.

[33] K. Liu, Y. Li, L. Tao, C. Liu, R. Xiao, Synthesis and characterization of inherently flame retardant polyamide 6 based on a phosphine oxide derivative, Polym. Degrad. Stab. 163 (2019) 151–160. https://doi.org/10.1016/j.polymdegradstab.2019.03.004.

[34] A.C. Draye, O. Persenaire, J. Brožek, J. Roda, T. Košek, P. Dubois, Thermogravimetric analysis of poly(ε-caprolactam) and poly[(ε-caprolactam)-co-(ε-caprolactone)] polymers, Polymer (Guildf). 42 (2001) 8325–8332. https://doi.org/10.1016/S0032-3861(01)00352-4.

[35] M. Coquelle, S. Duquesne, M. Casetta, J. Sun, S. Zhang, S. Bourbigot, Investigation of the decomposition pathway of polyamide 6/ammonium sulfamate fibers, Polym. Degrad. Stab. 106 (2014) 150–157. https://doi.org/10.1016/j.polymdegradstab.2014.02.007.

[36] G. Socrates, Infrared and Rafman Characteristic Group Frequencies: Tables and Charts, 3rd Edition Wiley, (2004)

[37] I. Butnaru, M.P. Fernández-Ronco, J. Czech-Polak, M. Heneczkowski, M. Bruma, S. Gaan, Effect of meltable triazine-DOPO additive on rheological, mechanical, and flammability properties of PA6, Polymers 7 (2015) 1541–1563. https://doi.org/10.3390/polym7081469

[38] D. Jia, J. He, R. Yang, The synthesis andcharacterization of a DOPOderivative bearing an activeterminal epoxy group:e-DOPO and its application inrigid polyurethane foam, J. Fire Sci. 37 (2019) 47–66. https://doi.org/10.1177/0734904118812227

[39] H. Luo, W. Rao, Y. Liu, P. Zhao, L. Wang, C. Yu, Novel multi- element DOPO derivative toward low- flammability epoxy resin, J. Appl. Polym. Sci. 137 (2020) 49427. https://doi.org/10.1002/app.49427

New sustainable flame retardant DOPO-NH-functionalized polyamide 6 and filament yarn

Marija Čolović[1], Jelena Vasiljević[2], Žiga Štirn[1], Nataša Čelan Korošin[3], Matic Šobak[1], Barbara Simončič[2], Andrej Demšar[2], Giulio Malucelli[4], Ivan Jerman[1]

[1]*National Institute of Chemistry, Hajdrihova 19, 1000 Ljubljana, Slovenia*

[2]*University of Ljubljana, Faculty of Natural Sciences and Engineering, Aškerčeva 12, 1000 Ljubljana, Slovenia*

[3]*University of Ljubljana, Faculty of Chemistry and Chemical Technology, Večna pot 113, 1000 Ljubljana, Slovenia*

[4]*Politecnico di Torino, Department of Applied Science and Technology and local INSTM Unit, Viale Teresa Michel 5, 15121 Alessandria, Italy*

*Author for correspondence (e-mail: ivan.jerman@ki.si)

Graphical abstract

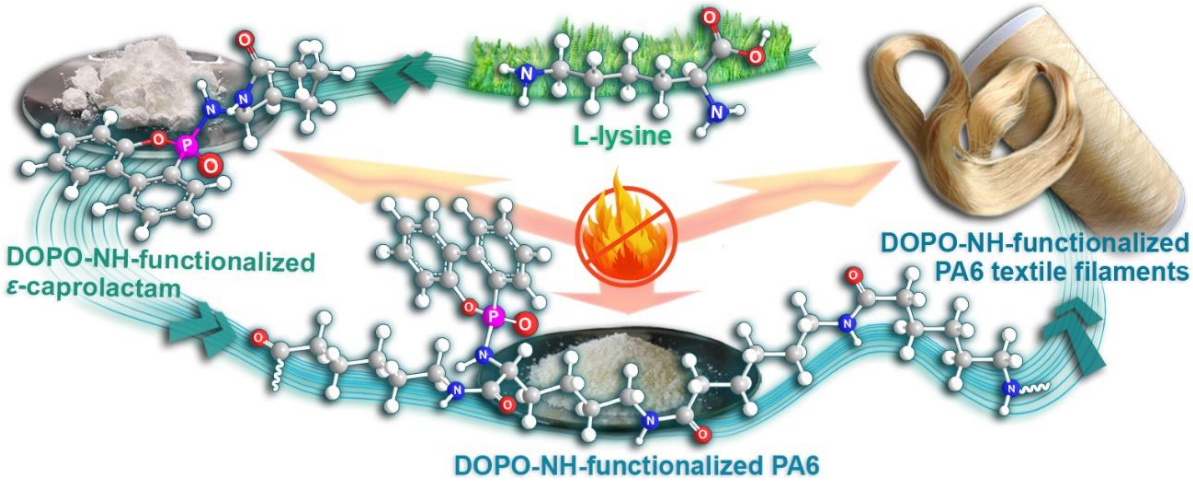

Highlights

- *New DOPO-NH-functionalized caprolactam comonomer was synthesized.*
- *New FR PA6 with pendant DOPO-NH– group was produced.*
- *DOPO-NH– group increased thermo-oxidative residue of PA6 at 500 °C by 35%.*
- *FR PA6 was successfully melt spun into multi-filaments of 65 µm in diameter.*
- *Melt spun filaments were self-extinguishing in 1 s by vertical flame spread test.*

~~α-amino-ε-caprolactam was modified with DOPO to produce new DOPO-A-CLM co-monomer~~

~~ε-caprolactam and DOPO-A-CLM were co-polymerized into new DOPO-NH-functionalized PA6~~

~~DOPO-NH-functionalized PA6 was used in melt spinning process to produce filament yarn~~

~~DOPO-NH– pendant group enhanced thermal and thermo-oxidative stability of PA6 polymer~~

~~DOPO-NH– group enhanced flame retardancy and self-extinguishment of filament yarn~~

ABSTRACT

This work presents a unique approach for the preparation of a flame retardant (FR) polyamide 6 (PA6) polymer with chemically bonded 9,10-dihydro-9,10-oxa-10-phosphaphenanthrene-10-oxide (DOPO) as a pendant group bridged to the polymer via an -NH- group. A novel phosphonamidate co-monomer (DOPO-A-CLM) was synthesized from DOPO and *α*-amino-*ε*-caprolactam (A-CLM). This co-monomer was subsequently used in the hydrolytic polymerization with *ε*-caprolactam (CLM) in different weight ratios to prepare DOPO-NH-functionalized PA6 (PA6-xDC, x = 7, 10, and 15 wt % DOPO-A-CLM). Chemical incorporation of DOPO-A-CLM into the PA6 backbone decreased the molecular weight of the polymer from 15387 for neat PA6 to 12375, 10516 and 9316 for PA6-7DC, PA6-10DC and PA6-15DC, respectively. The DOPO-NH– pendant group accelerated start of the PA6 thermal decomposition and increased the char residues at 500 °C from 1% for PA6 to 4.6, 4.9, and 5.0% for the PA6-7DC, PA6-10DC, and PA6-15DC samples, respectively, indicating crosslinking reactions in the condensed phase. The evolved phosphorus-active species in the gas phase inhibited the PA6 depolymerization, resulting in increased thermo-oxidative stability and about a fourfold higher residue at 500 °C in the case of PA6-15DC compared to PA6. The intrinsically flame retardant PA6 filament yarns with chemically bound FR pendant group were successfully melt spun from PA6-10DC, drawn and wound on bobbin. The DOPO-NH– pendant group decreased filament flammability and inhibited flame propagation, resulting in immediate self-

extinguishment after flame removal. Incorporation of DOPO-A-CLM decreased the filament tensile properties compared to the neat PA6, which correlates with the decreased polymer molecular weight.

Keywords: **α**-amino-*ε*-caprolactam; DOPO; Co-monomer; Polyamide 6; Filament yarn; Flame retardance

1. Introduction

The widespread use of polymeric materials has increased the demand for new, more sustainable solutions for their production. In fact, the production of plastics has accelerated to the point where 8.3 billion tons of new plastics were created by 2017, 79% of which was confined to landfills or ended up in the natural environment [1]. Considering this issue, environmental legislation, consumer concerns, and stringent waste management approaches are putting increasing pressure on polymer and polymer end-product manufacturers to consider the recyclability and sustainability of their products. The main challenges lie in the development of functional and durable polymer materials with reduced environmental impact and the possibility of implementing a circular economy strategy in their production [2–4].

Polyamide 6 (PA6) has proven to be an excellent candidate for the development of sustainable functional polymer materials. It is known as a high-performance fiber-forming industrial thermoplastic polymer belonging to aliphatic polyamides, the special group of engineering thermoplastics with excellent toughness, elasticity, abrasion resistance, and physical and chemical stability. Consequently, its wide applications include the automotive industry, the technical textile industry, the electrical and electronic industry, construction, and the packaging industry. tThe main advantage of PA6 compared to other engineering polymers

is its unique chemical structure, which allows for the chemical recycling of PA6 waste to the monomer ε-caprolactam (CLM) and subsequent re-polymerization into new PA6, while retaining value and usability. This enables the design of a closed loop production process, which is the guiding principle of the sustainability concept. Due to the possibility of obtaining the monomer CLM from the conversion of lysine from biomass fermentation [5,6], PA6 has been classified as a bio-based polymer. According to the literature, the amino acid lysine obtained by recycling biomass could be advantageously used as a renewable feedstock for the production of CLM [7,8], which is currently derived from fossil resources in petrochemical processing. The use of bio-based CLM in the production of PA6 can make an important contribution to reducing of greenhouse gas emissions and the environmental impact of petrochemical processing [9-11]. However, as the bio-renewable routes are still at an early stage of development, their commercial implementation is still a challenging scientific problem [12].

The development of synthesis reaction for ε-caprolactam from lysine [8] has opened new possibilities for the derivatization of α-amino-ε-caprolactam to produce co-monomers with moieties containing functionalities such as fluorine and benzyl [13,14]. In these studies, functionalized ε-caprolactam molecules were employed as co-monomers with CLM in the polymerization reaction at different weight/molar ratios and conditions to prepare a PA6 backbone with different side chain functionalities. Although there are also some reports on the performance of homo-polymerization of functionalized caprolactam, the resulting polymer shows a much shorter chain length and therefore poorer mechanical properties [15]. However, these studies confirm a multiple role of lysine as a precursor for the synthesis of CLM as well as of CLM-based co-monomers, enabling the development of bio-renewable synthetic routes for the preparation of PA6 co-polymers.

The preparation of functionalized PA6 materials by co-polymerization reactions is considered a practical solution to overcome the drawbacks of PA6 materials, such as their high

flammability. The covalent bonding of the functional group to the PA6 structure can prevent the migration and leaching of the flame retardant (FR)from the polymer, while improving the dispersion state of the FR in the polymer matrix, thereby lowering the concentration required for an efficient FR effect. It is well known that the covalent bonding of FRs into the polymer during the polymerization reaction can make an important contribution to solving environmental and fire safety problems [4]. Indeed, the release of FRs into the environment during the ageing process can cause environmental problems and can simultaneously decrease the FR efficiency of the polymer.

Based on the state of the art in FR polyamides, the use of organic phosphorous compounds as "green" FR alternatives is becoming greatly importance as part of efforts to replace toxic, persistent, and bio-accumulative halogenated FRs [16,17]. Among the phosphorus-based FR compounds, 9,10-dihydro-9,10-oxa-10-phosphaphenanthrene-10-oxide (DOPO) has been extensively explored, as it is known to release highly efficient radical scavenging species such as $PO^{\bullet}$ in the gas phase during its thermal decomposition [18]. Due to its excellent FR properties, DOPO is considered one of the model compounds for studying the effects of FR properties on phosphorous-based chemistry [17].

Various approaches have been conducted for the incorporation of DOPO functionality into the PA6 matrix, mostly involving the physical incorporation of DOPO by melt compounding, reactive extrusion, and the *in situ* polymerization of ε-caprolactam in the presence of DOPO [19-24] or the covalent incorporation of DOPO into the polyamide structure in co-polymerization reactions [25,26]. In this context, DOPO-functionalized dibasic acid and DOPO-functionalized diamine were used as co-monomers in combination with ε-caprolactam or with hexamethylene diamine and adipic acid to prepare polyamides with a different chemical structure. However, by incorporating dibasic acid and diamine into the main polymer chain, the unique backbone structure, characteristic of PA6, was lost. The disadvantage of this approach

is that the polymer modification worsens the recyclability of the products. Therefore, to preserve the PA6 backbone and thus the recyclability of the product, the DOPO derivatization of CLM or 6-aminocaproic acid and its incorporation with *ε*-caprolactam in the co-polymerization reaction remains the only approach, which is still completely unexplored.

The present work aims to synthesize a novel flame retardant DOPO-NH-functionalized PA6 by incorporating the DOPO-NH– functionality as a pendant group into the PA6 backbone structure. The main idea was to use the cyclic lysine, i.e., *α*-amino-*ε*-caprolactam (A-CLM), as a biomass resource for the one-step Atherton–Todd reaction, in which DOPO-NH-functionalized caprolactam (DOPO-A-CLM) was produced. The proposed co-monomer synthesis can be made more greener by using alternatives to standard chlorinating agents and has a high potential for implementation in an industrial setting. DOPO-A-CLM was further used as a co-monomer with CLM in the hydrolytic ring opening co-polymerization reaction to produce FR DOPO-NH-functionalized PA6 and multifilament yarn.

2. Experimental section

2.1. Materials

L-lysine hydrochloride, (L-Lys × HCl, ABCR, 99%), aluminum oxide, anhydrous (Al_2O_3, Grade I, 60 Mesh, Alfa Aesar), hexanol (Merck, 98%), 9,10-dihydro-9-oxa-10-phosphaphenanthrene-10-oxide (DOPO, ABCR, 97%), sulphuryl chloride (SO_2Cl_2, Sigma Aldrich, 97%), *N*-chlorosuccinimide (NCS, Sigma Aldrich, 98%), potassium hydroxide (KOH, Merck, pellets for analysis EMSURE), tri-ethylamine (TEA, Sigma Aldrich, 99,5%), dichloromethane (DCM, Honeywell, ≥99.8), tetrahydrofuran (THF, Honeywell, ≥99.9), acetone (Honeywell, ≥99.9), hexafluoro-isopropanol (HFIP, ABCR, 99%), and *ε*-caprolactam

(CLM) was kindly supplied by L. Brüggemann GmbH & Co. KG (Heilbronn, Germany). All chemicals were used as received.

2.2. Synthesis of DOPO-NH-functionalized PA6 (PA6-xDC)

A new procedure for the synthesis DOPO-NH-functionalized PA6 (PA6-xDC) is presented in Scheme 1. As shown, the synthesis includes three main steps: (a) synthesis of *α*-amino-*ε*-caprolactam (A-CLM) from L-Lys × HCl, (b) synthesis of DOPO-functionalized *α*-amino-*ε*-caprolactam phosphonamidate (DOPO-A-CLM), and (c) synthesis of DOPO-NH-functionalized PA6 (PA6-xDC) with the incorporated co-monomer DOPO-A-CLM at different wt % ratios (x = 7, 10, and 15 wt %).

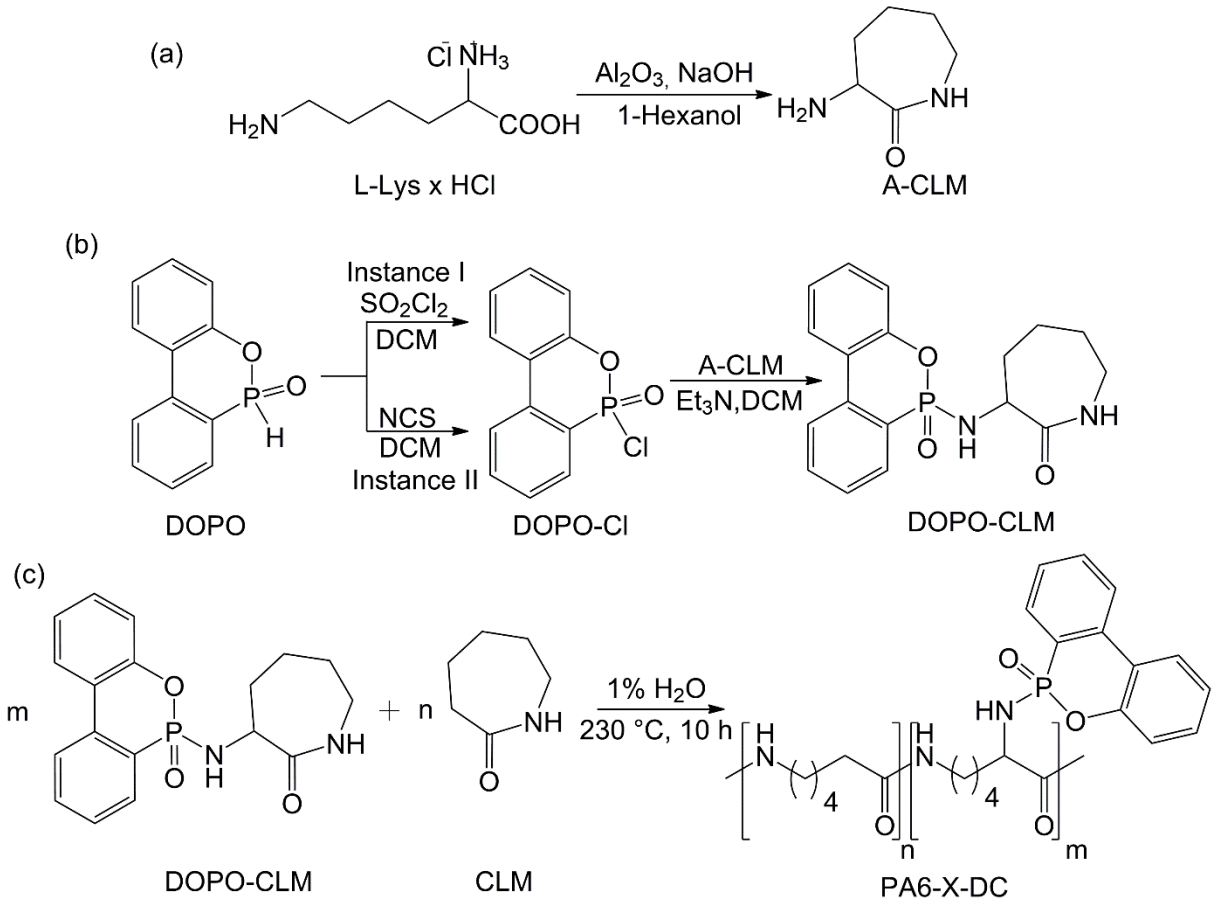

Scheme 1. (a) Synthesis of *α*-amino-*ε*-caprolactam (A-CLM). (b) Synthesis of DOPO-NH-functionalized caprolactam phosphonamidate (DOPO-A-CLM) using two different chlorinating agents, i.e., SO_2Cl_2 (Instance I) and NCS (Instance II). (c) Synthesis of DOPO-NH-functionalized PA6 (PA6-xDC; x = 7, 10, and 15 wt % DOPO-A-CLM).

a) Synthesis of *α*-amino-*ε*-caprolactam (A-CLM) according to the modified procedure [6] (Scheme 1a).

In a 10 L reaction vessel equipped with a mechanical stirrer and a nitrogen inlet, a suspension containing 0.8 mol (146.08 g) L-Lys x HCl, 0.8 mol (32 g) NaOH, and 7.2 mol (689.09 g) of Al_2O_3 was prepared in 4 L of hexanol. In a nitrogen atmosphere, the reaction mixture was vigorously stirred for 4 h under reflux (at approximately 155 °C). Afterwards, the cooled reaction mixture was filtered (removal of Al_2O_3), and the solvent evaporated under reduced pressure, which yielded a light orange resin-like substance (70% yield). The obtained A-CLM was used without further purification.

^{1}H NMR (DMSO-d$_6$, δ ppm): 7.57 (s, 1H, CON*H*), 3.41 (d, *J* = 8 Hz, 1H, COC*H*NH_2), 3.12-2.98 (m, 2H, CONHCH_2), 1.85-1.53 (m, 6H, NH_2 and ring) 1.36-1.26 (m, 1H, ring), 1.21-1.11 (m, 1H, ring).

^{1}H NMR spectrum of A-CLM is presented in the supporting information (Fig. S1).

b) Synthesis of DOPO-functionalized caprolactam phosphonamidate (DOPO-A-CLM) (Scheme 1b).

SO_2Cl_2 route (Scheme 1b, Instance I):

In a 2 L round bottom flask equipped with a magnetic stirrer, a nitrogen inlet, and a KOH trap (trapping evolved HCl and SO_2), a solution of 0.4 mol (86.48 g) DOPO in 400 mL of DCM was prepared and subsequently chilled to 0 °C, followed by a slow addition of 0.4 mol (54.24 g) SO_2Cl_2 dissolved in 200 mL of DCM (temperature in the flask did not exceed 10 °C during the addition). Afterwards, the reaction mixture was heated and refluxed for 3 h, removing HCl and SO_2 gases. The reaction mixture was chilled to 0 °C again, and two separate solutions of 0.44 mol (44.52 g) TEA in 200 mL of DCM and 0.4 mol (53.8 g) A-CLM in 200 mL of DCM were slowly added to the reaction mixture (the temperature in the flask did not exceed 10 °C during the addition). Afterwards, the reaction mixture was stirred overnight at room temperature. The solvent was removed under reduced pressure, and crude material was dissolved in THF, removing triethylamine hydrochloride by filtration. Subsequently, THF was removed under reduced pressure and the viscous residue was treated with DCM or acetone, leading to the precipitation of a white powder upon standing at 2–8 °C. The white precipitate was collected and dried, yielding 109.8 g (80%) of DOPO-A-CLM product.

NCS route (Scheme 1b, Instance II):

N-chloro succinimide, NCS (58.7 g, 0.44 mol) was gradually added at 0 °C under nitrogen to a stirred solution of DOPO (86.48 g, 0.4 mol) in 400 mL of DCM. The reaction mixture was left to warm up to ambient temperature and stirred overnight. Afterwards, it was cooled to 0 °C again, followed by dropwise addition of TEA (44.52 g, 0.44 mol) and A-CLM (53.8 g, 0.4 mol) dissolved in 200 mL of DCM. The reaction mixture was stirred overnight and then subjected to extraction with water in order to remove TEA × HCl. The solvent removal gave rise to an oily residue, which was treated with acetone or DCM to precipitate 68.6 g (50%) of a white powder product.

DOPO-A-CLM was found to be in the form of two enantiomeric pairs of diastereomers with a 1:2 ratio between Isomer I and II.

Isomer I (DS-I)

^{1}H NMR (DMSO-d$_6$, δ ppm): 8.19-8.16 (m, 2H, Ar), 8.08-8.04 (m, 1H, Ar), 7.84-7.82 (m, 1H, CON*H*CH$_2$), 7.77-7.74 (m, 1H, Ar), 7.59-7.56 (m, 1H, Ar), 7.46-7.43 (m, 1H, Ar), 7.32-2.29 (m, 2H, Ar), 5.51-5.47 (dd, J_1 = 8.5 Hz J_2 =13.5 Hz, COC*H*NH), 4.17-4.12 (m, 1H, CONHC*H*$_2$), 3.09-3.05 (m, 2H, cyclic), 1.87-1.84 (m, 2H, cyclic and COCHN*H*), 1.71-1.68 (m, 1H, cyclic), 1.57-1.51 (m, 2H, cyclic); **^{31}P NMR (DMSO-d6, δ ppm):** 13.28.

^{1}H NMR (HFIP, insert C$_6$D$_6$, δ ppm): 8.13-8.10 (m, 1H, Ar), 8.06-8.04 (m, 1H, Ar), 7.98-7.94 (m, 1H, Ar), 7.84-7.82 (m, 1H, Ar), 7.63-7.60 (m, 1H, Ar), 7.48-7.45 (m, 1H, Ar), 7.38-7.35 (m, 1H, Ar), 7.29-7.27 (m, 1H, Ar), 6.44 (m, 1H, CON*H*CH$_2$), 4.49 (dd, J_1 = 9 Hz, J_2 = 12, 1H, COC*H*NH), 4.19-4.14 (m, 1H, CONHC*H*), 3.27-3.22 (m, 1H, cyclic), 3.17-3.12 (m, 1H, cyclic), 1.98-1.96 (m, 2H, cyclic and COCHN*H*), 1.79-1.75 (m, 1H, cyclic), 1.68-1.62 (m, 1H, cyclic), 1.59-1.52 (m, 1H, cyclic), 1.42-1.35 (m, 1H, cyclic); **^{31}P NMR (HFIP, insert C$_6$D$_6$, δ ppm):** 19.98.

Isomer II (DS-II)

^{1}H NMR (DMSO-d$_6$, δ ppm): 8.21-8.18 (m, 2H, Ar), 7,89-7,87 (m, 1H, CON*H*CH$_2$), 7.81-7.74 (m, 2H, Ar), 7.60-7.56 (m, 1H, Ar), 7.47-7.44 (m, 1H, Ar) 7.33-7.28 (m, 2H, Ar), 5.45-5.42 (dd, J_1 = 9 Hz, J_2 = 12, 1H, COC*H*NH), 3.91-3.85 (m, 1H, CONHC*H*$_2$), 3.03-2.98 (m, 1H, CONHC*H*$_2$), 2.96-2.91 (m, 1H, cyclic), 1.99-1.96 (m, 1H, cyclic), 1.84-1.80 (m, 1H, cyclic) 1.66-1.62 (m, 1H, cyclic), 1.60-1.53 (m, 1H, cyclic), 1.47-1.39 (m, 1H, cyclic), 1.18-1.11 (m, 1H, cyclic). **^{31}P NMR (DMSO-d$_6$, δ ppm):** 13.29.

^{1}H NMR (HFIP, insert C$_6$D$_6$, δ ppm): 8.11-8.09 (m, 1H, Ar), 8.04-8.03 (m, 1H, Ar), 7.85-7.78 (m, 2H, Ar), 7.59-7.55 (m, 1H, Ar), 7.46-7.43 (m, 1H, Ar), 7.36-7.33 (m, 1H, Ar), 7.28-7.26 (m, 1H, Ar), 6.41-6.39 (m, 1H, CON*H*CH$_2$), 4.62 (dd, J_1 = 9 Hz, J_2 = 12 Hz, 1H, COC*H*NH), 3.91-3.86 (m, 1H, CONHCH$_2$), 3.20-3.15 (m, 1H, Cyclic), 3.02-2.97 (m, 1H, Cyclic), 2.12-2.09(m, 1H, Cyclic), 1.97-1.93 (m, 1H, Cyclic), 1.74-1.67(m, 2H, COCHN*H* and

Cyclic), 1.47-1.40 (m, 1H,Cyclic), 1.38-1.30 (m, 1H,Cyclic). **^{31}P NMR (HFIP, insert C_6D_6, δ ppm):** 20.28.

^{1}H NMR and ^{31}P NMR spectra of DOPO-A-CLM, DC-I and DC-II in DMSO-d_6 and HFIP are presented in the supporting information (Figs. S2 – S11).

c) Synthesis of DOPO-NH-functionalized PA6 (PA6-xDC) with incorporated DOPO-A-CLM (Scheme 1c).

Three different compositions of PA6-xDC with incorporated DOPO-A-CLM synthesized by an NCS route at different wt % ratios (x = 7, 10 and 15 wt %), namely PA6-7DC, PA6-10DC, and PA6-15DC, were produced. Under inert conditions (glove box), 7, 10, or 15 wt % of the co-monomer DOPO-A-CLM was introduced into melted CLM (92, 89, or 84 wt %, respectively). Afterwards, 1% H_2O was introduced outside the glove box, and the reaction mixture was homogenized. In the hermetically sealed autoclave, the reaction mixture was left to react for 10 h at 230 °C. The obtained co-polymers were crunched and refluxed for 24 h, first in water and then in DCM, to remove unreacted reagents and water-soluble oligomers, and then dried in an oven overnight at 90 °C under vacuum before any further analysis. Gravimetrically calculated yield ranged between 85 and 88%.

^{1}H-NMR of 10DC-PA6 (HFIP/benzene-d_6, δ ppm): 8.08-8.04 (m, 2H, Ar), 7.94-7.90 (m, 1H, Ar), 7,77-7.75 (m, 1 H), 7,59-7.56 (m, 1H, Ar), 7.48-7.45 (m, 1H, Ar), 7.37-7.26 (m, 1H, Ar), 6.70-6.67 (m, 1H, CON*H*CH_2-DOPO), 6.38-6.36 (m, 25H (1H),CON*H*CH_2-CL), 3.35-3.31 (m, 50H (2H), chain-CL), 2.34-2.32 (m, 50H (2H), chain-CL), 1.74-1.69 (m, 50H (2H), chain-CL), 1.67-1.62 (m, 50H (2H), chain-CL), 1.47-1.43 (m, 50H (2H), chain-CL).

^{1}H NMR spectrum of PA6-10DC sample is presented in the supporting information (Fig. S12).

d) Synthesis of PA6

PA6 was produced under identical conditions as PA6-xDC. Inside the glove box, the reactor's Teflon insert containing 0.875 mol (99 g) CLM was heated until melting; then, 1 wt % (1 g, 5.56 mmol) water was added into the melt outside the glove box. After homogenization, the Teflon insert was placed in the autoclave and hermetically sealed. Reaction continued in the oven for 10 h at 230 °C. The obtained product was crunched, refluxed in water for 24 h, filtered, and dried overnight in the oven at 90 °C under vacuum; the final yield was 87%.

^{1}H NMR (HFIP, insert C_6D_6, δ ppm): 6.38 (s, 1H, CON*H*CH_2), 3.38 (m, 2H, CONHC*H*$_2$), 2.35 (m, 2H, chain), 1.7 (m, 4H, chain), 1.46 (m, 2H, chain).

^{1}H NMR spectrum of PA6 is presented in the supporting information (Fig. S13).

2.3. Production of filament yarns by melt-spinning

PA6 and PA6-10DC filament yarns, coded as PA6(f) and PA6-10DC(f), were produced using a laboratory-scale melt-spinning and drawing device (Extrusion System Ltd, Bradford, Great Britain). PA6-15DC(f) filament yarns were not produced due to the poor spinnability with respect to the used melt-spinning process conditions. PA6 and PA6-10DC polymer samples were ground into granules (size: 1-3 mm) and fed into the extruder. The temperature of the extruder (three zones), the metering pump, and the spin pack (two zones) was set at 220 °C for the melt-spinning of PA6(f). In the case of the melt spinning of PA6-10DC(f), the temperature of the extruder was set at 200 °C, and the temperatures of the metering pump and spin pack were set at 190 °C. The extruder screw speed was 3 rpm. The spinneret for multifilament spinning had 10 holes with diameters of 0.35 mm. The extruded filaments were quenched in air at room temperature and were wound using a winder operating at 80 m min^{-1}.

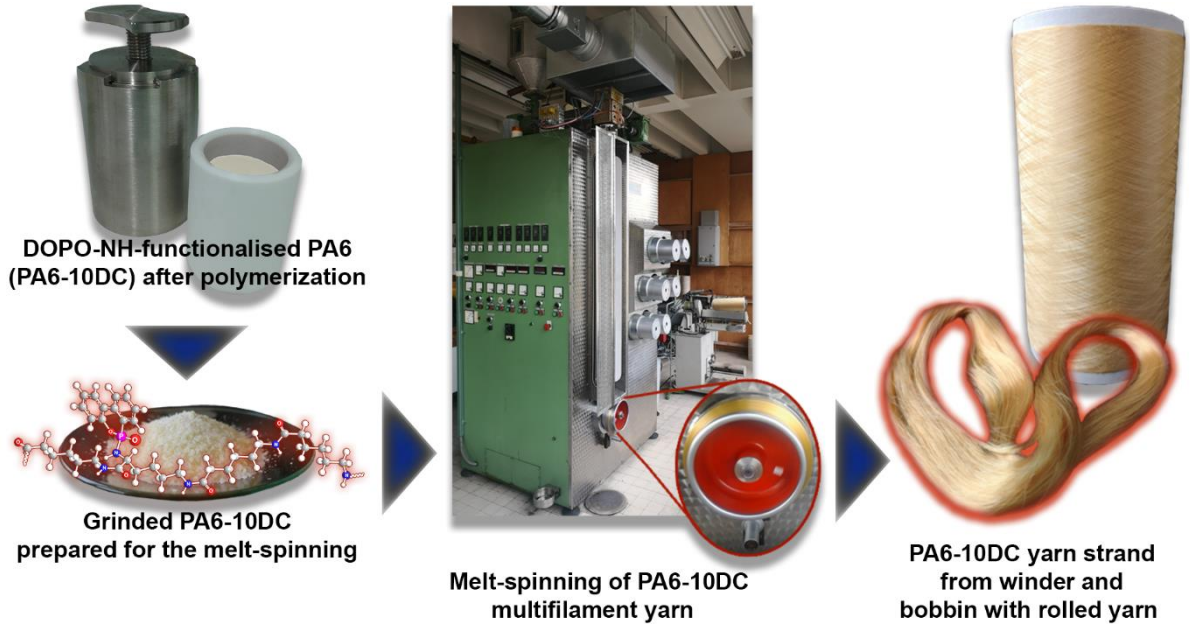

Fig. 1. Illustration of the fabrication process.

2.4. Characterization

^{1}H and ^{31}P NMR spectra were recorded on a Bruker AVANCE NEO 600 MHz NMR or on a Varian 300 MHz NMR Unity INOVA. Samples were prepared in deuterated dimethyl sulfoxide (dmso-d6) with tetramethylsilane (TMS) as an internal standard (δ TMS = 0.0 ppm) and/or in HFIP (hexafluoroisopropanol) with deuterated benzene (C_6D_6) as an internal standard. ^{31}P was calibrated relative to the signal of 85% H_3PO_4.

Ubbelohde viscometer of size 0a was used in order to measure relative viscosity of three polymer solutions with nominal concentrations of 0.01%, 0.05% and 0.09%. Sample solutions were prepared in 85% COOH and measured at 25.0 °C. Huggins (Eq. 1), Kreamer (Eq. 2) and Solomon-Ciuta (Eq. 3) equations were used to evaluate intrinsic viscosities of samples. The

obtained intrinsic viscosities were used in Mark–Houwink-Sakurada (Eq. 4) equation to give molecular weights named as $M_{Huggins}$, $M_{Kreamer}$ and $M_{Solomon\text{-}Ciuta}$ ($M_{Solomon\text{-}Ciuta}$ represents average molecular weight determined from the three used sample concentrations).

$$\frac{\eta_{sp}}{c} = [\eta] + k_2[\eta]^2 c \quad \text{(Eq. 1)}$$

$$\frac{\ln \eta_{rel}}{c} = [\eta] + k_1[\eta]^2 c \quad \text{(Eq. 2)}$$

$$[\eta] = \frac{\left[2\cdot(\eta_{sp} - \ln \eta_{rel})\right]^{1/2}}{c} \quad \text{(Eq. 3)}$$

$$[\eta] = K\mathrm{M}^{\alpha} \quad \text{(Eq. 4)}$$

In the equations, $[\eta]$ represents intrinsic viscosity (dL/g), η_{sp} specific viscosity (/), η_{rel} relative viscosity (/), c is solution concentration (g/dL), K is Mark–Houwink-Sakurada constant (0.000226 dL × mol/g^2) and α is scalar equal to 0.82 and related to stiffness of polymer chains in solvent. Relative viscosities and actual concentrations of sample solutions are presented in the supporting material (Table S1, Figures S16-S18).

Differential scanning calorimetry (DSC) was employed for measuring the melting (T_m) and crystallization (T_c) temperatures using a Mettler Toledo (CH) DSC1 instrument operating from 25 to 230 °C (or just above T_m of each sample) with heating and cooling rates of 10 °C/min in a nitrogen atmosphere (30 mL/min flow rate) and using aluminum-standard 40 µL crucibles with a pierced lid. The second heating runs were analyzed to determine the melting temperatures of each sample.

Thermogravimetric (TG) analyses of 10 mg samples in either air or nitrogen atmosphere at a gas flow rate of 50 mL/min were performed with a Mettler Toledo (CH) TGA/DSC1 Thermogravimetric Analyser from 25 to 800° C with a heating rate of 10 °C/min in open 150 µL platinum pans. Blank curves were subtracted for all measurements. Alternatively, TGA (SDT 2960, TA Instruments) was coupled with infrared spectroscopy (Nicolet iS10 by Thermo-Scientific); these analyses were carried out in a nitrogen atmosphere.

Scanning electron microscopy (SEM) and energy-dispersive X-ray spectroscopy (EDS) were performed on an SEM Cambridge 360 microscope equipped with an energy dispersive X-ray spectrometer (EDS) INCA 250. The samples were coated with a Cr layer in order to make them electrically conductive.

The tensile properties of the PA6(f) and PA6-10DC(f) multifilament yarns were tested on an Instron 5567 dynamometer in accordance with SIST ISO 2062:1997. For this purpose, the PA6(f) and PA6-10DC(f) multifilament yarns were wound onto bobbins at a 132 and 156 m min^{-1} speed, respectively, wherein they were partially drowned. The method was adjusted so that the gauge length was 100 mm and the deformation rate was 350 m min^{-1}. The linear densities of the partially oriented PA6 and PA6-10DC filament yarns were 386 and 481 dtex, respectively.

The standard vertical flame spread test (ASTM D6413) was performed on fiber strand samples (approximately 12.5 cm long, 1.5 cm wide, and 1.2 cm thick), which were prepared by twisting several filaments together.

Cone calorimetry (Fire Testing Technology, FTT) tests were performed using knitted fabric samples (100 cm × 100 cm) under an irradiative heat flux of 35 kW m^{-2} in horizontal configuration. The fabrics were placed in a sample holder and maintained in the correct configuration by a metallic grid. Time to ignition (TTI), heat release rate (HRR), total heat release (THR), peak of HRR (PHRR), and effective heat of combustion (EHC) were measured. Total smoke release (TSR), the average specific extinction area (SEA), CO, and CO_2 yield ([CO] and [CO_2]) were also evaluated.PA6(f) and PA6-10DC(f) knitted fabric samples with a right–right structure were prepared from the filament yarns wound on bobbin on a hand knitting machine RIMACH operating with 10-gauge needles. For each sample, three multifilament yarns were used for knitting.

3. Results and discussion

3.1. Synthesis strategy of DOPO-A-CLM and PA6-xDC

In this research, a unique approach for the synthesis of flame retardant DOPO-NH-functionalized PA6 (PA6-xDC) is presented. For this purpose, the DOPO-functionalized *α*-amino-*ε*-caprolactam molecule (DOPO-A-CLM) was first synthesized and used as a co-monomer with CLM in the polymerization process, since DOPO-A-CLM is compatible with the nature of CLM and its polymerization conditions. As the name of the DOPO-A-CLM molecule suggests, it consists of two structural parts, DOPO and CLM, and the bond between them is established by phosphonamidate bonding.

The DOPO-A-CLM molecule was prepared by reaction of A-CLM with DOPO species. Initially, A-CLM was prepared by converting L-lysine into A-CLM through an intermolecular condensation/cyclization reaction (Scheme 1a) [6]. Since the reaction in butanol at 155 °C in the presence of Al_2O_3 favors an intramolecular over an intermolecular condensation reaction, the reaction preferentially leads to cyclic amide A-CLM over oligomeric or polymeric polyamide linear structures. The use of Al_2O_3 as an efficient water absorber is crucial for achieving a high degree of conversion and a high-yield reaction process (70% isolation yield). The applied synthesis approach for the preparation of A-CLM is classified as green and renewable, since the main component L-lysine is one of the essential amino acids abundant in nature (animal and plant organisms) [27]. Industrial lysine is mainly produced by microbiological fermentation of sugary feeds, and current research is focused on increasing the conversion yield [28]. Butanol, which is used as a solvent in this process, is considered an environmentally friendly and potentially bio-based material [29,30].

The functionalization of A-CLM with DOPO was carried out by the Atherton–Todd reaction under two different synthesis conditions (Scheme 1b). In the first case, SO_2Cl_2 was used as chlorinating agent. However, the release and capture of SO_2 gas as a by-product of the chlorination reaction poses a financial and possibly an environmental risk in industrial-scale synthesis. To circumvent the aforementioned risk, a second synthesis approach using *N*-chlorosuccinimide (NCS) as a chlorinating agent was used as an alternative, which is more environmentally friendly and greener than SO_2Cl_2 [31]. Moreover, the by-product after the reaction is succinimide, which can be regenerated to NCS. Although in this latter approach the reaction yield was reduced to 50%, adjusting the reaction conditions allowed for an increase in the reaction yield. Nevertheless, this new approach proved the possibility of using NCS as a more environmentally friendly alternative to the chlorinating agent in DOPO-A-CLM synthesis with additional potential for cost savings, as the SO_2 capture and conversion technology is not required.

3.2. Characterization of DOPO-A-CLM

3.2.1. NMR characterization of DOPO-A-CLM

The successful synthesis of DOPO-A-CLM was confirmed by ^{1}H and ^{31}P NMR analyses. The comparison of the ^{1}H spectra of DOPO-A-CLM and the initial compound A-CLM (Fig. 2) reveals significant differences in the molecular structure of these two molecules. The major difference is the presence of aromatic signals in DOPO-A-CLM, corresponding to DOPO functionalization (marked as Ar in Fig. 2). The second obvious and important difference includes the chemical shift and the change in multiplicity for the proton bound to the alpha carbon (marked with number 2 in Fig. 2). The signal shifted from 3.55 in A-CLM to 5.50 ppm in DOPO-A-CLM, while the multiplicity changed from *d* to *dd*, indicating the presence of the

second coupling center with ½ spin, such as ^{31}P. All the changes observed in ^{1}H NMR are logical consequences of successful chemical bond formation between P and N atoms of DOPO-Cl and A-CLM molecules. The presence of ^{31}P was further confirmed by the ^{31}P NMR spectrum shown in Fig. S3.

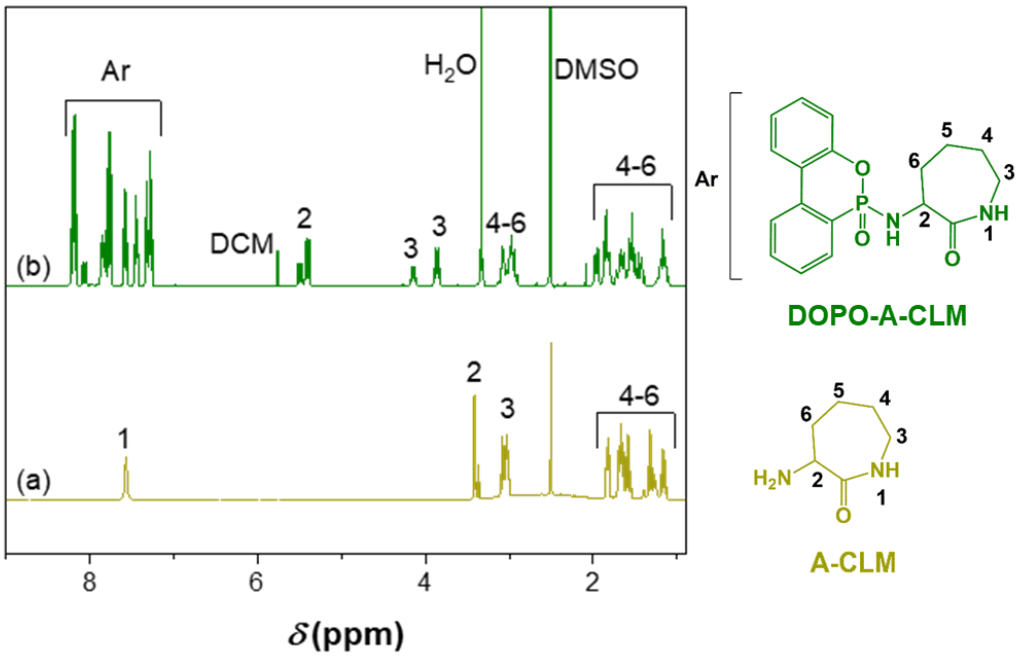

Fig. 2. ^{1}H NMR spectra of A-CLM (a) and DOPO-A-CLM (b).

A closer examination of the ^{1}H NMR (Fig. 3) and ^{31}P NMR (Fig. S3) spectra revealed that DOPO-A-CLM consists of two diastereomeric species, identified as DS-I and DS-II (Fig. 4). The diastereomeric mixture is a consequence of the two chiral centers in the DOPO-A-CLM molecule, the first originating from the A-CLM molecule (alpha positioned C atom next to the carbonyl group) and the second originating from the DOPO molecule (phosphorous atom). Considering that the lysine used as the initial reactant for the preparation of A-CLM was natural L-Lysine, its *S*$_C$ configuration was retained in the synthesized A-CLM product. On the other hand, the phosphorous atom introduced by the DOPO bond was racemic (50:50 *RP*/*SP* configuration), which accounted for the appearance of diastereomeric compounds classified as *R*$_P$*Sc* and *S*$_P$*Sc* (Fig. 4). The obtained diastereomeric products were further selectively

crystallized and characterized by ^{1}H and ^{31}P and DSC analysis. Although the absolute configuration of the diastereomers was not determined, their characteristic differences can be identified and described.

Though the differences between the diastereomers found in the ^{1}H NMR spectrum were quite significant (Fig. 3), there are some signals that stand out more than the others and could be classified as characteristic signals for the two diastereomers. In particular in the aromatic region at 8.06 ppm (1 in Fig. 3), the characteristic (isolated) multiple signal integrated for 1 proton and belonging to DS-I can be seen. Furthermore, signals representing the proton bound to α-C related to the CO group in the ε-caprolactam ring were found close to each other at 5.49 and 5.43 ppm (2 and 2' in Fig. 3) for DS-I and DS-II, respectively. The signals in the two diastereomers belonging to the proton bound on δ-C, which is attached to the amide group of the ε-caprolactam ring, exhibited significantly different chemical shifts; the signals at 4.15 and 3.88 ppm (3 and 3' in Fig. 3) correspond to DS-I and DS-II, respectively. The signals at 1.97 and 1.43 ppm, attributable to some of the aliphatic protons of the ε-caprolactam ring, appeared to be isolated and therefore characteristic of DS-II (4' and 5' in Fig. 3). Although many of the signals appear to be characteristic of individual diastereomers, only those at 4.15 and 3.88 ppm (3 and 3' in Fig. 3) provide reliable integration in the case of DS-mix, where one of the diastereomers is present in significant excess relative to the other. The quantitative evaluation of the ^{1}H NMR signals corresponding to DS-I also revealed the traces of DS-II with a DS-I/DS-II ratio equal to 93:7.

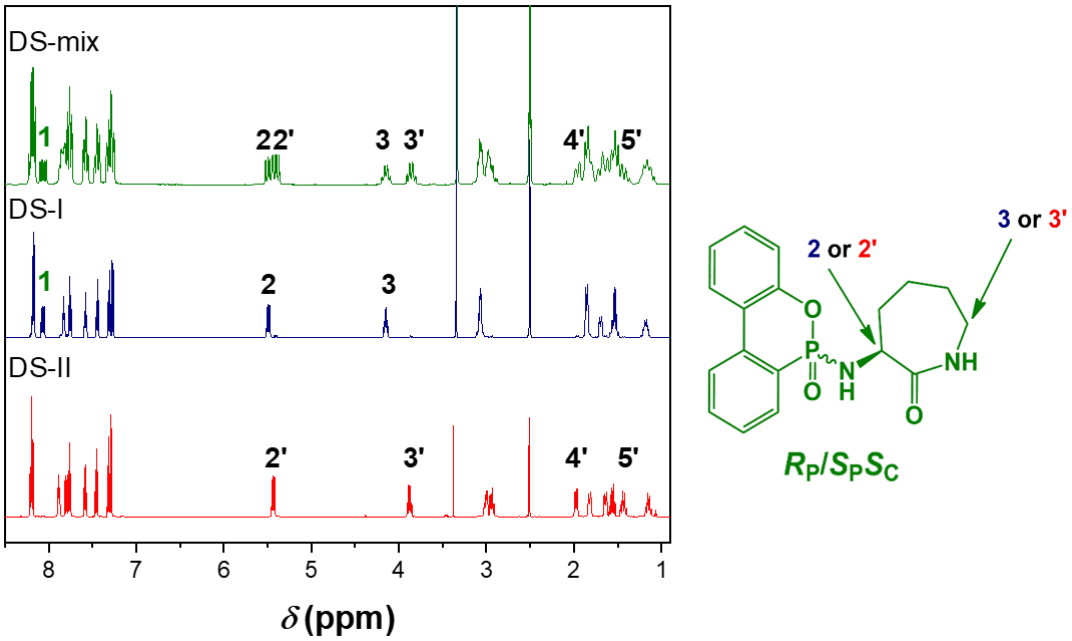

Fig. 3. ^{1}H NMR spectra of DOPO-A-CLM diastereomers DS-I, DS-II, and their 50:50 mixture, DS-mix.

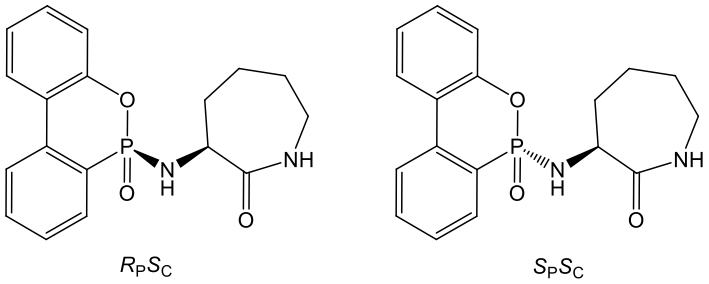

Fig. 4. Two possible diastereomers of DOPO-A-CLM.

3.2.2. DSC characterization of DOPO-A-CLM

Based on DSC analysis (Fig. 5), CLM was found to have the lowest melting point (72 °C), while the highest melting point was observed in the case of DS-II (190 °C), which is significantly higher compared to DS-I (melting point of 123 °C). Interestingly, in the case of a 50:50 mixture of DS-I and DS-II (DS-mix in Fig. 5), there is virtually no detectable endothermic peak that corresponds to the melting of the mixture. The reason for the above phenomena is

probably due to the amorphous nature of DS-mix. Amorphous substances normally become completely liquid over a wider temperature range and are therefore not detected as an endothermic effect by the DSC instrument. Due to this significant difference between the DSs, it is evident that DSC analysis is much more sensitive to the impurity profile than NMR. The observed additional melting peak in the case of DS-I, which occurs at 133 °C, can be attributed to impurities, e.g., traces of DS-II, affecting the melting behavior of the pure DS-I compound. This is consistent with the results of ^{1}H NMR analysis discussed earlier.

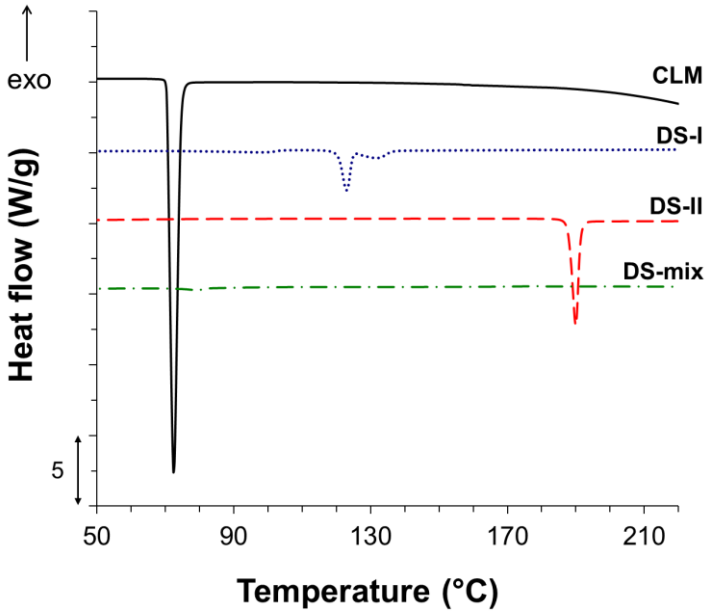

Fig. 5. DSC curves of ε-caprolactam (CLM), DOPO-A-CLM diastereomers DS-I, DS-II, and their 50:50 mixture, DS-mix.

3.3. Characterization of DOPO-NH-functionalized PA6 (PA6-xDC)

3.3.1. NMR characterization of PA6-xDC

The structure of DOPO-NH-functionalized PA6 was confirmed by ^{1}H NMR spectroscopy (Fig. 6), where the presence of signals of aromatic protons indicated the

chemically bound DOPO as a pendant group of the PA6 backbone. The presence of aliphatic proton signals confirmed the opening of the ε-caprolactam ring in the DOPO-A-CLM, while ^{1}H NMR signals of the DOPO-A-CLM molecule were not detected, mainly due to the large molar difference between the monomers used in the co-polymerization reaction (CLM/DOPO-A-CLM was 27:1 in the case of PA6-10DC). Therefore, the aliphatic signals are probably hidden by those belonging to the opened form of CLM.

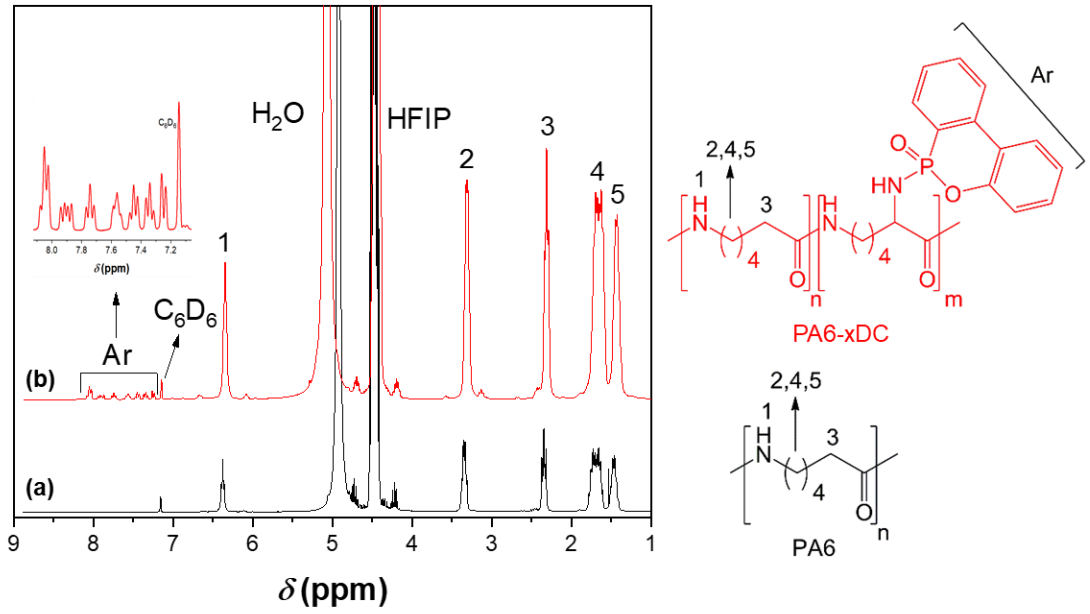

Fig. 6. ^{1}H NMR spectra of PA6 (a) and PA6-10DC (b).

Quantitative analysis of the ^{1}H NMR signals allowed determination of the molar ratio of the DOPO-A-CLM incorporated into the backbone of PA6-xDC (Table 1) based on the aromatic signals (Fig. 6b). The results show that the weight fraction of the incorporated DOPO-A-CLM was slightly higher than the added weight fraction, which was a consequence of the PA6-xDC purification process in water and DCM. Namely, the purification process allowed the removal of unreacted DOPO-A-CLM as well as of the water-soluble CLM-based oligomers.

Obviously, this extraction process slightly increased the concentration of the chemically bound DOPO group, mainly due to the complete extraction of unreacted CLM. The fact that even after the extensive extraction of the samples, the DOPO concentration in the sample remained high proves that the DOPO functionality is chemically bound into the PA6 backbone. Furthermore, this indicates that the DOPO is evenly distributed throughout the PA6 matrix, otherwise a lower level of DOPO functionality would be expected in the final sample due to the leaching of smaller fragments.

The chemical incorporation of the DOPO functionality into the PA6 backbone affected the molecular weight, M_{mean}, of the samples, which gradually decreased from neat PA6 towards PA6-15DC (Table 1, Table S2, Fig. S19). This suggests that the integration of DOPO-A-CLM into the PA6 matrix hindered the chain growth of PA6 backbones.

Table 1. Amounts of added and chemically incorporated DOPO-A-CLM, CLM/DOPO-A-CLM molar rations in different samples of PA6-xDC and the mean value of molecular weight, M_{mean}, calculated form $M_{Huggins}$, $M_{Kreamer}$ and $M_{Solomon-Ciuta}$ (Table S2).

Sample	**DOPO-A-CLM added (wt %)**	**Reaction yield (%)**	**DOPO-A-CLM incorporated (wt %)**	**CLM/ DOPO-A-CLM (molar ratio)**	**M_{mean} (g/mol)**
PA6	0	88	0	100	15387
PA6-7DC	7	88	7.56	40.5	12375
PA6-10DC	10	88	11.40	27.2	10516
PA6-15DC	15	85	16.28	15.9	9316

3.3.2. DSC and TGA characterization of PA6-xDC

A comparison of thermal properties between PA6-xDC and pure PA6 was investigated using DSC and TGA (Figs. 7-10, Tables 2-5). The DSC curves are shown in Fig. 7, and the results for the characteristic melting, T_m, and crystallization, T_c, temperatures, and the degree of crystallinity, *Xc*, are summarized in Table 2. The endothermic melting peaks from the second heating runs corresponding to the melting of the original crystallites of the PA6, PA6-7DC, PA6-10DC, and PA6-15DC samples appeared at 222, 212, 208, and 200 °C, respectively. This trend suggests hindered hydrogen bonding between the PA6 backbones caused by the bulky DOPO-NH– pendant group, which, being chemically bonded to the PA6 backbones, may affect their linear alignment required for the hydrogen bonding and the crystalline phase formation. The second melting peak, which occurred at 215, 206, 201, and 193 °C for the PA6, PA6-7DC, PA6-10DC, and PA6-15DC samples, respectively, was caused by the non-isothermal recrystallization in the DSC analyses and can be attributed to both the γ-crystalline phase and α-crystallites of different sizes and perfection. As the chemically bonded DOPO-NH– pendant group affected the packing of the PA6 backbones, T_m and X_c also decreased as the concentration of the incorporated DOPO-A-CLM increased.

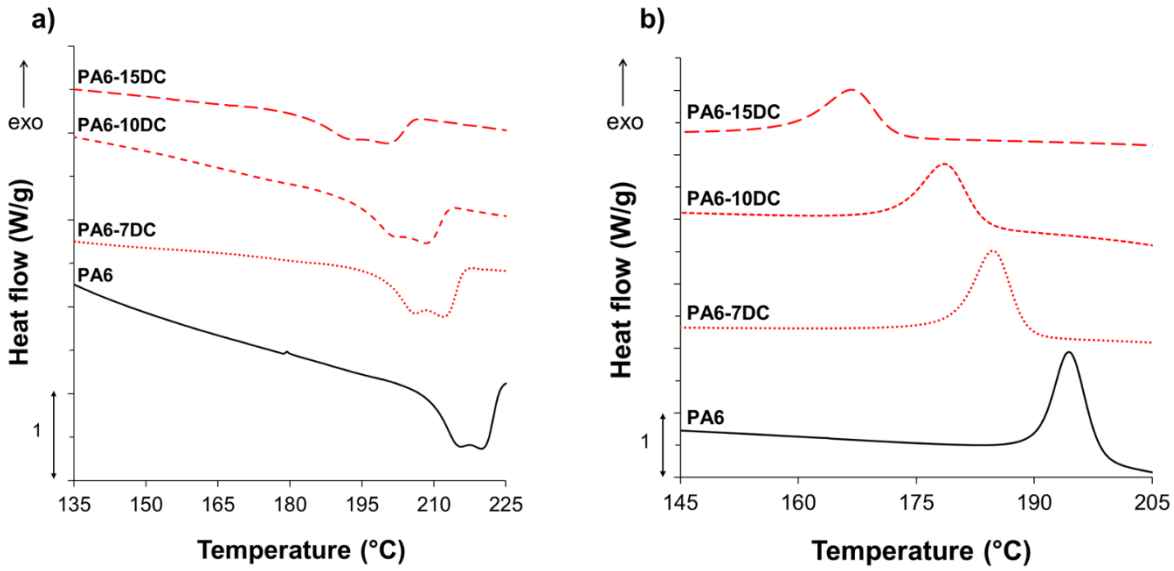

Fig. 7. DSC curves in nitrogen: (a) the second heating run; (b) the first cooling run.

Table 2. Melting temperature, T_m, enthalpy, ΔH_m, crystallization temperature, T_c, and the degree of crystallinity, X_c, of PA6 and PA6-xDC in nitrogen.

Sample	T_m (°C)	ΔH_m (J/g)	T_c (°C)	X_c (%)
PA6	215 / 222	-56.08	196	29.4
PA6-7DC	206 / 212	-46.29	185	28.5
PA6-10DC	201 / 208	-41.99	179	25.9
PA6-15DC	193 / 200	-31.32	167	19.8

To gain insight into the effect of the DOPO-NH– pendant group chemically bonded to the PA6 backbone on the thermal stability of the polymer, the thermal decomposition process of the DOPO-A-CLM, PA6, PA6-7DC, PA6-10DC and PA6-15DC samples were investigated by TGA in a nitrogen atmosphere (Fig. 8 and Table 3). The results showed that the thermal decomposition of DOPO-A-CLM started at about 279 °C (the temperature at 5% weight loss, $T_{5\%}$) and proceeded through two decomposition steps. The second decomposition step on the DOPO-A-CLM thermogravimetric curve, where 69.9% weight loss occurred, was considered as the main decomposition step with the temperature of the maximum of the weight loss rate (T_{max1}) of 417 °C. This step was preceded by an initial decomposition step with the temperature of the maximum of the weight loss rate of 297 °C and the weight loss of 9.1%. Considering that the temperature of the maximum in the weight loss rate for ε-caprolactam is about 120 °C [32] and that ε-caprolactam decomposes without residue, the bridging of DOPO and ε-caprolactam with the –NH– group significantly increased the thermal stability of ε-caprolactam. This finding also confirmed the successful functionalization of the ε-caprolactam ring. It can be assumed that the cleavage of the C–N in the bridge between the ε-caprolactam and DOPO-NH– group

ring occurs concurrently with the cleavage of the peptide C(O)–NH bond or the alkyl-amide NH–CH_2 bond. Since the weight loss during the decomposition step, which preceded T_{max1}, was equal to 9.1%, it can be assumed that some low-molecular-weight gaseous products were formed during this step. However, the chemical interactions occurring between the decomposition products increased the thermal stability of DOPO, as the initial decomposition temperature of DOPO alone is at about 237 °C [18]. Further interactions between the decomposition products formed during the thermal decomposition apparently induce some crosslinking reactions, as the residue fraction of about 10% remains stable in the temperature range from 500 to 800 °C. Since the initial decomposition temperature of DOPO-A-CLM is 279 °C, it can be suggested that this co-monomer could be safely processed at temperatures up to, for example, 260 °C.

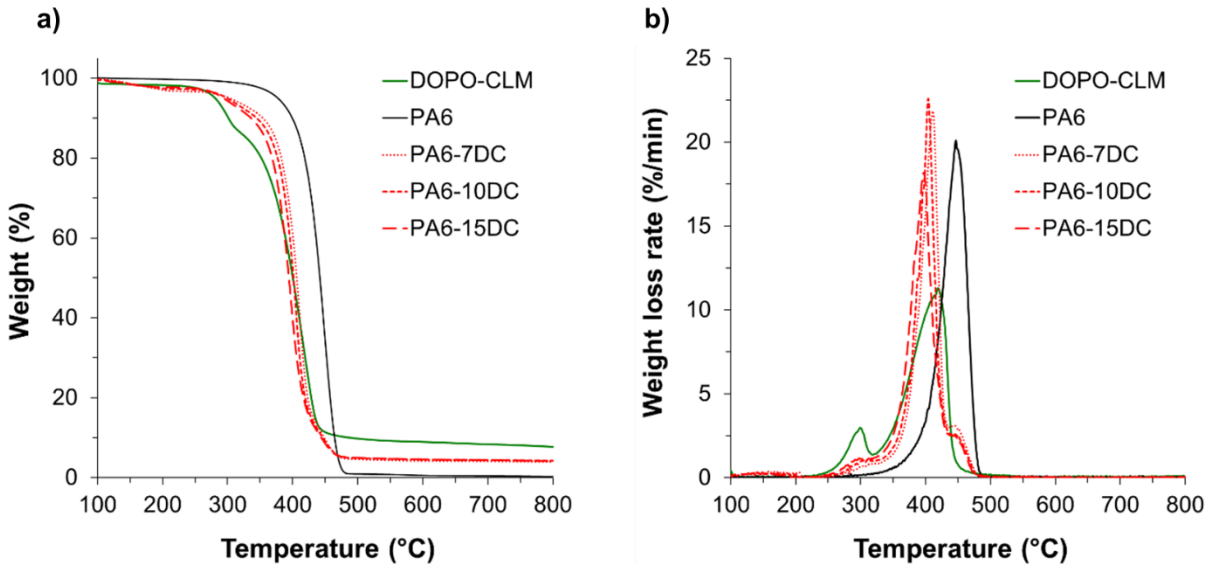

Fig. 8. (a) TG and (b) dTG graphs of DOPO-A-CLM, PA6, PA6-7DC, PA6-10DC, and PA6-15DC analyzed in a nitrogen atmosphere.

Table 3. TG data obtained in a nitrogen atmosphere.

Sample	$T_{5\%}$ (°C)	T_{max1} (°C)	Residue at T_{max1} (%)	T_{max2} (°C)	Residue at T_{max2} (%)	Residue at 500 °C (%)
DOPO-A-CLM	279	417*	30.1	-	-	9.8
PA6	379	449	40.5	-	-	1.0
PA6-7DC	303	412	39.8	448	10.7	4.6
PA6-10DC	301	405	43.8	447	10.3	4.9
PA6-15DC	295	399	44.8	448	9.7	5.0

* In the case of DOPO-A-CLM, this step was preceded by the initial decomposition step at 297 °C.

While the decomposition of PA6 under a nitrogen atmosphere is a one-step process, the thermal decomposition of PA6-7DC, PA6-10DC, and PA6-15DC samples was characterized by two decomposition steps, T_{max1} and T_{max2}. Chemical bonding of the DOPO-NH– pendant group to the PA6 backbone shifted $T_{5\%}$ and T_{max1} of the PA6-7DC, PA6-10DC, and PA6-15DC samples toward lower temperatures compared to those of the PA6 sample by 76, 78, and 84 °C, respectively, for $T_{5\%}$ and by 37, 44, and 50 °C, respectively, for T_{max1} (Fig. 8 and Table 3). This phenomenon intensified when the concentration of the incorporated DOPO-A-CLM was increased. The decrease in $T_{5\%}$ and T_{max1} could be attributed to the accelerated start of the thermal decomposition of PA6 due to the decomposition of organophosphorus group, as already reported in the literature [19,33] with respect to the MW of the studied polymers. Since the dTG curves of the PA6-7DC, PA6-10DC, and PA6-15DC samples also show shoulder at about 300 °C, as in the case of DOPO-A-CLM (Fig. 9b), it can be assumed that thermal decomposition of the PA6-7DC, PA6-10DC, and PA6-15DC samples is initiated with the cleavage between the DOPO-NH– group and the PA6 backbone. From the heat flow rates, which were measured

simultaneously with the weight change during thermal decomposition (Fig. S14), it can be concluded that DOPO-A-CLM decomposes exothermically, indicating the exothermic cleavage of the C–N in the bridge between the PA6 backbone and the DOPO-NH– group. This could also promote the start of the thermal decomposition of PA6-7DC, PA6-10DC, and PA6-15DC at a lower temperature compared with that of PA6.

Furthermore, the occurrence of the second decomposition step, T_{max2}, in the temperature range 447-448 °C for samples PA6-7DC, PA6-10DC, and PA6-15DC may coincide with T_{max1} of PA6. This phenomenon could be explained by a partial block structure in the PA6-7DC, PA6-10DC, and PA6-15DC polymers [34]. Moreover, the increase in char residues at 500 °C from 1% for PA6 to 4.6, 4.9, and 5.0% for the PA6-7DC, PA6-10DC, and PA6-15DC samples, respectively, suggests that the DOPO-NH– pendant functionality promotes the crosslinking reactions in the condensed phase of the polymer during the main decomposition step.

To further understand the decomposition pathway, an investigation of the gaseous products of the thermal decomposition of PA6 and PA6-10DC was carried out using TG-FTIR. The evaluated results for the gaseous products formed are shown in Fig. 9, while the assignments of the detected FTIR bands are collected in Table 4. The decomposition of PA6 in a nitrogen atmosphere was followed by the generation of ε-caprolactam, NH_3, CO, CO_2, and H_2O, as well as primary aliphatic amines and hydrocarbons, and carboxylic acid monomer (Fig. 9a and Table 4). These products were confirmed in the spectra collected at $T_{5\%}$, T_{max1}, and 500 °C. Spectra corresponding to the PA6-10DC sample showed significantly reduced band intensities (2400–2266 cm^{-1}, 668 cm^{-1}) in the case of CO_2 emission compared to PA6. The source of the CO_2 emission bands is probably the decarboxylation reaction of the acidic ends that occurs during the hydrolytic cleavage of the peptide C(O)–NH bonds [34]. Therefore, it can be assumed the cleavage of the peptide C(O)–NH bonds and, thus, the depolymerization of the PA6 backbone was inhibited during the thermal decomposition of the PA6-10DC sample in

comparison to that of PA6. This was confirmed by the disappearance of the band at 1761 cm^{-1} in the spectra of the PA6-10DC sample recorded at $T_{5\%}$, T_{max1}, and 500 °C, where the band at 1761 cm^{-1} represents the C=O stretching vibration belonging to the carboxylic acid monomer. Additional bands at 1234, 1219, 1095, and 753 cm^{-1}, which appeared in the spectra of PA6-10DC at 500 °C, are assigned to the phosphorus compounds (Table 4), confirming the existence of the phosphorus-active species in the gas phase. Moreover, the time-evolution profiles for the total absorption intensity and the intensity of the peaks characteristic of ε-caprolactam and ammonium (Fig. 9b,c,d) confirmed that the DOPO-NH– pendant functionality initiated the release of the gaseous products of the decomposed PA6 at lower temperatures with respect to PA6.

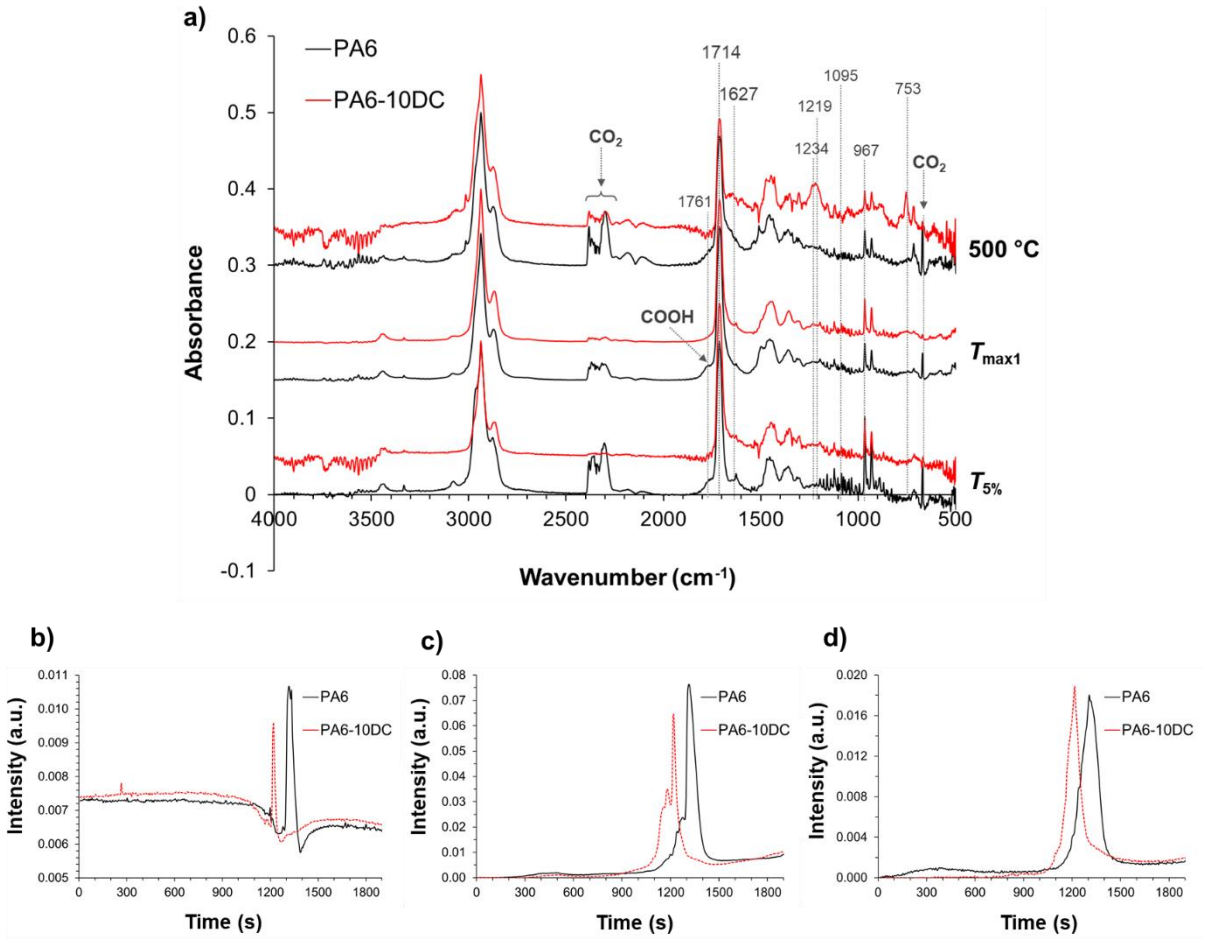

Fig. 9. (a) FTIR spectra of the evolved gases during the thermal decomposition of the PA6 and PA6-10DC at $T_{5\%}$, T_{max1}, and 500 °C; (b) the total absorbance intensity calculated as the root mean square (RMS) plotted as as a function of decomposition time; (c) intensity of the band at 1714 cm^{-1} representing the ε-caprolactam peak plotted as a function of decomposition time; (d) intensity of the band at 967 cm^{-1} representing ammonium peak plotted as a function of decomposition time.

Table 4. FTIR peak assignment [35,36].

Wavenumber (cm^{-1})	Vibration assignment	Functional group or compound
3441, 3332	amine N-H stretching vibrations	Primary aliphatic amines
2938, 2873	CH_2 stretching vibrations	ε-caprolactam
1713	C=O stretching vibration in the CONH group (Amide I)	
2400 – 2266, 668	CO_2 asymmetric stretching and bending vibrations	CO_2
2185, 2107	CO stretching vibration, doublet	CO
1761	C=O stretching vibration band in the COOH	Carboxylic acid monomer
1470-1360	C-H deformation vibrations	Hydrocarbons
964, 930	NH_3 bending vibrations	NH_3
753	P-C stretching vibration	Organic phosphorus
1095	P-O stretching vibration	Organic phosphorus
1219, 1234	P=O stretching vibration, doublet	Organic phosphorus

The results of thermo-oxidative decomposition may give an indication of the ability of the polymer to resist combustion since the flaming combustion is preceded by interaction of the polymer with heat and oxygen. When heat-induced decomposition is assisted by oxygen, the decomposition products react chemically with oxygen, shifting the onset of polymer decomposition to lower temperatures compared to the decomposition under a nitrogen atmosphere. The thermo-oxidative decomposition of PA6, PA6-7DC, PA6-10DC, and PA6-15DC samples in an air atmosphere confirmed that the chemically bonded DOPO-NH– pendant group caused a shift of $T_{5\%}$ (Fig. 10a, Table 5) to lower values compared to PA6. The T_{max1} of PA6-7DC, PA6-10DC, and PA6-15DC samples also decreased as compared to PA6, but the DOPO-NH– group significantly decreased the rate of weight loss during the first main decomposition step, resulting in increased residues at T_{max1} and 500 °C (Table 5). Comparing the initial decomposition step for DOPO-A-CLM occurring at 288 °C with the initial decomposition steps for PA6-7DC, PA6-10DC, and PA6-15DC samples occurring at 333, 325 and 320 °C, respectively, it can be observed that the thermo-oxidative stability of the DOPO-NH– functionality bound to the PA6 backbone is more stable compared to that in DOPO-A-CLM. The increased thermo-oxidative stability resulted in about a fourfold higher residue at 500 °C in the case of PA6-15DC compared to PA6. In addition, the increased thermo-oxidative stability of PA6-7DC, PA6-10DC, and PA6-15DC residues shifted T_{max2} to higher temperatures as compared to PA6, leading to the increased char residues in this decomposition step. The increased thermo-oxidative stability of the PA6-7DC, PA6-10DC, and PA6-15DC samples also resulted in decreased heat flow rates (Fig. S15) compared to PA6, which confirmed the successful inhibition of oxidative radicals by the phosphorus radical scavenging species. Additionally, since the $T_{5\%}$ corresponding to DOPO-A-CLM is significantly lower in comparison to the $T_{5\%}$ corresponding to PA6, it could be assumed that the physical

incorporation of DOPO-A-CLM into the PA6 matrix, would cause DOPO-A-CLM to decompose prematurely at temperatures lower than the onset of PA6 decomposition. This would result in the premature evolution of the flame retardant radical species into the gas phase, which would not be able to provide the increased residue at 500°, as was the case with the chemically bonded DOPO-NH–group to the PA6 backbone.The dTG curves of the PA6-7DC, PA6-10DC, and PA6-15DC samples (Fig. 10b) clearly showed an additional third decomposition step occurring above 650 °C, which was not observed for the PA6 sample. This finding can be ascribed to the blocky structure of the PA6-7DC, PA6-10DC, and PA6-15DC samples. Based on the collected evidence, the chemically bonded DOPO-NH– pendant group may provide the flame retardant effect for the PA6 in both gas and condensed phases.

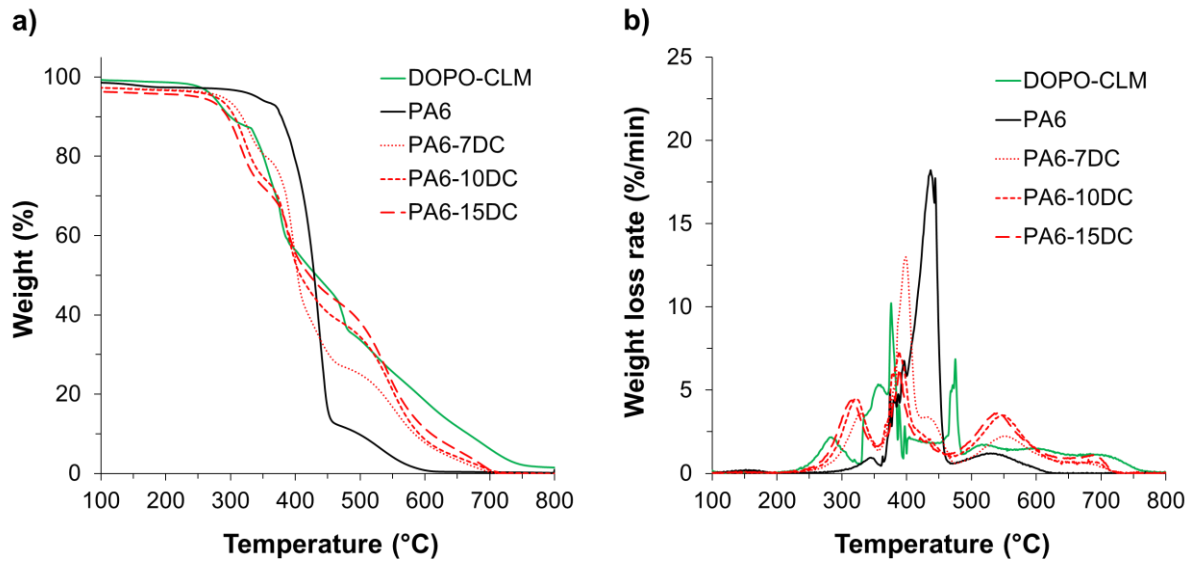

Fig. 10. (a) TG and (b) dTG graphs of DOPO-A-CLM, PA6, PA6-7DC, PA6-10DC, and PA6-15DC samples analyzed in an air atmosphere.

Table 5: TG data obtained in an air atmosphere.

Sample	$T_{5\%}$ (°C)	T_{max1} (°C)	Residue at T_{max1} (%)	T_{max2} (°C)	Residue at T_{max2} (%)	T_{max3} (°C)	Residue at T_{max3} (%)	Residue at 500 °C (%)
DOPO-A-CLM	277	379	66.5	478	39.0	-	-	34.1
PA6	343	449	36.5	527	7.2	-	-	10.0
PA6-7DC	290	403	57.0	552	17.0	656	2.9	25.2
PA6-10DC	280	392	61.1	551	22.0	679	2.2	34.9
PA6-15DC	253	392	61.0	543	26.8	684	2.5	38.8

3.4. Characterization of PA6-10DC(f) filament yarn

3.4.1. Morphology

Some typical SEM images of the PA6(f) and PA6-10DC(f) filament yarns are shown in Fig. 11. A comparison of the PA6(f) and PA6-10DC(f) filament surfaces revealed no significant differences in the surface morphology of the filament yarns. In both cases, the surface was relatively smooth, while oligomeric microfibrils were visible on both the PA6(f) and PA6-10DC(f) filament surfaces. SEM images also showed that the diameter of the PA6-10DC(f) sample was 65.4 ± 2.2 μm, which is slightly larger than that of PA6 (62.7 ± 1.4 μm).

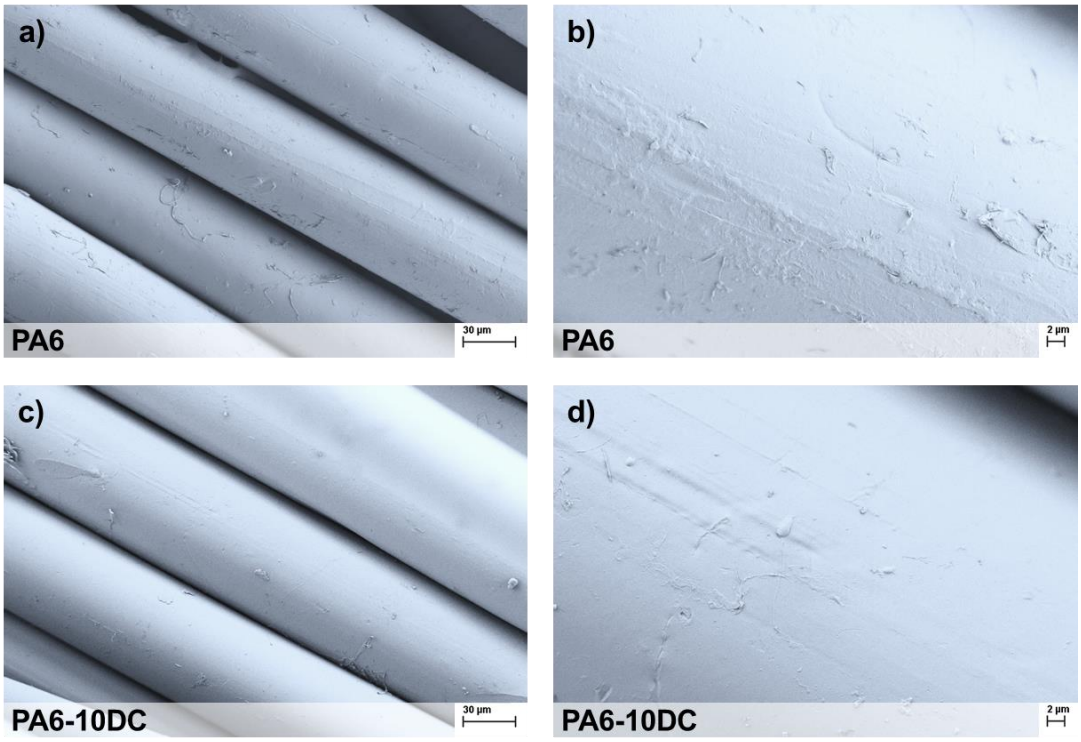

Fig. 11. Typical SEM images of longitudinal views of multifilament yarns: (a,b) PA6(f); (c,d) PA6-10DC(f) (lower (a,c) and higher (b,d) magnification).

3.4.2. Tensile properties

Tensile analysis was performed to evaluate the effects of incorporating the DOPO-NH– functionality on the mechanical properties of the multifilament yarns. The force versus tensile strain curves obtained for the PA6(f) and PA6-10DC(f) samples are shown in Fig. 12a. The results show that the tenacity and tensile strain at break decreased for PA6-10DC(f) compared to PA6(f). This finding can be attributed to the influence of chemically bonded DOPO-NH– functionality as the pendant group in the PA6 backbone, which reduces the H-bonding occurring between the PA6 chains, as well as slowing down the polymer crystallization and orientation. Therefore, further efforts should be made to investigate the chemical systems with a minimal effect on the mechanical properties of PA6 bulk materials. There is also much scope for optimizing the melt spinning process conditions, as they are known to have a direct effect

on the mechanical properties of the filament yarns. However, in this work, it was shown that the PA6-10DC(f) filament yarn could be successfully melt-spun as well as drawn and wound on bobbins (Fig. 12b).

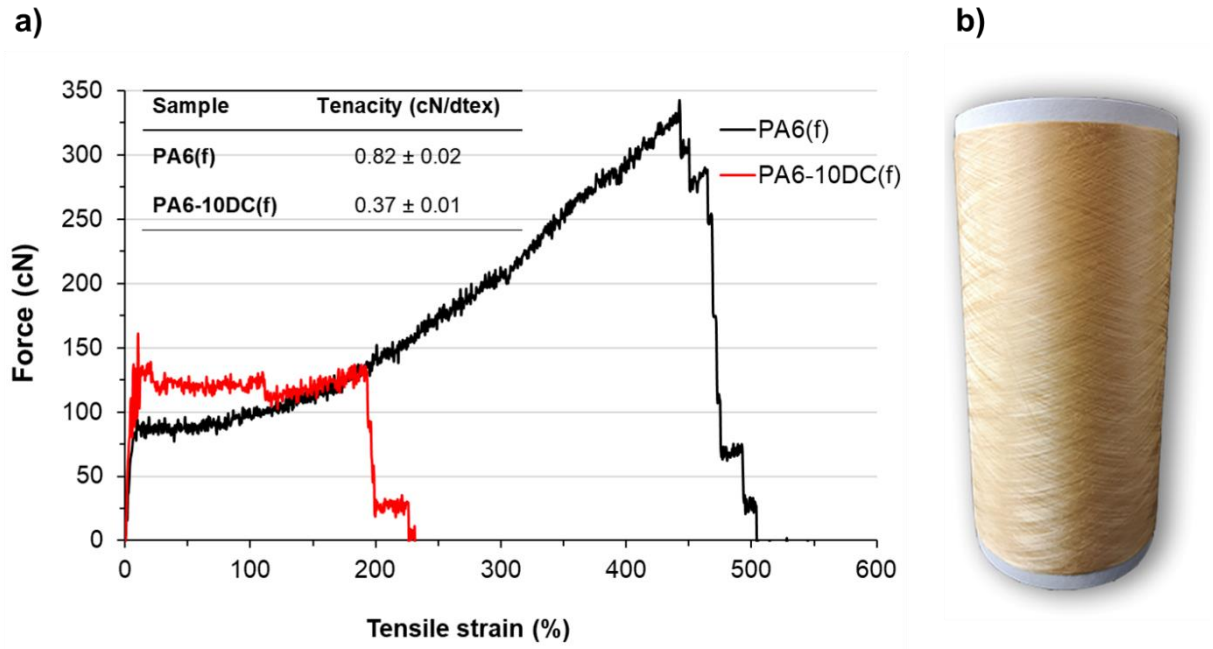

Fig. 12. (a) Force-tensile strain curves; (b) PA6-10DC(f) multifilament yarn wound on bobbin.

3.4.3. Vertical flame spread and forced-combustion tests

The vertical burning behavior of PA6(f) and PA6-10DC(f) filament samples was investigated according to the standardized vertical flame spread test (ASTM D6413); the results are shown in Fig. 13 and Table 6. The high surface-to-volume ratio of the fiber strand samples prolonged the burning and dripping of PA6(f). The flame retardant action of the DOPO-NH– pendant functionality successfully retarded both burning and melt-dripping, and provided self-extinction within 1 s for the PA6-10DC(f) sample (Fig. 13a). Self-extinction occurred immediately after the first drop, which significantly reduced the weight loss.

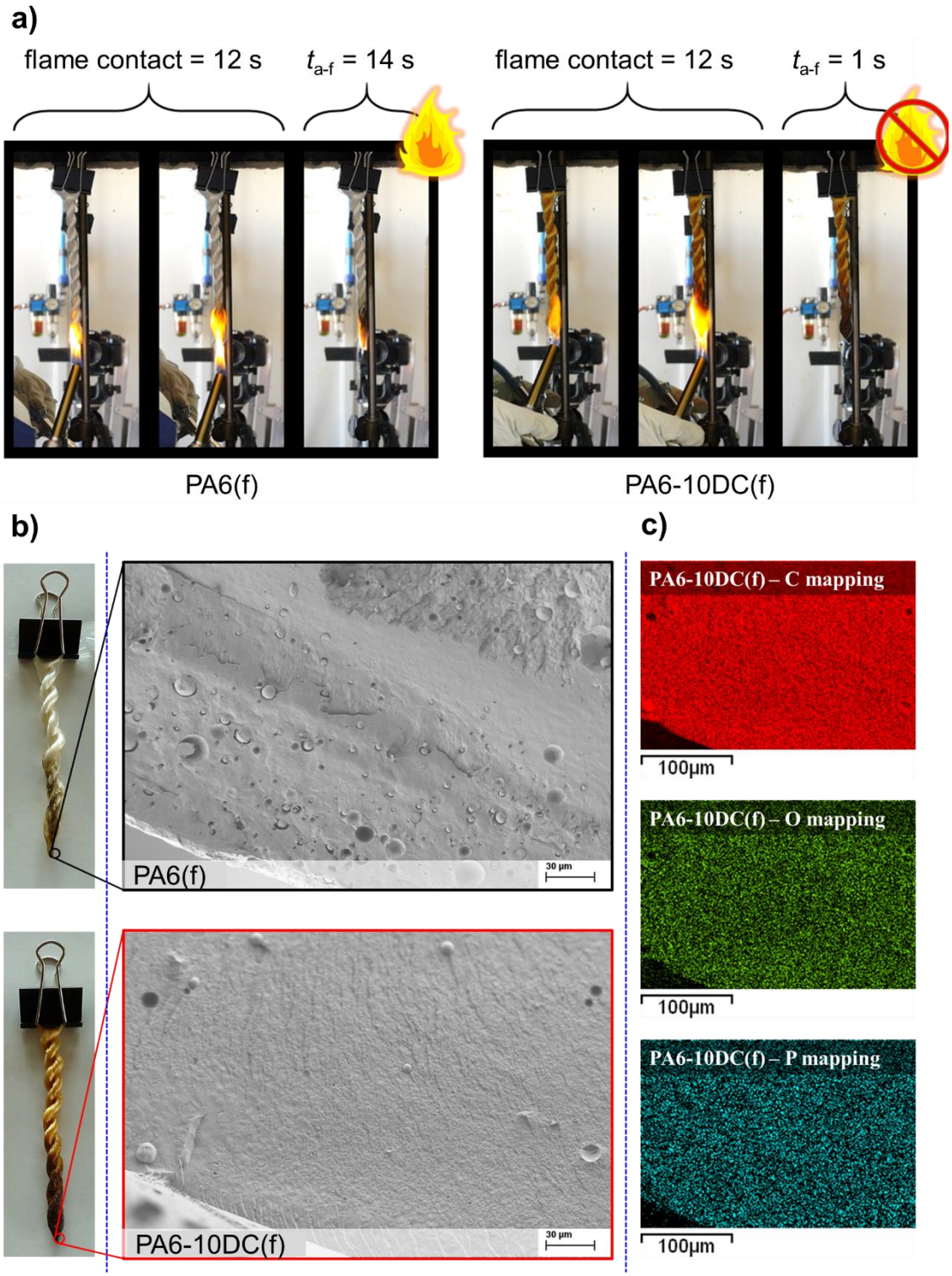

Fig. 13. (a) Snapshot photos from the videos of the ASTM D6143 vertical flame spread testing of the PA6(f) and PA6-DC(f) fiber strand samples and the corresponding residues after testing, (b) SEM images of the polymer bulk near the surface of bottom edge samples being exposed to

the flame, and (c) EDS carbon, oxygen, and phosphorus mapping of the surface of bottom edge of the PA6-DC(f) fiber strand being exposed to the flame.

Some typical SEM images of the polymer bulk spots in close proximity to the charred surfaces of the PA6(f) and PA6-10DC(f) fibre strand residues that were in direct contact with the flame are presented in Fig. 13b. The PA6(f) polymer bulk appeared to be much more porous as compared to that of PA6-10DC(f). The observed voids resulted from the released gases formed during the decomposition of the polymer, which was much more intense in the case of PA6(f) than PA6-10DC(f), which appeared to be much more compact. These results undoubtedly confirm that the thermo-oxidative stability of the PA6 backbone provided by the chemically bonded DOPO-NH– pendant group in the PA6-10DC(f) sample was efficient enough to confer acceptable flame retardant properties to PA6. In addition to the action of the flame retardant radicals in the gas phase during the decomposition of the DOPO-NH– pendant groups, their partial effect in the condensed phase can also be suspected, as the EDS mapping of the PA6-10DC polymer bulk near the surface of the lower edge sample exposed to the flame (Fig. 13c) confirms the presence of phosphorus.

Table 6. The results of the ASTM D6143 vertical flame spread tests performed on PA6(f) and PA6-10DC(f) fibre strand samples.

Sample	$t_{a\text{-}f}$ [a)] (s)	Weight loss (%)	Number of drips
PA6(f)	14	22.5 ± 3.2	12
PA6-10DC(f)	1	3.5 ± 1.1	1

[a)] $t_{a\text{-}f}$ – after flame time.

The resistance of the PA6(f) and PA6-10DC(f) knitted fabric samples to a heat flux of 35 kW/m^2 was investigated by cone calorimetry (Fig. 14, Tables 7 and 8). These results confirmed that the chemically bonded DOPO-NH– pendant functionality decreased the time to ignition (TTI, Table 7) and increased the mean heat release rate (HRR, Fig. 14a) and total heat released (THR, Table 7) of the PA6 polymer. These findings seem to contradict the results from the vertical flame spread tests, as the presence of the chemically bonded DOPO-NH– pendant group in the PA6-10DC(f) sample degrades the forced-combustion behavior of PA6. However, since the forced flaming combustion of polymers in cone calorimetry proceeds as a pyrolysis process with limited oxygen diffusion, the increased HRR, PHRR, and THR could be primarily attributed to the limited condensed phase effect, as the flame retardant DOPO's radicals act primarily in the gas phase [37]. Additionally, the exothermic effect of the cleavage between the DOPO-NH– group and the PA6 backbone, as determined by DSC analyses (Fig. S14) could also additionally degrade the forced-combustion behavior of PA6. The decrease in the mean effective heat of combustion (EHC, Table 7) of the volatiles generated during the decomposition of the PA6-10DC(f) sample compared to that of the PA6(f) indicates inhibited combustion in the gas phase. At the same time, the chemical interactions occurring in the gas phase caused a significant increase of the total smoke release (TSR, Fig. 14b) and the mean specific extinction area (SEA, Table 8) of the PA6-10DC(f) sample compared to those of the PA6(f). This was followed by a 4-hold higher mean [CO] yield and a 30% lower mean [CO_2] yield for the PA6-10DC(f) sample compared to that of the PA6(f) (Table 8).

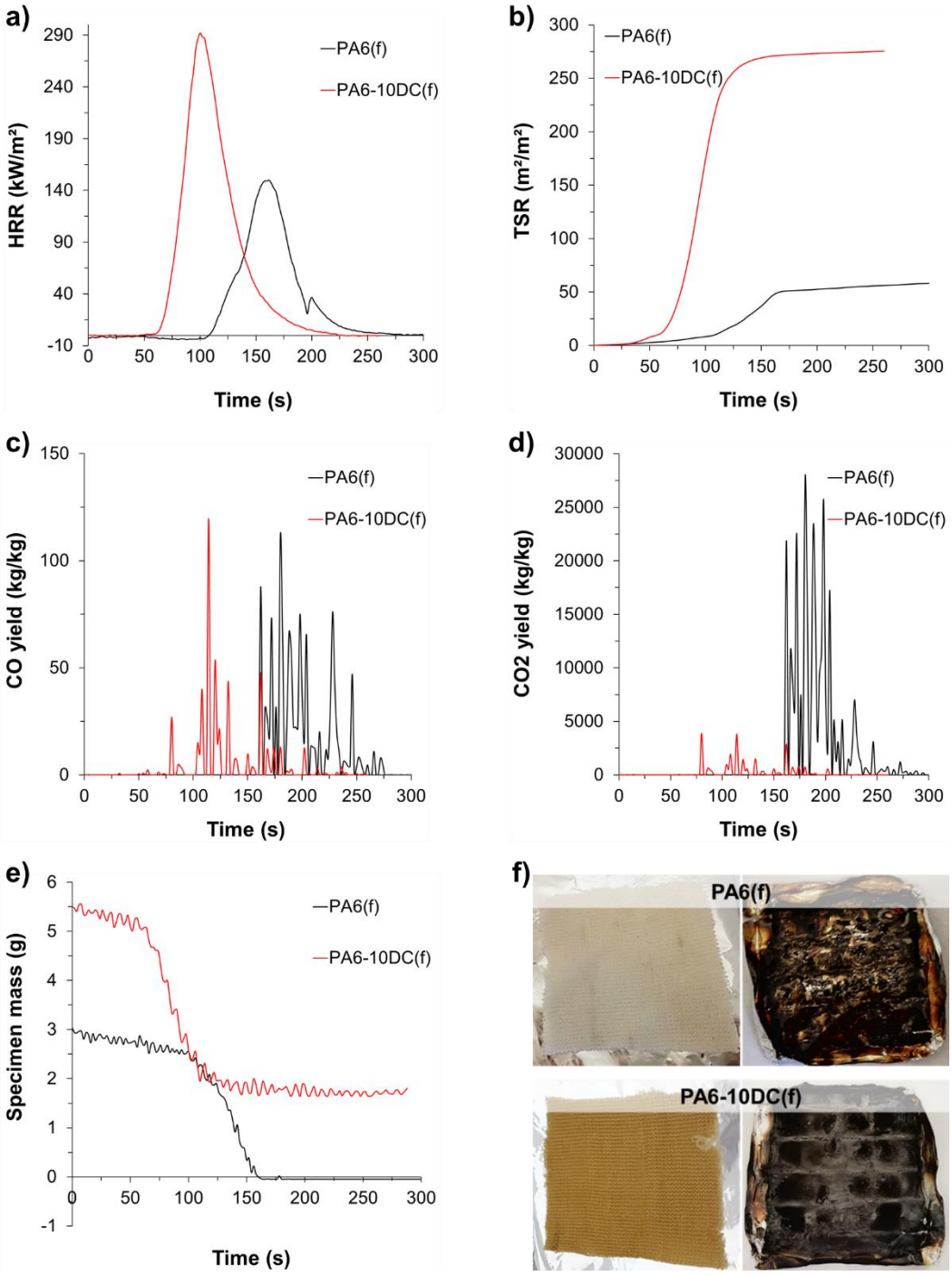

Fig. 14. (a) Heat release rate (HRR) vs. total combustion time, (b) total smoke release (TSR) vs. total combustion time, (c) and (d) carbon monoxide and carbon dioxide yields, respectively, vs. total combustion time, (e) specimen mass loss vs. total combustion time for the PA6(f) and PA6-10DC(f) knitted fabric samples, and (f) photographs of the PA6(f) and PA6-10DC(f) knitted fabric samples and their charred residues after cone calorimetry tests.

Table 7. Combustion data collected by cone calorimetry (heat flux: 35 kW/m^2).

Sample	TTI (s)	PHRR (kW/m^2)	THR (MJ/m^2)	EHC (MJ/kg)
PA6(f)	110 ± 30	190 ± 5	8.0 ± 0.2	32.8 ± 2.9
PA6-10DC(f)	51 ± 5	295 ± 12	13.3 ± 0.4	27.7 ± 0.4

Table 8. Smoke data collected by cone calorimetry (heat flux: 35 kW/m^2).

Sample	SEA (m^2/kg)	[CO] yield (kg/kg)	[CO_2] yield (kg/kg)	[CO]/[CO_2]
PA6(f)	191 ± 27	0.010 ± 0.001	2.911 ± 0.169	0.004
PA6-10DC(f)	546 ± 9	0.046 ± 0	1.985 ± 0.089	0.023

Furthermore, it can be observed that the production of both CO and CO_2 for the PA6-10DC(f) sample occurred at lower combustion times compared to those of the PA6(f) (Fig. 14c,d). However, the mass of CO_2 yield per mass of the PA6-10DC(f) sample burned was significantly lower compared to the PA6(f) (Fig 14d), confirming the results of the TG-FTIR analysis. Consequently, the ratio between the [CO] and [CO_2] yields (Table 8) was fivefold higher for the PA6-10DC(f) sample with respect to that of the PA6(f) sample, which could be due to the retardation of the OH• radicals in the oxidation of CO to CO_2 as well as the inhibited cleavage of the peptide C(O)–NH bonds. This eventually leads to the inhibited decomposition of the PA6-10DC(f) sample in the solid phase, as evidenced by the sample mass loss values shown in Fig. 14e. The charred residue of the PA6-10DC(f) sample, also displayed in Fig. 14f, was significantly higher as compared to that of the PA6(f). The initial weights of the 1 dm^2 samples of PA6(f) and PA6-10DC(f) knitted fabrics were 3.0 and 5.5 g, respectively, which could be partly responsible for the increased HRR and THR, since almost twice the mass of the

PA6-10DC(f) sample was burned under the continuous heat flux compared to PA6(f). However, the increased TSR is characteristic of the phosphorus-based FRs active in the gas phase, and this phenomenon should be further researched by simultaneously introducing smoke suppressants and investigating their influence on the flame retardant effects of DOPO-NH– functionality [33,38,39].

4. Conclusion

In this work, the idea of producing FR PA6 by chemical modifications of the polymer chain, while completely preserving the structure of the PA6 backbone, was fulfilled for the first time. For this purpose, a novel phosphonamidate derivative of A-CLM, containing the DOPO-NH– pendant functional group, was synthesized for the first time by a one-step Atherton–Todd reaction. Due to the presence of two chiral centers, DOPO-A-CLM consists of two diastereomeric species DS-I and DS-II. The co-polymerization of DOPO-A-CLM with CLM was conducted as a hydrolytic polymerization process, and DOPO-A-CLM was successfully integrated into the polymer matrix at different weight ratios.

The results showed that the bridging of DOPO and ε-caprolactam with the –NH– group significantly enhances the thermal stability of ε-caprolactam. Consequently, the chemical bonding of the DOPO-NH– pendant group to the PA6 backbone increases the thermal stability of polymer in nitrogen and air, as compared to PA6. The promoted thermal decomposition at lower temperatures, and the inhibition of the cleavage of peptide C(O)–NH bonds and thus depolymerization of PA6, increased char residues at 500 °C with respect to PA6. The increased thermal stability of PA6-xDC was enhanced by increasing the concentration of the incorporated DOPO-A-CLM co-monomer.

The chemically bonded DOPO-NH– pendant group affected the packing of PA6 backbones, leading to decreased crystallinity. This phenomenon caused a decrease in the tensile properties of PA6-10DC as compared to PA6. However, the filament yarns were successfully melt-spun from PA6-10DC, then partially drawn during winding onto bobbins, and knitted into the fabric samples. The surface morphology of the PA6-10DC(f) filament yarns was not significantly different from that of PA6.

The flame retardant effect of the DOPO-NH– functionality successfully slowed down both the burning and melt dripping of the PA6-10DC(f) sample that achieved self-extinction within 1 s, immediately after the first drop. The presence of phosphorus near the surface of the lower edge sample exposed to the flame confirms, in addition to the gas phase action of DOPO, a possible effect taking place in the condensed phase.

We believe that the discussed high-performance flame retardant polyamide yarn material fabricated from bio-mass holds great potential for a wide variety of future products in, e.g., the automotive, aerospace, and technical textile industries, where safety plays an important role.

Acknowledgements

This work was supported by the Slovenian Research Agency (Basic Postdoc Project Z2-9250, Programmes P2-0213, P2-0393, and P1-0134b, the Infrastructural Centre RIC UL-NTF), and the European COST Action CONTEXT, "European Network to connect research and innovation efforts on advanced Smart Textiles". The authors thank Helena Spreizer and Gregor Žitko for technical support in the synthesis of co-polymer, Tomaž Stergar for technical support during the melt-spinning process, and Andrej Vilar for the preparation of the knitted fabric samples.

Appendix A. Supplementary information

References

[1] R. Geyer, J.R. Jambeck, K.L. Law, Production, use, and fate of all plastics ever made, Sci. Adv. 3 (2017) e1700782. https://doi.org/10.1126/sciadv.1700782.

[2] J.C. Worch, A.P. Dove, 100th Anniversary of Macromolecular Science Viewpoint: Toward Catalytic Chemical Recycling of Waste (and Future) Plastics, ACS Macro Lett. (2020) 1494–1506. https://doi.org/10.1021/acsmacrolett.0c00582.

[3] J.B. Williamson, S.E. Lewis, R.R. Johnson, I.M. Manning, F.A. Leibfarth, C−H Functionalization of Commodity Polymers, Angew. Chemie Int. Ed. 58 (2019) 8654–8668. https://doi.org/10.1002/anie.201810970.

[4] A.B. Morgan, The Future of Flame Retardant Polymers–Unmet Needs and Likely New Approaches, Polym. Rev. 59 (2019) 25–54. https://doi.org/10.1080/15583724.2018.1454948.

[5] B. Claus, K. Rudolf, S. Joachim, W. Reinhard, Process for the production of caprolactam from waste containing polyamide, 2002.

[6] Frost W. John, Synthesis of caprolactam from lysine, WO2005123669A1, 2005.

[7] Frost W. John, Catalytic Deamination for Caprolactam Production, US20100145003A1, 2008.

[8] J. Sebastian, M. Zheng, Y. Jiang, Y. Zhao, H. Wang, Z. Song, X. Li, J. Pang, T. Zhang, One-pot conversion of lysine to caprolactam over Ir/H-Beta catalysts, Green Chem. 21 (2019) 2462–2468. https://doi.org/10.1039/c9gc00415g.

[9] J. Zhang, X. Mi, S. Chen, Z. Xu, D. Zhang, M. Miao, J. Wang, A bio-based hyperbranched flame retardant for epoxy resins, Chem. Eng. J. 381 (2020) 122719. https://doi.org/10.1016/j.cej.2019.122719.

[10] W. Huang, X. Hu, J. Zhai, N. Zhu, K. Guo, Biorenewable furan-containing polyamides,

Mater. Today Sustain. 10 (2020) 100049. https://doi.org/10.1016/j.mtsust.2020.100049.

[11] H. Vahabi, H. Rastin, E. Movahedifar, K. Antoun, N. Brosse, M.R. Saeb, Flame Retardancy of Bio-Based Polyurethanes: Opportunities and Challenges, Polymers (Basel). 12 (2020) 1234. https://doi.org/10.3390/polym12061234.

[12] R. Beerthuis, G. Rothenberg, N.R. Shiju, Catalytic routes towards acrylic acid, adipic acid and ε-caprolactam starting from biorenewables, Green Chem. 17 (2015) 1341–1361. https://doi.org/10.1039/c4gc02076f.

[13] D. Tunc, H. Bouchekif, B. Améduri, C. Jérôme, P. Desbois, P. Lecomte, S. Carlotti, Synthesis of aliphatic polyamide bearing fluorinated groups from ε-caprolactam and modified cyclic lysine, Eur. Polym. J. 71 (2015) 575–584. https://doi.org/10.1016/j.eurpolymj.2015.08.030.

[14] D. Tunc, C. Le Coz, M. Alexandre, P. Desbois, P. Lecomte, S. Carlotti, Reversible cross-linking of aliphatic polyamides bearing thermo- and photoresponsive cinnamoyl moieties, Macromolecules. 47 (2014) 8247–8254. https://doi.org/10.1021/ma502083p.

[15] J. Chen, M. Li, W. He, Y. Tao, X. Wang, Facile Organocatalyzed Synthesis of Poly(ε-lysine) under Mild Conditions, Macromolecules. 50 (2017) 9128–9134. https://doi.org/10.1021/acs.macromol.7b02331.

[16] C. Hirsch, B. Striegl, S. Mathes, C. Adlhart, M. Edelmann, E. Bono, S. Gaan, K.A. Salmeia, L. Hoelting, A. Krebs, J. Nyffeler, R. Pape, A. Bürkle, M. Leist, P. Wick, S. Schildknecht, Multiparameter toxicity assessment of novel DOPO-derived organophosphorus flame retardants, Arch. Toxicol. 91 (2017) 407–425. https://doi.org/10.1007/s00204-016-1680-4.

[17] M.M. Velencoso, A. Battig, J.C. Markwart, B. Schartel, F.R. Wurm, Molecular firefighting—How modern phosphorus chemistry can help solve the challenge of flame

retardancy. Angew. Chem. 2018, 57, 10450–10467. https://doi.org/10.1002/anie.201711735..

[18] N.M. Neisius, M. Lutz, D. Rentsch, P. Hemberger, S. Gaan, Synthesis of DOPO-Based Phosphonamidates and their Thermal Properties, Ind. Eng. Chem. Res. 53 (2014) 2889–2896. https://doi.org/10.1021/ie403677k.

[19] A. Buczko, T. Stelzig, L. Bommer, D. Rentsch, M. Heneczkowski, S. Gaan, Bridged DOPO derivatives as flame retardants for PA6, Polym. Degrad. Stab. 107 (2014) 158–165. https://doi.org/10.1016/j.polymdegradstab.2014.05.017.

[20] L. Long, W. Zhou, Y. Xiang, J. Li, S. Huang, S. Qin, G. Xu, J. Yu, Function of the aryl group in bis DOPO phosphonate on reducing fire hazards of polyamide 6 composites, J. Appl. Polym. Sci. 137 (2020) 49188. https://doi.org/10.1002/app.49188.

[21] M. Li, Y. Zhong, Z. Wang, A. Fischer, F. Ranft, D. Drummer, W. Wu, Flame retarding mechanism of Polyamide 6 with phosphorus-nitrogen flame retardant and DOPO derivatives, J. Appl. Polym. Sci. 133 (2016) n/a-n/a. https://doi.org/10.1002/app.42932.

[22] P. Simonetti, R. Nazir, A. Gooneie, S. Lehner, M. Jovic, K.A. Salmeia, R. Hufenus, A. Rippl, J.P. Kaiser, C. Hirsch, B. Rubi, S. Gaan, Michael addition in reactive extrusion: A facile sustainable route to developing phosphorus based flame retardant materials, Compos. Part B Eng. 178 (2019) 107470. https://doi.org/10.1016/j.compositesb.2019.107470.

[23] J. Vasiljević, M. Čolović, N. Čelan Korošin, M. Šobak, Ž. Štirn, I. Jerman, Effect of Different Flame-Retardant Bridged DOPO Derivatives on Properties of in Situ Produced Fiber-Forming Polyamide 6, Polymers (Basel). 12 (2020) 657. https://doi.org/10.3390/polym12030657.

[24] J. Vasiljević, M. Čolović, I. Jerman, B. Simončič, A. Demšar, Y. Samaki, M. Šobak, E. Šest, B. Golja, M. Leskovšek, V. Bukošek, J. Medved, M. Barbalini, G. Malucelli, S.

Bolka, In situ prepared polyamide 6/DOPO-derivative nanocomposite for melt-spinning of flame retardant textile filaments, Polym. Degrad. Stab. 166 (2019) 50–59. https://doi.org/10.1016/j.polymdegradstab.2019.05.011.

[25] G. Mourgas, E. Giebel, T. Schneck, J. Unold, M.R. Buchmeiser, Syntheses of intrinsically flame- retardant polyamide 6 fibers and fabrics, J. Appl. Polym. Sci.136 (2019) 47829. https://doi.org/10.1002/app.47829.

[26] D. XUAN, F. XINXING, J. LIPENG, W. XING, WENHUA XIAO, Preparation method of halogen-free flame retardant nylon 66 polymer, CN104211954A, 2014.

[27] I. Leinonen, P.P.M. Iannetta, R.M. Rees, W. Russell, C. Watson, A.P. Barnes, Lysine Supply Is a Critical Factor in Achieving Sustainable Global Protein Economy, Front. Sustain. Food Syst. 3 (2019) 27. https://doi.org/10.3389/fsufs.2019.00027.

[28] F.K. do C. Félix, L.A.J. Letti, G. Vinícius de Melo Pereira, P.G.B. Bonfim, V.T. Soccol, C.R. Soccol, L-lysine production improvement: a review of the state of the art and patent landscape focusing on strain development and fermentation technologies, Crit. Rev. Biotechnol. 39 (2019) 1031–1055. https://doi.org/10.1080/07388551.2019.1663149.

[29] B.O. Abo, M. Gao, Y. Wang, C. Wu, Q. Wang, H. Ma, Production of butanol from biomass: recent advances and future prospects, Environ. Sci. Pollut. Res. 26 (2019) 20164–20182. https://doi.org/10.1007/s11356-019-05437-y.

[30] E. Ketabchi, L. Pastor-Pérez, T.R. Reina, H. Arellano-García, Catalytic upgrading of acetone, butanol and ethanol (ABE): A step ahead for the production of added value chemicals in bio-refineries, Renew. Energy. 156 (2020) 1065–1075. https://doi.org/10.1016/j.renene.2020.04.152.

[31] P. Losch, J.F. Kolb, A. Astafan, T.J. Daou, L. Pinard, P. Pale, B. Louis, Eco-compatible zeolite-catalysed continuous halogenation of aromatics, Cite This Green

Chem. 18 (2016) 4714. https://doi.org/10.1039/c6gc00731g.

[32] K. Shakeela, V.L. Sinduri, G.R. Rao, Hydrophobic supramolecular assemblies of Keggin anions with lactam-lactim cationic tautomers, Polyhedron. 137 (2017) 43–51. https://doi.org/10.1016/j.poly.2017.07.023.

[33] K. Liu, Y. Li, L. Tao, C. Liu, R. Xiao, Synthesis and characterization of inherently flame retardant polyamide 6 based on a phosphine oxide derivative, Polym. Degrad. Stab. 163 (2019) 151–160. https://doi.org/10.1016/j.polymdegradstab.2019.03.004.

[34] A.C. Draye, O. Persenaire, J. Brožek, J. Roda, T. Košek, P. Dubois, Thermogravimetric analysis of poly(ε-caprolactam) and poly[(ε-caprolactam)-co-(ε-caprolactone)] polymers, Polymer (Guildf). 42 (2001) 8325–8332. https://doi.org/10.1016/S0032-3861(01)00352-4.

[35] M. Coquelle, S. Duquesne, M. Casetta, J. Sun, S. Zhang, S. Bourbigot, Investigation of the decomposition pathway of polyamide 6/ammonium sulfamate fibers, Polym. Degrad. Stab. 106 (2014) 150–157. https://doi.org/10.1016/j.polymdegradstab.2014.02.007.

[36] G. Socrates, Infrared and Rafman Characteristic Group Frequencies: Tables and Charts, 3rd Edition Wiley, (2004)

[37] I. Butnaru, M.P. Fernández-Ronco, J. Czech-Polak, M. Heneczkowski, M. Bruma, S. Gaan, Effect of meltable triazine-DOPO additive on rheological, mechanical, and flammability properties of PA6, Polymers 7 (2015) 1541–1563. https://doi.org/10.3390/polym7081469

[38] D. Jia, J. He, R. Yang, The synthesis andcharacterization of a DOPOderivative bearing an activeterminal epoxy group:e-DOPO and its application inrigid polyurethane foam, J. Fire Sci. 37 (2019) 47–66. https://doi.org/10.1177/0734904118812227

[39] H. Luo, W. Rao, Y. Liu, P. Zhao, L. Wang, C. Yu, Novel multi- element DOPO derivative toward low- flammability epoxy resin, J. Appl. Polym. Sci. 137 (2020) 49427. https://doi.org/10.1002/app.49427

Declaration of Interest Statement

The authors have no competing **interests** to **declare**.